Doctoral Dissertation

Phenomenological study on classically scale invariant models towards natural realization of the Higgs mass
(ヒッグス質量の自然な理解に向けた古典的スケール不変性を持つ模型の現象論的研究)

Yuya Yamaguchi

Department of Physics, Graduate school of Science, Hokkaido University

March, 2017

Abstract

Although the standard model (SM) can explain almost all experimental results obtained until now, there are unsolvable problems with the SM: active neutrino masses, baryon asymmetry of the Universe, dark matter relic abundance, dark energy, and so on. This fact clearly suggests existence of the beyond the SM. It is, however, well known that the hierarchy problem arises if new particles exist in a high energy scale compared to the electroweak scale. As an idea avoiding the hierarchy problem, classically scale invariant extensions have recently drawn a lot of attention. The classical scale invariance should be broken by some quantum effects, and there are roughly two breaking mechanisms: one is the Coleman-Weinberg mechanism, which is based on perturbation theory; another is the strong-coupling dynamics like the QCD, which is based on non-perturbation theory. In this thesis, we investigate these two types of models, and show the phenomenological consequences. In addition, we propose a new dynamics of the electroweak symmetry breaking in a classically scale invariant model, i.e., bosonic seesaw mechanism, and find that a dark matter candidate naturally exits in the model.

Acknowledgment

I would like to express the deepest appreciation to my supervisor, Naoyuki Haba, for insightful inspiration and constant encouragement throughout my study. I also would like to thank Hiroyuki Ishida for fruitful discussion and valuable advice. It has been a great pleasure to work in collaboration with Tetsutaro Higaki, Kunio Kaneta, Noriaki Kitazawa, Tatsuo Kobayashi, Shinya Matsuzaki, Nobuchika Okada, Osamu Seto, Kyousuke Shimada, Ryo Takahashi, Koji Tsumura, Masatoshi Yamada, and Yukari Yoshimochi. Without their important contributions, my work would have never been possible.

I gratefully acknowledge the past and present members of theoretical particle physics group at Hokkaido University. My stay in Shimane would have been so pleasant without friends and members of Shimane University. My work is financially supported by Research Fellowships of the Japan Society for the Promotion of Science for Young Scientists (Grants No. 26·2428).

Finally, I would like to thank my family for continuing support.

Contents

Chapter 1

Introduction

The standard model (SM) has been established by the discovery of the Higgs boson [1, 2], and it can explain almost all of experimental results obtained so far. However, the SM cannot explain some phenomenological issues: active neutrino masses, neutrino dark matter (DM) relic abundance, baryon asymmetry of the Universe, inflation in the early Universe, dark energy, and so on. To explain these issues, the SM should be extended. In almost all extended models, there are one or more additional particles, which usually have heavier masses compared to the electroweak (EW) scale. These particles would cause a hierarchy problem, i.e. a fine-tuning problem of the Higgs mass correction. The fine-tuning problem may give us a hint to construct the extended model.

It is well known that the hierarchy problem can be solved by the supersymmetry (SUSY), in which the Higgs mass corrections coming from fermions and bosons are canceled each other. Since there is no SUSY in the present Universe, the SUSY must be broken above the EW scale. When one introduces the SUSY breaking term, its value should be not so far from the EW scale to avoid the hierarchy problem. The current collider experiments, however, suggest that the SUSY breaking scale should be larger than the TeV scale, which might cause the hierarchy problem. Thus, other solution of the hierarchy problem should be expected.

In recent years, a lot of classically scale invariant models have been studied for the solution of the hierarchy problem. In the next chapter, we will explain the hierarchy problem in more detail, and explicitly show the essence of the classical scale invariance. It is our main motivation, and we concentrate on classical scale invariant models in the rest of this thesis.

Before explaining the classical scale invariance, we should clarify questions for the Higgs mass. The Higgs mass is measured by the LHC experiments as

$$M_h = 125.09 \pm 0.21 \text{ (stat.)} \pm 0.11 \text{ (syst.)} \,\text{GeV}\,, \tag{1.1}$$

with a relative uncertainty of 0.2% [3], while we do not know why it is so small compared

with a UV cutoff scale, e.g., the GUT scale ($\sim 10^{16}$ GeV) or the Planck scale ($\sim 10^{18}$ GeV). In addition, the origin of the EW symmetry breaking is the negativeness of Higgs mass term, which is given by hand in the SM. Thus, there are two fundamental questions about the Higgs mass parameter m_H^2, which is a coefficient of the Higgs mass term:

- why the Higgs mass is $\mathcal{O}(100)$ GeV?
- why the sign of Higgs mass term is negative?

They are denoted by "why $m_H^2 \sim -(100\,\mathrm{GeV})^2$ is realized?". Within the SM, since m_H^2 is just a parameter which cannot be determined from the physical system, there is no meaning to consider the above questions. We, however, expect that a UV complete model can give physically natural answer to them. Actually, we will find that our models can naturally explain the above problem.

Chapter 2

Classical scale invariance

In this chapter, we explain the SM briefly, and the hierarchy problem in detail.

2.1 Standard model

We first briefly review the SM. In the SM, the Lagrangian is given by

$$\mathcal{L} = \mathcal{L}_{\text{kin}} + \mathcal{L}_{\text{Yukawa}} - V(H)\,, \tag{2.1}$$

with

$$\begin{aligned}
\mathcal{L}_{\text{kin}} = {} & \overline{q_L} i\gamma^\mu \left(\partial_\mu - ig_Y \frac{Y_q}{2} B_\mu - ig_2 \frac{\sigma^i}{2} W^i_\mu - ig_3 \frac{\lambda^a}{2} G^a_\mu\right) q_L \\
& + \overline{u_R} i\gamma^\mu \left(\partial_\mu - ig_Y \frac{Y_u}{2} B_\mu - ig_3 \frac{\lambda^a}{2} G^a_\mu\right) u_R \\
& + \overline{d_R} i\gamma^\mu \left(\partial_\mu - ig_Y \frac{Y_d}{2} B_\mu - ig_3 \frac{\lambda^a}{2} G^a_\mu\right) d_R \\
& + \overline{\ell_L} i\gamma^\mu \left(\partial_\mu - ig_Y \frac{Y_\ell}{2} B_\mu - ig_2 \frac{\sigma^i}{2} W^i_\mu\right) \ell_L \\
& + \overline{e_R} i\gamma^\mu \left(\partial_\mu - ig_Y \frac{Y_e}{2} B_\mu\right) e_R \\
& + \left|\left(\partial_\mu - ig_Y \frac{Y_H}{2} B_\mu - ig_2 \frac{\sigma^i}{2} W^i_\mu\right) H\right|^2 \\
& - \frac{1}{4} B_{\mu\nu} B^{\mu\nu} - \frac{1}{4} W^i_{\mu\nu} W^{i\,\mu\nu} - \frac{1}{4} G^a_{\mu\nu} G^{a\,\mu\nu}\,,
\end{aligned} \tag{2.2}$$

$$\mathcal{L}_{\text{Yukawa}} = -Y_U \overline{q_L} \tilde{H} u_R - Y_D \overline{q_L} H d_R - Y_E \overline{\ell_L} H e_R + \text{h.c.}\,, \quad (\tilde{H} = i\sigma^2 H^*) \tag{2.3}$$

$$V(H) = \lambda_H (H^\dagger H)^2 + m_H^2 (H^\dagger H)\,, \tag{2.4}$$

where representations of the SM fields are summarized in Table 2.1. For the ($U(1)_Y$, $SU(2)_L$, $SU(3)_C$) gauge interactions, gauge couplings are (g_Y, g_2, g_3), and Y_α ($\alpha = q, u, d, \ell, e, H$), σ^i ($i = 1 \sim 3$), λ^a ($a = 1 \sim 8$) represent the hypercharge, the Pauli matrix

		Representation	Spin
Quark doublet	q_L^i	$(\mathbf{3}, \mathbf{2}, 1/3)$	1/2
Up-type quark singlet	u_R^i	$(\mathbf{3}, \mathbf{1}, 4/3)$	1/2
Down-type quark singlet	d_R^i	$(\mathbf{3}, \mathbf{1}, -2/3)$	1/2
Lepton doublet	ℓ_L^i	$(\mathbf{1}, \mathbf{2}, -1)$	1/2
Charged lepton singlet	e_R^i	$(\mathbf{1}, \mathbf{1}, -2)$	1/2
Higgs doublet	H	$(\mathbf{1}, \mathbf{2}, 1)$	0
$U(1)_Y$ gauge boson	B_μ	$(\mathbf{1}, \mathbf{1}, 0)$	1
$SU(2)_L$ gauge boson	W_μ^i	$(\mathbf{1}, \mathbf{3}, 0)$	1
$S(3)_C$ gauge boson	G_μ^a	$(\mathbf{8}, \mathbf{1}, 0)$	1

Table 2.1: Representations of the SM fields under $(SU(3)_C, SU(2)_L, U(1)_Y)$. For fermions, i (=1, 2, and 3) is a generation index. Electric charge is given by $Q_{\rm em} = I_3 + Y/2$ with the isospin I_3 and the hypercharge Y.

and the Gell-Mann matrix, respectively. The gauge filed strength are given by

$$\begin{aligned} B_{\mu\nu} &= \partial_\mu B_\nu - \partial_\nu B_\mu \,, \\ W_{\mu\nu}^i &= \partial_\mu W_\nu^i - \partial_\nu W_\mu^i + g_2 \epsilon^{ijk} W_\mu^j W_\nu^k \,, \\ G_{\mu\nu}^a &= \partial_\mu G_\nu^a - \partial_\nu G_\mu^a + g_3 f^{abc} G_\mu^b G_\nu^c \,, \end{aligned} \tag{2.5}$$

where ϵ^{ijk} and f^{abc} are the structure constants for $SU(2)_L$ and $SU(3)_C$ gauge groups, which obey $[\sigma^i/2, \sigma^j/2] = \epsilon^{ijk}\sigma^k/2$ and $[\lambda^a/2, \lambda^b/2] = f^{abc}\lambda^c/2$, respectively.

When the Higgs mass parameter m_H^2 is negative, the Higgs field has nonzero vacuum expectation value (VEV), and thus, the EW symmetry $(SU(2)_L \times U(1)_Y)$ is spontaneously broken into $U(1)_{\rm em}$. In the unitary gauge, the Higgs doublet is written by the expansion around the VEV, v_H, as

$$H = \begin{pmatrix} G^+ \\ \frac{1}{\sqrt{2}}\left(v_H + h + iG^0\right) \end{pmatrix} , \tag{2.6}$$

where G^+ and G^0 are the Nambu-Goldstone (NG) bosons, and h is the physical Higgs boson. From the stationary condition of the Higgs potential (2.4), one can find the VEV given by $v_H = \sqrt{-m_H^2/\lambda_H}$, whose value is around 246 GeV. In addition, the physical Higgs mass is given by

$$M_h = \sqrt{2\lambda_H} v_H = \sqrt{-2m_H^2} \,, \tag{2.7}$$

and its value is around 125 GeV.

Substituting Eq. (2.6) for the kinetic term of the Higgs doublet in Eq. (2.2), three massive gauge bosons arise as

$$\begin{aligned} W_\mu^\pm &= \frac{1}{\sqrt{2}}\left(W_\mu^1 \mp iW_\mu^2\right) \quad \text{with mass} \quad M_W = g_2 \frac{v_H}{2} \,, \\ Z_\mu &= \frac{1}{\sqrt{g_Y^2 + g_2^2}}\left(g_2 W_\mu^3 - g_Y B_\mu\right) \quad \text{with mass} \quad M_Z = \sqrt{g_Y^2 + g_2^2}\frac{v_H}{2} \,, \end{aligned} \tag{2.8}$$

while one gauge boson remains massless as

$$A_\mu = \frac{1}{\sqrt{g_Y^2 + g_2^2}} \left(g_Y W_\mu^3 + g_2 B_\mu \right) \quad \text{with mass} \quad M_A = 0 \,, \tag{2.9}$$

which corresponds to the $U(1)_{\rm em}$ gauge boson, or photon. The $U(1)_{\rm em}$ gauge coupling is given by

$$e = \frac{g_Y g_2}{\sqrt{g_Y^2 + g_2^2}} = g_2 \sin\theta_W = g_Y \cos\theta_W \,, \tag{2.10}$$

where θ_W is the Weinberg angle defined by $\cos\theta_W = M_W/M_Z$.

In the same way, substituting Eq. (2.6) for the Yukawa terms in Eq. (2.3), the fermion mass matrices are given by

$$\begin{aligned} M_U &= Y_U \frac{v_H}{\sqrt{2}} \quad \text{for up-type quarks } (u,\, c,\, t) \,, \\ M_D &= Y_D \frac{v_H}{\sqrt{2}} \quad \text{for down-type quark } (d,\, s,\, b) \,, \\ M_E &= Y_E \frac{v_H}{\sqrt{2}} \quad \text{for charged lepton } (e,\, \mu,\, \tau) \,, \end{aligned} \tag{2.11}$$

while the neutrinos remain massless because of the absence of right-handed neutrino, which is a SM-gauge singlet fermion. The mass matrices, which are generic complex 3×3 matrices, can be diagonalized by bi-unitary transformation like $V_L^\dagger M V_R = M_{\rm diag}$ with unitary matrices V_L and V_R. For the fermion fields, flavor (or gauge) eigenstates are written by

$$\begin{aligned} q_L^i &= \begin{pmatrix} u_L^i \\ d_L^i \end{pmatrix} = \left(\begin{pmatrix} u_L \\ d_L \end{pmatrix}, \begin{pmatrix} c_L \\ s_L \end{pmatrix}, \begin{pmatrix} t_L \\ b_L \end{pmatrix} \right) , \\ u_R^i &= (u_R \,,\ c_R \,,\ t_R) \,, \qquad d_R^i = (d_R \,,\ s_R \,,\ b_R) \,, \\ \ell_L^i &= \begin{pmatrix} \nu_L^i \\ e_L^i \end{pmatrix} = \left(\begin{pmatrix} \nu_{eL} \\ e_L \end{pmatrix}, \begin{pmatrix} \nu_{\mu L} \\ \mu_L \end{pmatrix}, \begin{pmatrix} \nu_{\tau L} \\ \tau_L \end{pmatrix} \right) , \\ & \qquad e_R^i = (e_R \,,\ \mu_R \,,\ \tau_R) \,, \end{aligned} \tag{2.12}$$

and the mass eigenstates, which are denoted with hat, are given by the following unitary transformations

$$\begin{aligned} u_L^i &= (V_L^u)_{ij} \hat{u}_L^j \,, & u_R^i &= (V_R^u)_{ij} \hat{u}_R^j \,, \\ d_L^i &= (V_L^d)_{ij} \hat{d}_L^j \,, & d_R^i &= (V_R^d)_{ij} \hat{d}_R^j \,, \\ \nu_L^i &= (V_L^\nu)_{ij} \hat{\nu}_L^j \,, \\ e_L^i &= (V_L^e)_{ij} \hat{e}_L^j \,, & e_R^i &= (V_R^e)_{ij} \hat{e}_R^j \,. \end{aligned} \tag{2.13}$$

Then, diagonalized mass matrices can be given by bi-unitary matrices as mentioned above:

$$\begin{aligned} V_L^{u\dagger} M_U V_R^u &= {\rm diag}(m_u \,,\ m_c \,,\ m_t) \,, \qquad V_L^{d\dagger} M_D V_R^d = {\rm diag}(m_d \,,\ m_s \,,\ m_b) \,, \\ & \qquad V_L^{e\dagger} M_E V_R^e = {\rm diag}(m_e \,,\ m_\mu \,,\ m_\tau) \,. \end{aligned} \tag{2.14}$$

Using the mass eigenstates, the kinetic terms (2.2) include the $W^\pm$ interaction terms, i.e., $g_2/\sqrt{2}\, W^\pm_\mu J^{\mu\pm}$, where the charged currents are given by

$$\begin{aligned} J^{\mu+} &= \overline{u^i_L}\gamma^\mu d^i_L + \overline{\nu^i_L}\gamma e^i_L = \overline{\hat{u}^i_L}\left(V^{u\dagger}_L V^d_L\right)_{ij}\gamma^\mu \hat{d}^j_L + \overline{\hat{\nu}^i_L}\left(V^{\nu\dagger}_L V^e_L\right)_{ij}\gamma \hat{e}^j_L\,, \\ J^{\mu-} &= \overline{d^i_L}\gamma^\mu u^i_L + \overline{e^i_L}\gamma \nu^i_L = \overline{\hat{d}^i_L}\left(V^{d\dagger}_L V^u_L\right)_{ij}\gamma^\mu \hat{u}^j_L + \overline{\hat{e}^i_L}\left(V^{e\dagger}_L V^\nu_L\right)_{ij}\gamma \hat{\nu}^j_L\,. \end{aligned} \tag{2.15}$$

Thus, the quark and lepton charged currents have the mixing matrices

$$V_{\rm CKM} \equiv V^{u\dagger}_L V^d_L\,, \qquad V_{\rm PMNS} \equiv V^{\nu\dagger}_L V^e_L\,, \tag{2.16}$$

which are known as the Cabibbo-Kobayashi-Maskawa [4, 5] and the Pontecorvo-Maki-Nakagawa-Sakata [6, 7] matrices, respectively. However, since there is no neutrino mass matrix, V^ν_L is an arbitrary unitary matrix, and thus, $V_{\rm PMNS}$ can become the identity matrix by taking $V^\nu_L = V^e_L$. Therefore, the neutrino oscillations do not occur within the SM, and we have to extend the SM to explain the neutrino mass generation.

Renormalization group equation (RGE) of physical parameter A is defined by

$$\mu\frac{dA}{d\mu} = \beta_A\,, \tag{2.17}$$

where μ is a renormalization scale. β functions of the SM parameters are given by

$$\begin{aligned} \beta_{g_1} &= \frac{g_1^3}{16\pi^2}\frac{41}{10}\,, \qquad \beta_{g_2} = \frac{g_2^3}{16\pi^2}\left(-\frac{19}{6}\right)\,, \qquad \beta_{g_3} = \frac{g_3^3}{16\pi^2}\left(-7\right)\,, \\ \beta_{Y_U} &= \frac{Y_U}{16\pi^2}\left\{\frac{3}{2}Y_U^\dagger Y_U - \frac{3}{2}Y_D^\dagger Y_D + {\rm tr}\left[3Y_U^\dagger Y_U + 3Y_D^\dagger Y_D + Y_E^\dagger Y_E\right] - \frac{17}{20}g_1^2 - \frac{9}{4}g_2^2 - 8g_3^2\right\}, \\ \beta_{Y_D} &= \frac{Y_D}{16\pi^2}\left\{\frac{3}{2}Y_D^\dagger Y_D - \frac{3}{2}Y_U^\dagger Y_U + {\rm tr}\left[3Y_U^\dagger Y_U + 3Y_D^\dagger Y_D + Y_E^\dagger Y_E\right] - \frac{1}{4}g_1^2 - \frac{9}{4}g_2^2 - 8g_3^2\right\}, \\ \beta_{Y_E} &= \frac{Y_E}{16\pi^2}\left\{\frac{3}{2}Y_E^\dagger Y_E + {\rm tr}\left[3Y_U^\dagger Y_U + 3Y_D^\dagger Y_D + Y_E^\dagger Y_E\right] - \frac{9}{4}g_1^2 - \frac{9}{4}g_2^2\right\}, \\ \beta_{\lambda_H} &= \frac{1}{16\pi^2}\left\{\lambda_H\left(24\lambda_H - \frac{9}{5}g_1^2 - 9g_2^2 + 4\,{\rm tr}\left[3Y_U^\dagger Y_U + 3Y_D^\dagger Y_D + Y_E^\dagger Y_E\right]\right)\right. \\ &\quad \left. + \frac{9}{8}\left(\frac{3}{25}g_1^4 + \frac{2}{5}g_1^2 g_2^2 + g_2^4\right) - 2\,{\rm tr}\left[3Y_U^\dagger Y_U Y_U^\dagger Y_U + 3Y_D^\dagger Y_D Y_D^\dagger Y_D + Y_E^\dagger Y_E Y_E^\dagger Y_E\right]\right\}, \\ \beta_{m_H^2} &= \frac{m_H^2}{16\pi^2}\left\{12\lambda_H - \frac{9}{10}g_1^2 - \frac{9}{2}g_2^2 + 2\,{\rm tr}\left[3Y_U^\dagger Y_U + 3Y_D^\dagger Y_D + Y_E^\dagger Y_E\right]\right\}, \end{aligned} \tag{2.18}$$

at one-loop level, where $U(1)_Y$ gauge coupling has been normalized by $g_1 = \sqrt{5/3}g_Y$. Solving the RGEs with using the experimentally observed values as in Ref. [8] for the top quark mass, Ref. [3] for the Higgs mass and Ref. [9] for others, we can find energy dependence of the parameters as shown in Figs. 2.1 and 2.2.[1] In Fig. 2.2, the Higgs

[1] We have used two-loop RGEs as shown in App. A.1.

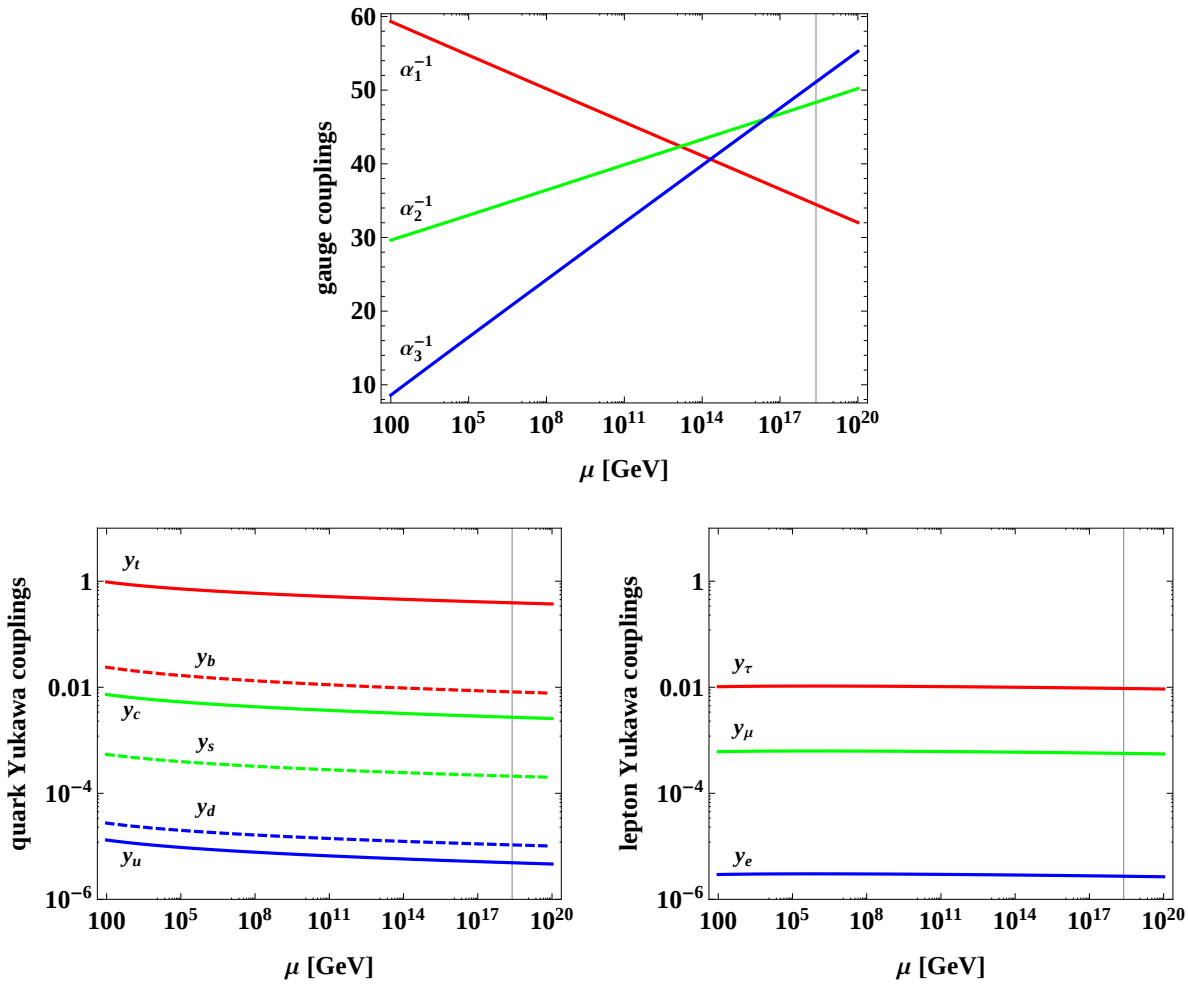

Figure 2.1: Renormalization group evolution of the SM couplings. The vertical line corresponds to the reduced Planck mass $M_{\rm Pl} = 2.4 \times 10^{18}$ GeV.

self-coupling λ_H becomes negative around $\mu \sim 10^{10}$ GeV. Then, the Higgs potential has another minimum besides the EW vacuum, and the EW vacuum can decay into other vacuum. Actually, this decay rate is enormously longer than the age of our Universe, so the EW vacuum is meta-stable (within the SM).

When we consider the extension of the SM, we focus on, e.g., the following issues:

- Origin of the negative mass term of the Higgs doublet
- Mechanism of neutrino mass generation
- How to stabilize the EW vacuum

Once we introduce a new field into the SM, the Higgs self-coupling λ_H often becomes larger than the SM one, which induces the vacuum stability. For example, a coupling between the Higgs doublet and new scalar (or gauge) field positively contributes to β_{λ_H};

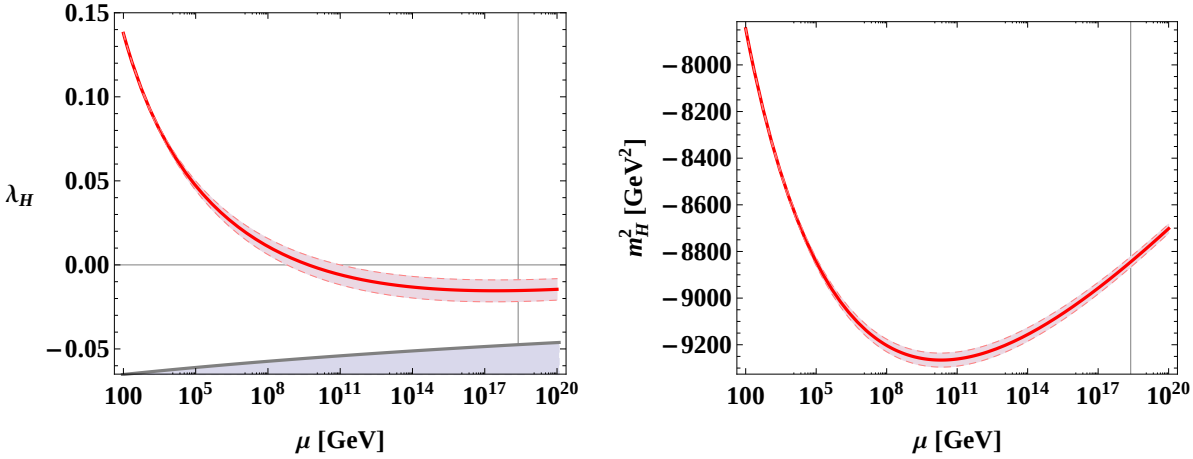

Figure 2.2: Renormalization group evolution of the Higgs self-couplings and the Higgs mass parameter. We take the world average values for top quark mass and the strong coupling as $M_t = 173.34 \pm 0.76$ [8] and $\alpha_3 = 0.1185 \pm 0.0006$ [9], respectively. The red thick line corresponds to the central values of them. In the left panel, the gray shaded region means vacuum instability. The vertical line corresponds to the reduced Planck mass $M_{\rm Pl} = 2.4 \times 10^{18}$ GeV.

new fermion field with the SM-gauge charges make the SM-gauge couplings become larger, and then, the larger gauge couplings induce smaller Yukawa couplings and larger λ_H; tree-level threshold correction lifts up the self-coupling. However, the additional fields often causes hierarchy problem. In the next section, we explain the hierarchy problem in detail.

2.2 Hierarchy problem

In this section, to generalize the hierarchy problem, we explain it with real scalars $S = (s_1, s_2, \cdots)^T$, gauge fields V, and Weyl fermions F. In the effective field theory, which is valid up to a UV cutoff scale Λ, renormalized scalar mass, $m_S^2(\mu)$ ($|m_A| < \mu < \Lambda$), is given by [10]

$$\begin{aligned}(m_S^2(\mu))_{ab} &= (\bar{m}_S^2(\Lambda))_{ab} + (\delta m_S^2(\Lambda,\mu))_{ab} \\ &= (\bar{m}_S^2(\Lambda))_{ab} + \sum_{A=S,V,F} (-1)^{2J_A}(2J_A+1)\frac{(g_A)_{abcd}}{16\pi^2}\left[\Lambda^2\delta_{cd} - (\bar{m}_A^2(\Lambda))_{cd}\ln\frac{\Lambda^2}{\mu^2}\right],\end{aligned} \tag{2.19}$$

where $\bar{m}_A^2(\Lambda)$ is the bare mass for the field A with spin J_A and coupling g_A, which is defined by

$$\frac{1}{4!}(g_S)_{abcd}S_aS_bS_cS_d\,, \qquad \frac{1}{2}(g_V)_{abcd}V_aV_bS_cS_d\,, \qquad (y_F)_{abc}\overline{F_a}F_bS_c\,, \tag{2.20}$$

and $(y_F)_{abe}(y_F)_{cde} = (g_F)_{abcd}$. In the correction term, there are two types of divergence: one is a quadratic divergence proportional to Λ^2, and another is a logarithmic divergence proportional to $\bar{m}_A^2(\Lambda)$.

It is often said that the hierarchy problem arises for $m_S^2 \ll \Lambda^2$, which requires a fine-tuning between $\bar{m}_S^2(\Lambda)$ and Λ^2. However, $\bar{m}_S(\Lambda)$ is just a parameter in the Lagrangian, and Λ is an upper limit of loop integral, that is, the both quantities are unphysical.[2] Even in the limit of $\Lambda \to \infty$, the renormalized quantity $m_S^2(\mu)$ can become finite. In addition, once the quadratic divergence is renormalized (or subtracted), it does not arise again in the theory, while the logarithmic correction should arise [12]. If a theory have only small explicit (renormalized) mass terms $m_S^2 \ll \Lambda^2$, the theory possesses an approximate scale invariance, and its stability depends on logarithmic corrections. Thus, the hierarchy problem arises only when the corrections are much larger than the explicit mass. In this sense, the SM possesses an approximate scale invariance, which is softly broken by the Higgs mass term ($\sim 100\,\mathrm{GeV}$), and dynamically broken by the quark condensate ($\sim 100\,\mathrm{MeV}$). The scale of the Higgs mass parameter is stable during the RG evolution as shown in the left panel of Fig. 2.2. Therefore, if the cutoff scale is much larger than the Higgs mass, there is no hierarchy problem within the SM. The above discussion was firstly mentioned in Ref. [13].

On the other hand, one might wonder why the observed Higgs mass is much smaller than a UV scale, e.g., the GUT scale ($\sim 10^{16}\,\mathrm{GeV}$) and the Planck scale ($\sim 10^{18}\,\mathrm{GeV}$). It is not a fine-tuning problem, but a problem why explicit breaking of the scale invariance is so small compared to the UV scale, which rather may be a philosophical or ideological problem. We cannot guess what scale is natural for the explicit symmetry breaking. Actually, even if there is no explicit mass term, scale invariance can be broken "anomalously" by, e.g., strong-coupling dynamics like quark condensate in the QCD, and the Coleman-Weinberg (CW) mechanism [14]. Then, the breaking scale can be determined by a physical system, which is completely different from the explicit symmetry breaking case. Thus, when the scale invariance is imposed into the theory, in which there is no explicit mass term, the smallness of the Higgs mass can be naturally explained by an anomalous breaking of the "classical" scale invariance.

It is known that, within the SM, the observed Higgs mass cannot be explained by the CW mechanism. Thus, a lot of works have been done in classically scale invariant models to naturally realize the observed Higgs mass. There are almost two types of the model: one depends on the CW mechanism, and another depends on the strong-coupling dynamics.[3]

[2] Using the dimensional regularization, there is no quadratic divergence in the first place. From the viewpoint of the Wilsonian renormalization group, the quadratic divergence can always be absorbed into a position of the critical surface [11]. We can regard such a scheme dependent quantity as unphysical.

[3] Other models depend on modified gravity, e.g., as in Ref. [15].

The CW type has been considered in non-gauge extended models (Refs. [16]-[37]), $U(1)$ (Refs. [27], [38]-[73]) and/or $SU(N)$ (Refs. [52, 57, 58], [74]-[83]) gauge extended models. The strong-coupling dynamics type has been considered in the $SU(N)$ gauge extended model (Refs. [84]-[104]). In this thesis, we consider these two types of classically scale invariant models.

Chapter 3

$U(1)$ gauge extended model I

In this chapter, we consider the flatland scenario, in which a model has the scale invariance, and a scalar potential vanishes at the Planck scale [47, 53, 55]. This chapter is based on our work [64].

3.1 $U(1)_\chi$ gauge extension and flatland scenario

We consider $U(1)$ gauge extension of the SM, in which filed contents are shown in Table 3.1. The $U(1)_X$ charge are given by $B - L + x_H Y$, where x_H, B, L, and Y denote an arbitrary real number, the baryon and lepton numbers, and the $U(1)_Y$ hypercharge, respectively. In particular, $x_H = 0$, -1 and $-2/5$ correspond to $U(1)_{B-L}$, $U(1)_R$ and $U(1)_\chi$, respectively. In this chapter, we concentrate on the $U(1)_\chi$ model. Note that we have to introduce three generations of right-handed neutrinos ν_R to make the model free from all the gauge and gravitational anomalies.

A scalar potential is given by

$$V = \lambda_H |H|^4 + \lambda_\Phi |\Phi|^4 + \lambda_{\rm mix} |H|^2 |\Phi|^2 \,, \tag{3.1}$$

where Φ is a SM-gauge singlet complex scalar field. Since we have assumed the classical scale invariance, there is no dimensionful parameter like a mass term. In the flatland scenario, we impose that all the quartic couplings vanish at the (reduced) Planck scale. The Lagrangian including right-handed neutrinos is given by

$$\mathcal{L}_N = -Y_\nu^{\alpha i} \overline{\ell_L^\alpha} H \nu_R^i - Y_M^{ij} \Phi \overline{\nu_R^{ic}} \nu_R^j + (h.c.) \,, \tag{3.2}$$

where α and i show the indices of the flavor and generation, respectively. The type-I seesaw mechanism [105] can explain the active neutrino masses, and the Dirac Yukawa coupling Y_ν is typically $\mathcal{O}(10^{-6})$ for the right-handed neutrinos with TeV scale masses. Thus, we can neglect Y_ν for the RG analyses.

	$SU(3)_C \times SU(2)_L \times U(1)_Y$	$U(1)_X$
q_L^i	$(\mathbf{3}, \mathbf{2}, 1/3)$	$(x_H+1)/3$
u_R^i	$(\mathbf{3}, \mathbf{1}, 4/3)$	$(4x_H+1)/3$
d_R^i	$(\mathbf{3}, \mathbf{1}, -2/3)$	$(-2x_H+1)/3$
ℓ_L^i	$(\mathbf{1}, \mathbf{2}, -1)$	$-x_H-1$
e_R^i	$(\mathbf{1}, \mathbf{1}, -2)$	$-2x_H-1$
ν_R^i	$(\mathbf{1}, \mathbf{1}, 0)$	-1
H	$(\mathbf{1}, \mathbf{2}, 1)$	x_H
Φ	$(\mathbf{1}, \mathbf{1}, 0)$	2

Table 3.1: Charge assignments, where x_H is an arbitrary real number.

In this model, there are two $U(1)$ gauge bosons. When we take their kinetic terms are diagonal, the covariant derivative is given by

$$D_\mu = \partial_\mu - ig_Y \frac{Y}{2} B_\mu - i\left(g_{\rm mix}\frac{Y}{2} + g_\chi X\right) Z'_\mu - ig_2 \frac{\sigma^i}{2} W^i_\mu - ig_3 \frac{\lambda^a}{2} G^a_\mu \,, \tag{3.3}$$

where Y and X denote $U(1)_Y$ and $U(1)_\chi$ charges, respectively. The additional $U(1)$ gauge boson is conventionally called the Z' boson [see Ref. [106] for a review of Z' boson]. The gauge coupling of $U(1)_\chi$ is g_χ, and there is a $U(1)$ mixing coupling $g_{\rm mix}$, because it appears through loop corrections of fermions having both $U(1)_Y$ and $U(1)_\chi$ charges even if $g_{\rm mix}$ is vanishing at some scale. In this chapter, we impose $g_{\rm mix}(M_{\rm Pl}) = 0$, which would arise from breaking a simple unified gauge group into $SU(3)_C \times SU(2)_L \times U(1)_Y \times U(1)_\chi$. Particularly, it is well known the decomposition of the $SO(10)$ GUT as $SO(10) \to SU(5) \times U(1)_\chi$. Thus, when the $SO(10)$ GUT is broken at the Planck scale, $g_{\rm mix}(M_{\rm Pl}) = 0$ is naturally expected.

Let us explain the mechanism of the $U(1)_\chi$ gauge symmetry breaking and the subsequently occurred EW symmetry breaking. The $U(1)_\chi$ gauge symmetry breaking is caused by the one-loop CW potential for $U(1)_\chi$ sector, which is given by

$$V_\Phi(\phi) = \frac{1}{4}\lambda_\Phi(M)\phi^4 + \frac{1}{8}\tilde{\beta}_{\lambda_\Phi}(M)\phi^4 \left(\ln\frac{\phi^2}{M^2} - \frac{25}{6}\right) , \tag{3.4}$$

where $\tilde{\beta}_{\lambda_\Phi} \equiv \beta_{\lambda_\Phi} - \lambda_\Phi \gamma_{\lambda_\Phi}$ (γ_{λ_Φ} is the anomalous dimension of Φ). Using Eq. (A.13), the CW potential is approximately given by

$$V_\Phi(\phi) \simeq \frac{1}{4}\lambda_\Phi(M)\phi^4 + \frac{1}{8\pi^2}\left(6g_\chi^4(M) - {\rm tr}Y_M^4(M)\right)\phi^4 \left(\ln\frac{\phi^2}{M^2} - \frac{25}{6}\right) , \tag{3.5}$$

around $\phi = M$ [14], where we have taken $\Phi = \phi/\sqrt{2}$ in the unitary gauge. We assume that the Majorana Yukawa couplings of the right-handed neutrinos are diagonal as $Y_M^{ij} = y_{M_i}\delta_{ij}$. In the following analyses, we will take ${\rm tr}Y_M^4 = \sum y_{M_i}^4 = N_\nu y_M^4$ for simplicity, where N_ν stands for the number of large Majorana Yukawa couplings that are enough to

be effective in the RGE. Equation (3.5) satisfies the following renormalization conditions

$$\left.\frac{\partial^2 V_\Phi}{\partial\phi^2}\right|_{\phi=0} = 0\,, \qquad \left.\frac{\partial^4 V_\Phi}{\partial\phi^4}\right|_{\phi=M} = 6\lambda_\Phi\,. \tag{3.6}$$

Due to the one-loop corrections, ϕ can obtain a nonzero VEV $\langle\phi\rangle = v_\Phi$, and we choose the renormalization scale at $M = v_\Phi$ to avoid large logarithmic corrections, which have an uncertainty in large $\ln(\phi^2/v_\Phi^2)$ region. The stationary condition of the potential (3.5) induces

$$\lambda_\Phi(v_\Phi) = \frac{11}{6\pi^2}\left(6g_\chi^4(v_\Phi) - N_\nu y_M^4(v_\Phi)\right)\,. \tag{3.7}$$

When this relation is satisfied, the $U(1)_\chi$ gauge symmetry is broken.

Once ϕ obtains the nonzero VEV, the singlet scalar boson , the Z' boson, and the right-handed neutrinos become massive as

$$M_\phi = \sqrt{\frac{6}{11}\lambda_\Phi(v_\Phi)}v_\Phi\,, \qquad M_{Z'} = 2g_\chi(v_\Phi)v_\Phi\,, \qquad M_N = \sqrt{2}y_M(v_\Phi)v_\Phi\,, \tag{3.8}$$

respectively. To realize the CW mechanism successfully, logarithmic terms of the potential (3.5) should be effective compared to the first term. Thus, $\lambda_\Phi(v_\Phi)$ should be much smaller than $g_\chi(v_\Phi)$ and $y_M(v_\Phi)$, and the mass hierarchy $M_\phi \ll M_{Z'}$, M_N is expected. As will be shown later, the typical value of M_ϕ is a few GeV, and then the singlet scalar field does not decouple at the EW scale, while the Z' boson and the right-handed neutrinos decouple. From Eq. (3.7), the masses are approximately written by

$$M_\phi^2 \approx \beta_{\lambda_\Phi}(v_\Phi)v_\Phi^2 > 0\,, \qquad \frac{M_{Z'}}{M_N} \approx \left(\frac{2N_\nu}{3}\right)^{1/4}\,. \tag{3.9}$$

When the approximation is valid, $\beta_{\lambda_\Phi}(v_\Phi) > 0$ is required, since the physical scalar mass must be real. On the other hand, since we have imposed $\lambda_\Phi(M_{\rm Pl}) = 0$, $\beta_{\lambda_\Phi}(M_{\rm Pl}) \leq 0$ should be satisfied to avoid $\lambda_\Phi < 0$, which might cause the vacuum instability. Therefore, RG evolution of λ_Φ is typically curved upward in the flatland scenario.

Condition of the curved upward λ_Φ is given by an analysis of one-loop β functions, which are given in App. A.2, as [55]

$$K = \frac{41x_H^2 + 32x_H + 27}{3(2+N_\nu)}\sqrt{\frac{N_\nu}{6}} < 1\,, \tag{3.10}$$

which is shown in Fig. 3.1. In our case, i.e., the $U(1)_\chi$ model, the values of K are

$$K = (0.9417,\ 0.9988,\ 0.9786) \quad \text{for } N_\nu = (1,\ 2,\ 3)\,, \tag{3.11}$$

respectively. Thus, in the $U(1)_\chi$ model, the flatland scenario can work for any $N_\nu = 1$–3. However, in the $U(1)_R$ and $U(1)_{B-L}$ models, the flatland scenario cannot work because of

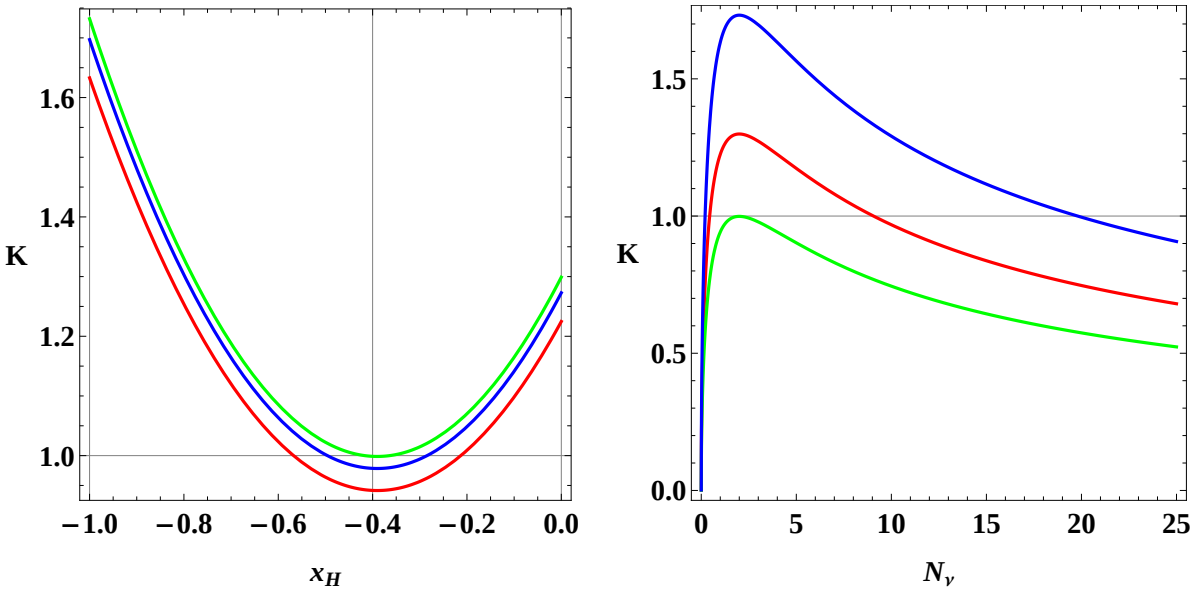

Figure 3.1: x_H (left) and N_ν (right) dependences of K. *Left*: The red, green and blue lines correspond to $N_\nu = 1$, 2 and 3, respectively. The vertical lines denote $x_H = 0$, $-2/5$ and -1. *Right*: The red, green and blue lines correspond to $x_H = 0$, $-2/5$ and -1, respectively.

$K > 1$ for $N_\nu < 10$ and 20, respectively. For $N_\nu = 0$, λ_Φ becomes negative in any energy scale below the Planck scale, because β_{λ_Φ} almost depends on the gauge quartic terms [see Eq. (A.13)]. Thus, the flatland scenario cannot work for $N_\nu = 0$.

Here, we comment on RG evolution of λ_Φ in $N_\nu = 2$ case, in which the value of K is almost equal to 1. It means that the terms $48g_\chi^4 - 8N_\nu y_M^4$ in β_{λ_Φ}, Eq. (A.13), almost vanish. Then, two-loop order terms of β_{λ_Φ} are comparable to one-loop order terms, and β_{λ_Φ} becomes negative in all energy scale. Thus, the RG evolution of λ_Φ monotonically and very slowly decreases from the EW scale to the Planck scale [see Fig. 3.2 (b)], which is a quite different situation from the typically expected flatland scenario. It is worth noting that the CW mechanism can also work in $N_\nu = 2$ case, since the stationary condition (3.7) can be satisfied at $\mu = v_\Phi$.

After the $U(1)_\chi$ gauge symmetry breaking, the scalar mixing term becomes Higgs mass term as

$$m_H^2(v_\Phi) = \frac{1}{2}\lambda_{\rm mix}(v_\Phi)v_\Phi^2\,, \tag{3.12}$$

and the tree-level Higgs potential at $\mu = v_\Phi$ is given by

$$V_H(H) = \lambda_H(v_\Phi)(H^\dagger H)^2 + m_H^2(v_\Phi)(H^\dagger H)\,, \tag{3.13}$$

which is the same form as the SM case. To obtain the observed Higgs mass, we have to

calculate the RGE of the Higgs mass parameter, which is given by

$$\mu\frac{dm_H^2}{d\mu} = \frac{1}{16\pi^2}\left[m_H^2\left(12\lambda_H + 6y_t^2 - \frac{9}{2}g_2^2 - \frac{3}{2}g_Y^2 - \frac{3}{2}\left(g_{\rm mix} - \frac{4}{5}g_\chi\right)^2\right) + 2\lambda_{\rm mix}M_\phi^2\right], \tag{3.14}$$

for $\mu < v_\Phi$. From Eq. (3.8), the last term in Eq. (3.14) is of the order of $\lambda_\Phi m_H^2$, and then it is negligible because of $\lambda_\Phi \ll 1$. In other word, $\lambda_{\rm mix} \sim (v_H/v_\Phi)^2$ is required to realize the EW scale of m_H^2, and then it is small enough to be neglected. After the Z' boson decouples, the terms including $g_{\rm mix}$ and/or g_χ are omitted from Eq. (3.14). However, the effects can be numerically neglected, since they are sufficiently small compared to other contributions in Eq. (3.14).

From the stationary condition of the Higgs potential, the VEV of the Higgs field is given by

$$v_H = \sqrt{\frac{-m_H^2(v_H)}{\lambda_H(v_H)}}, \tag{3.15}$$

where m_H^2 must be negative to realize the electroweak symmetry breaking. Note that $\lambda_{\rm mix}$, or m_H^2, naturally becomes negative in the flatland scenario. This is because $\beta_{\lambda_{\rm mix}}$ almost depends on the gauge quartic terms, and is always positive [see Eq. (A.14)]. Then, the Higgs mass is given by

$$M_h^2 = 2\lambda_H(v_H)v_H^2 + \Delta M_h^2, \tag{3.16}$$

where ΔM_h^2 is the Higgs self-energy correction to the Higgs pole mass [107]. The running of quartic couplings are controlled by the initial values of g_χ and y_M, which are determined to realize $v_H \simeq 246\,\text{GeV}$ and $M_h \simeq 125\,\text{GeV}$. On the other hand, once g_χ or y_M is fixed, the other is uniquely determined by Eq. (3.7). Therefore, there is only one free parameter in the flatland scenario, and the physical quantities are uniquely predicted.[1]

After the EW symmetry breaking, the singlet scalar and the Higgs bosons are mixed by the $\lambda_{\rm mix}$ term. The scalar mass squared matrix is given by

$$\mathcal{M}^2 = \begin{pmatrix} M_h^2 & \frac{1}{2}\lambda_{\rm mix}v_H v_\Phi \\ \frac{1}{2}\lambda_{\rm mix}v_H v_\Phi & M_\phi^2 \end{pmatrix}, \tag{3.17}$$

where M_h and M_ϕ are given by Eqs. (3.16) and (3.8), respectively. Then, the scalar mixing angle θ is expressed by

$$\tan 2\theta = \frac{\lambda_{\rm mix}v_H v_\Phi}{M_h^2 - M_\phi^2}. \tag{3.18}$$

[1]Actually, there are more degrees of freedom for the Majorana Yukawa coupling matrix Y_M^{ij}, but we have taken $\text{tr}[Y_M^{ij}] = N_\nu y_M$ for simplicity.

Since the flatland scenario expects $\lambda_\Phi \ll |\lambda_{\rm mix}| \ll \lambda_H$ at a low energy scale, the lighter mass eigenvalue is approximately given by

$$\begin{aligned} M_{\phi'}^2 &= \frac{1}{2}\left[\left(2\lambda_H v_H^2 + \frac{6}{11}\lambda_\Phi v_\Phi^2\right) - \left(2\lambda_H v_H^2 - \frac{6}{11}\lambda_\Phi v_\Phi^2\right)\sqrt{1+\tan^2 2\theta}\right] \\ &\approx M_\phi^2 - \frac{\lambda_{\rm mix}^2 v_H^2 v_\Phi^2}{4\left(M_h^2 - M_\phi^2\right)} . \end{aligned} \tag{3.19}$$

It would be negative for a large $|\lambda_{\rm mix}|$. We will discuss the positive definiteness of the scalar mass squared eigenvalues in the next section.

In the same way, the $U(1)$ gauge bosons are mixed by the $g_{\rm mix}$ term. It is potentially dangerous, because the ρ-parameter deviates from unity at the tree level. The mass term of the Z and Z' bosons are given by

$$\mathcal{L}_Z = \frac{1}{2}(Z_\mu,\ Z'_\mu) M_{ZZ'}^2 \begin{pmatrix} Z^\mu \\ Z'^\mu \end{pmatrix} , \tag{3.20}$$

with

$$M_{ZZ'}^2 = \begin{pmatrix} M_Z^2 & \delta M^2 \\ \delta M^2 & M_{Z'}^2 + \frac{1}{4}\left(g_{\rm mix} - \frac{4}{5}g_\chi\right)^2 v_H^2 \end{pmatrix} , \tag{3.21}$$

where M_Z is the SM one as $M_Z^2 = (g_Y^2 + g_2^2)v_H^2/4$. The second term of the Z' boson mass is obtained after the EW symmetry breaking, and it is much smaller than $M_{Z'}^2$ because of $v_H \ll v_\Phi$. The mixing term is given by

$$\delta M^2 = \frac{1}{4}\sqrt{g_Y^2 + g_2^2}\left(g_{\rm mix} - \frac{4}{5}g_\chi\right) v_H^2 , \tag{3.22}$$

and the mass matrix is diagonalized by

$$\tan 2\theta_Z = \frac{2\delta M^2}{M_Z^2 - \left(M_{Z'}^2 + \frac{1}{4}\left(g_{\rm mix} - \frac{4}{5}g_\chi\right)^2 v_H^2\right)} . \tag{3.23}$$

After diagonalizing the mass matrix, the lighter mass eigenvalue is approximately obtained by

$$M_1^2 \approx M_Z^2 - \frac{\left(\delta M^2\right)^2}{\left(M_{Z'}^2 + \frac{1}{4}\left(g_{\rm mix} - \frac{4}{5}g_\chi\right)^2 v_H^2\right) - M_Z^2} , \tag{3.24}$$

which is smaller than M_Z^2, and the ρ-parameter deviates from unity. We will also discuss the deviation of the ρ-parameter in the next section.

(a) $N_\nu = 1$ (b) $N_\nu = 2$

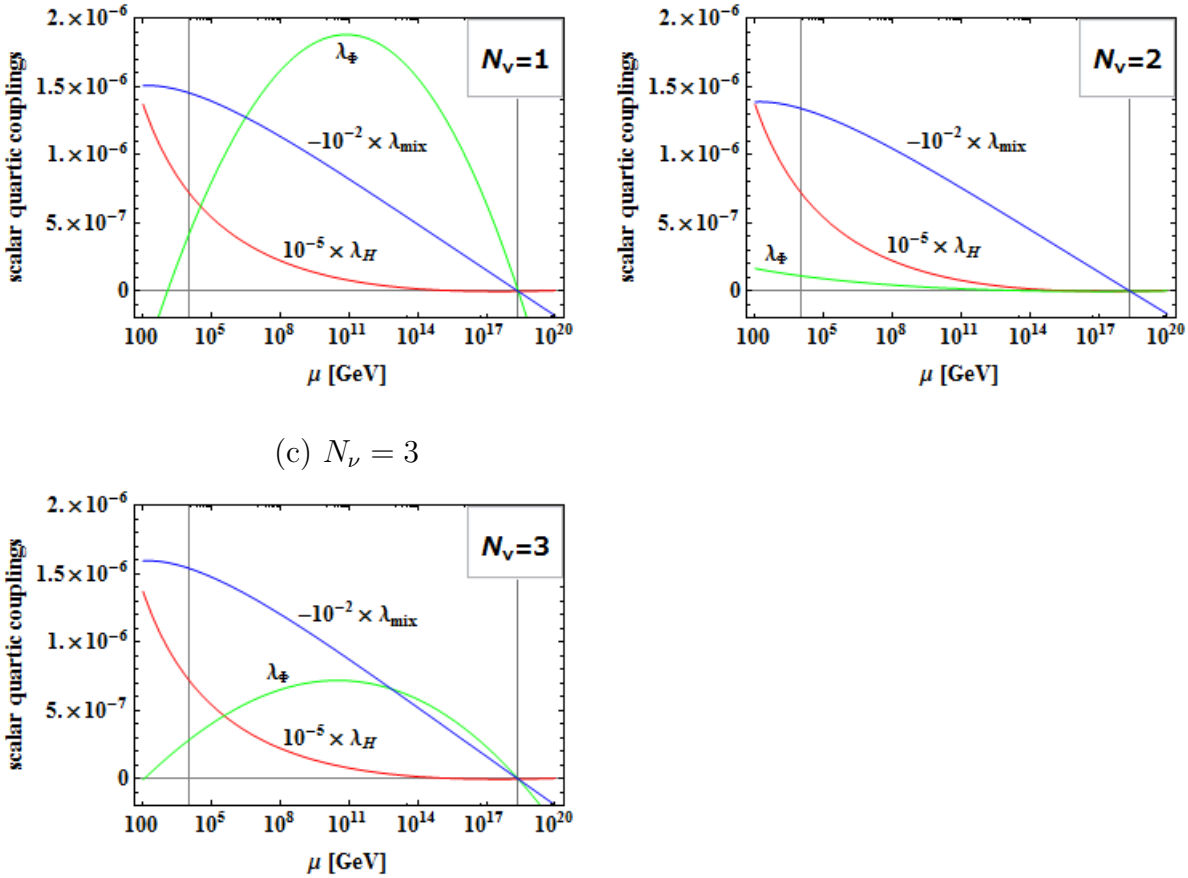

(c) $N_\nu = 3$

Figure 3.2: Example of running quartic couplings for $N_\nu = 1$, 2 and 3. The red, green, and blue lines correspond to $10^{-5} \times \lambda_H$, λ_Φ, and $-10^{-2} \times \lambda_{\rm mix}$, respectively. Two vertical grid lines represent v_Φ and $M_{\rm Pl}$. The decoupling effects of the Z' boson and the right-handed neutrinos are not considered in these figures.

3.2 Constraints from the vacuum stability

We show RG evolutions of the scalar quartic couplings in Fig. 3.2. In all cases, $\lambda_{\rm mix}$ naturally becomes negative to realize the negative Higgs mass term. For $N_\nu = 1$ and 3, the RG evolution of λ_Φ is curved upward, which is the same as the conventional flatland scenario. On the other hand, for $N_\nu = 2$, the behavior of λ_Φ is the quite different from $N_\nu = 1$ and 3 case. The RG evolution of λ_Φ monotonically and slowly decreases from the EW scale to the Planck scale as mentioned above. In all $N_\nu = 1$–3 cases, the Higgs mass of 125 GeV is realized with the top quark mass of 171 GeV, and the $U(1)_\chi$ gauge symmetry is broken at $\mu = v_\Phi \simeq 10$ TeV. The singlet scalar boson, the Z' boson, and the right-handed neutrino become massive for $N_\nu = (1,\ 2,\ 3)$ as $M_\Phi \simeq (5.0,\ 2.7,\ 3.9)$ GeV, $M_{Z'} \simeq (2.0,\ 2.0,\ 2.0)$ TeV, and $M_N \simeq (2.3,\ 1.9,\ 1.7)$ TeV, respectively. The values of ratio $M_{Z'}/M_N$ agree very well with the predicted values from Eq. (3.9). We investigate allowed

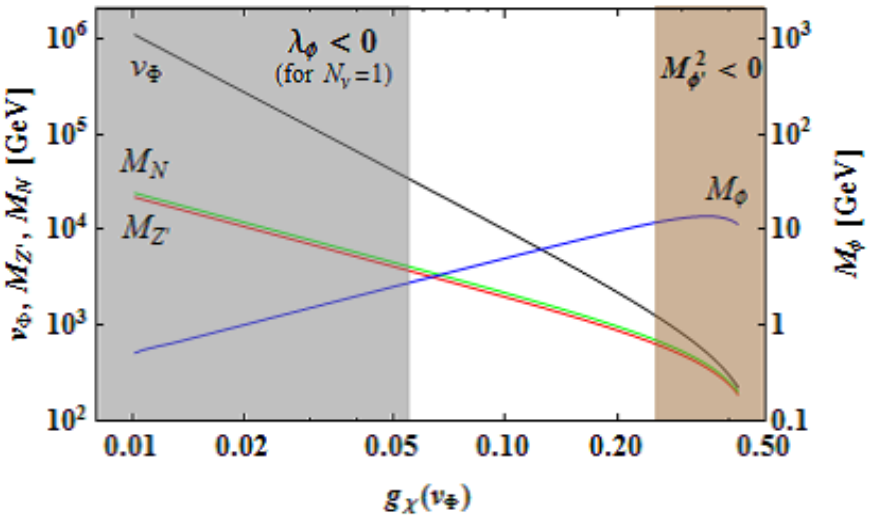

Figure 3.3: $U(1)_\chi$ gauge coupling dependences on the singlet scalar VEV and new particle masses obtained by Eq. (3.8). The left and right shaded regions are excluded by $\lambda_\Phi < 0$ and $M_{\phi'}^2 < 0$ conditions, respectively. This figure shows the $N_\nu = 1$ case, and the left shaded region does not appear in $N_\nu = 2$ and 3 cases.

parameter spaces by the vacuum stability with using two-loop RGEs. Adding the singlet scalar field into the SM, the vacuum stability conditions are given by [108]

$$\lambda_H > 0\,, \qquad \lambda_\Phi > 0\,, \qquad 4\lambda_H\lambda_\Phi - \lambda_{\rm mix}^2 > 0\,. \tag{3.25}$$

These conditions should be satisfied at any energy scale. If all quartic couplings are positive, the potential is obviously bounded from below, and the vacuum is stable. The last condition in Eq. (3.25) determines the upper bound of $|\lambda_{\rm mix}|$, which induces a non-trivial vacuum stability condition for $\lambda_{\rm mix} < 0$.

For our analyses, we take g_χ as a free parameter. Figure 3.3 shows g_χ dependences on other physical quantities. Since $M_{Z'}$ and M_N satisfy Eq. (3.9), they are almost the same values. Although this figure shows the result for $N_\nu = 1$, the predicted physical quantities are almost the same for $N_\nu = 2$ and 3. This is because that all running couplings, except for λ_Φ, are almost the same for any N_ν. The left and right shaded regions correspond to constraints obtained by the vacuum stability conditions and the positive definiteness of the scalar mass squared eigenvalue, respectively. We will explain these constraints below.

First, we consider the Higgs self-coupling λ_H. To realize $\lambda_H > 0$ at all energy scales, the β function of λ_H at the Planck scale should satisfy $\beta_{\lambda_H}(M_{\rm Pl}) \leq 0$ because of $\lambda_H(M_{\rm Pl}) = 0$. In the SM, once $\lambda_H(M_{\rm Pl}) = 0$ and $\beta_{\lambda_H}(M_{\rm Pl}) \leq 0$ is imposed, we can find $M_t \gtrsim 173\,$GeV and $M_h \gtrsim 129\,$GeV [109, 110], while this lower bound of the Higgs mass has been excluded

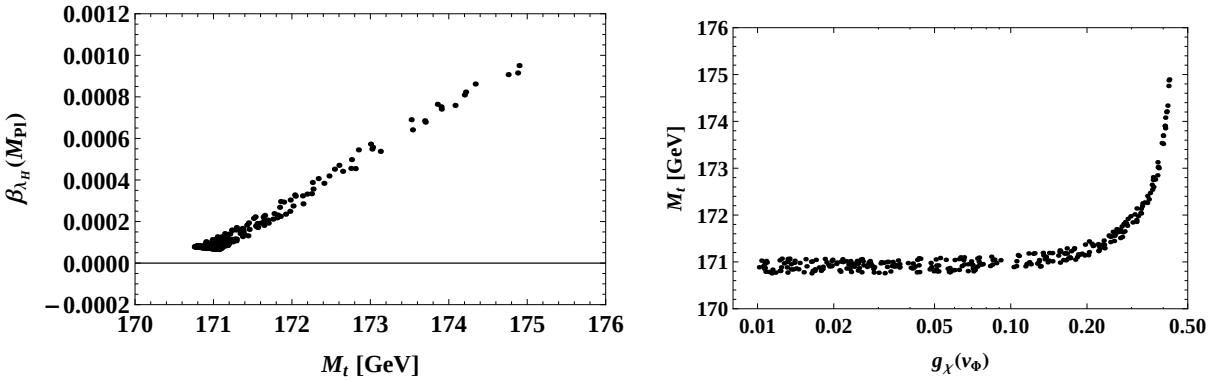

Figure 3.4: *Left*: Relation between the top quark mass and the β function of λ_H at the Planck scale. *Right*: g_χ dependences on the top quark mass. The dots realize the Higgs mass in the range of Eq. (1.1).

by the collider experiments. In the flatland scenario, $\beta_{\lambda_H}(M_{\rm Pl})$ is given by

$$\beta_{\lambda_H}(M_{\rm Pl}) = \frac{1}{(4\pi)^2}\left[-6y_t^4 + \frac{3}{8}\left\{2g_2^4 + \left(g_2^2 + g_Y^2 + \frac{16}{25}g_\chi^2\right)^2\right\}\right] , \tag{3.26}$$

up to the one-loop level. The larger g_χ becomes, the larger top Yukawa coupling y_t (or the top quark mass M_t) is required in order to realize 125 GeV Higgs mass. The left panel of Fig. 3.4 shows a relation between M_t and $\beta_{\lambda_H}(M_{\rm Pl})$, in which the dots realize the Higgs mass in the range of Eq. (1.1). Then, the larger M_t becomes, the larger $\beta_{\lambda_H}(M_{\rm Pl})$ becomes, while the Higgs mass cannot be realized by $M_t \lesssim 171$ GeV. We can find that it is impossible to simultaneously realize both $\beta_{\lambda_H}(M_{\rm Pl}) \leq 0$ (or $\lambda_H > 0$) and $M_h \simeq 125$ GeV.

On the other hand, once one gives up $\lambda_H > 0$ at all energy scales and imposes $\lambda_H(M_{\rm Pl}) = 0$, the observed Higgs boson mass $M_h \simeq 125$ GeV can be realized by $M_t \simeq 171$ GeV in the SM. Although λ_H becomes negative below the Planck scale, the vacuum is meta-stable, which is phenomenologically allowed. The same thing can be said in the flatland scenario unless the RG evolution of λ_H does not drastically change from that in the SM. As g_χ becomes larger, $M_h \simeq 125$ GeV can be realized by larger M_t compared to the SM case, which is shown in the right panel of Fig. 3.4. When we allow $\lambda_H < 0$ as long as the vacuum is meta-stable, $M_h \simeq 125$ GeV can be realized by $g_\chi \simeq 0.4$, which corresponds to the experimentally favored value of the top quark mass, $M_t \simeq 173$ GeV [8]. However, the large g_χ region as $g_\chi \gtrsim 0.2$ is excluded for $N_\nu = 1$ by the positive definiteness of the scalar mass squared eigenvalue as mentioned below.

Next, we consider the singlet scalar self-coupling λ_Φ. In Fig. 3.2 (a), λ_Φ seems to become negative an order of magnitude below $\mu = v_\Phi$. However, in fact, we can find $\lambda_\Phi > 0$ is realized as follows. After the $U(1)_\chi$ symmetry breaking, the Z' boson and the right-handed neutrinos become massive. Since their masses are the same order of magnitude as v_Φ, they would decouple and be integrated out from the theory before λ_Φ

becomes negative. Then, β functions of λ_Φ becomes

$$\beta_{\lambda_\Phi}(\mu < M_{Z'}, M_N) = \frac{1}{(4\pi^2)}\left[20\lambda_\Phi^2 + 2\lambda_{\rm mix}^2\right] , \tag{3.27}$$

up to the one-loop level. It does not include contributions of loop diagrams which have internal lines of the Z' boson and/or the right-handed neutrinos. Since both λ_Φ and $\lambda_{\rm mix}$ are numerically almost equal to zero around v_Φ, i.e., $\beta_{\lambda_\Phi}(\mu < M_{Z'}, M_N) \simeq 0$, it is reasonable to consider $\lambda_\Phi(\mu < M_{Z'}, M_N) \simeq \lambda_\Phi(M_{Z'}) \simeq \lambda_\Phi(M_N)$.[2] Thus, we can find that parameter space of $g_\chi(\simeq y_M) \lesssim 0.055$ is excluded by $\lambda_\Phi(\mu < M_{Z'}, M_N) < 0$, which is shown as the left shaded region in Fig. 3.3. This constraint corresponds to $v_\Phi \lesssim 3.3 \times 10^5\,$GeV, $M_\Phi \gtrsim 2.8\,$GeV, $M_{Z'} \lesssim 3.7\,$TeV, and $M_N \lesssim 4.1\,$TeV, respectively.

However, for $N_\nu = 2$ and 3, the condition of $\lambda_\phi > 0$ does not constrain the model parameter. For $N_\nu = 2$, the RG evolution of λ_Φ monotonically decreases from the EW scale to the Planck scale as shown in Fig. 3.2 (b). Since λ_Φ becomes rather larger at lower energy scale, λ_Φ is positive at all energy scales. Thus, the condition of $\lambda_\phi > 0$ gives no constraint for $N_\nu = 2$. For $N_\nu = 3$, the RG evolution of λ_Φ is similar to that for $N_\nu = 1$, but the gradient of the running is much gentler as in Fig. 3.2 (c). Then, even for $g_\chi \sim 0.01$, the Z' boson and the right-handed neutrinos are decoupled before λ_Φ becomes negative. Therefore, the small g_χ region is almost not constrained for $N_\nu = 3$.

Next, we consider the mixing coupling between the scalar fields $\lambda_{\rm mix}$. The vacuum stability requires $4\lambda_H\lambda_\Phi - \lambda_{\rm mix}^2 > 0$, which excludes the large mixing coupling. When both λ_H and λ_Φ are positive, the inequality is almost always satisfied because of $\lambda_H \gg |\lambda_{\rm mix}|$. On the other hand, the inequality cannot be satisfied when either λ_H or λ_Φ is negative. Then, the condition $4\lambda_H\lambda_\Phi - \lambda_{\rm mix}^2 > 0$ is almost the same as the condition $\lambda_H > 0$. Note that $4\lambda_H\lambda_\Phi - \lambda_{\rm mix}^2 > 0$ cannot be satisfied at all energy scales, since λ_H should be negative below the Planck scale in order to realize the Higgs mass of 125 GeV as mentioned above.

However, $\lambda_{\rm mix}$ is also constrained by the positive definiteness of the scalar mass squared eigenvalue. The lighter scalar mass squared $M_{\phi'}^2$ given by Eq. (3.19) would be negative for a sufficiently large $|\lambda_{\rm mix}|$. The left panel of Fig. 3.5 shows that $M_{\phi'}^2$ becomes negative for large g_χ region, which corresponds to large scalar mixing as shown in the right panel. Since the RG evolution of $\lambda_{\rm mix}$ is almost the same for any $N_\nu = 1$–3, the relation between g_χ and $\lambda_{\rm mix}$ is also the same. Thus, the positive definiteness of the scalar mass squared eigenvalue induces that large g_χ regions are excluded as $g_\chi \gtrsim 0.25$, 0.16, and 0.23 for $N_\nu = 1$, 2, and 3, respectively. For $N_\nu = 1$, it is shown as the right shaded region in Fig. 3.3. This constraint corresponds to $v_\Phi \gtrsim 1.3\,$TeV, $M_\phi \lesssim 12\,$GeV, $M_{Z'} \gtrsim 650\,$GeV, and $M_N \gtrsim 720\,$GeV, respectively. Therefore, the physical quantities are constrained

[2]Here, we have considered the tree-level matching condition, that is, the running couplings have no gaps at $\mu = M_{Z'}$ and $\mu = M_N$.

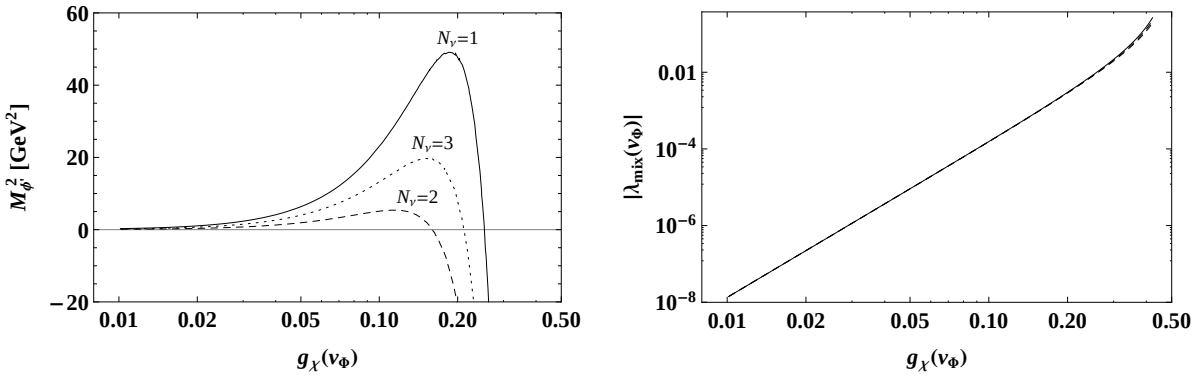

Figure 3.5: g_χ dependences on the lighter scalar mass squared eigenvalue (left) and the scalar mixing coupling (right). The solid, dashed, and dotted lines correspond to $N_\nu = 1$, 2, and 3, respectively.

	$N_\nu = 1$	$N_\nu = 2$	$N_\nu = 3$
g_χ	$0.055 \lesssim g_\chi \lesssim 0.25$	$g_\chi \lesssim 0.16$	$g_\chi \lesssim 0.23$
v_Φ	$1.3\,\text{TeV} \lesssim v_\Phi \lesssim 3.3 \times 10^5\,\text{GeV}$	$3.8\,\text{TeV} \lesssim v_\Phi$	$2.0\,\text{TeV} \lesssim v_\Phi$
M_ϕ	$2.8\,\text{GeV} \lesssim M_\phi \lesssim 12\,\text{GeV}$	$M_\phi \lesssim 4.2\,\text{GeV}$	$M_\phi \lesssim 7.7\,\text{GeV}$
$M_{Z'}$	$650\,\text{GeV} \lesssim M_{Z'} \lesssim 3.7\,\text{TeV}$	$1.2\,\text{TeV} \lesssim M_{Z'}$	$860\,\text{GeV} \lesssim M_{Z'}$
M_N	$720\,\text{GeV} \lesssim M_N \lesssim 4.1\,\text{TeV}$	$1.1\,\text{TeV} \lesssim M_N$	$720\,\text{GeV} \lesssim M_N$

Table 3.2: Allowed parameter regions for the physical quantities.

from both above and below for $N_\nu = 1$. The allowed parameter spaces for the physical quantities are summarized in Table 3.2. Actually, the ATLAS and CMS experiments have obtained larger lower bounds for $M_{Z'}$ than those as in Table 3.2 as mentioned below.

3.3 Experimental bounds

In this section, we mention the experimental bounds. When there is the gauge mixing between the Z and Z' bosons at the EW scale, it is dangerous since the ρ-parameter deviates from unity at the tree level. Let us estimate the deviation of the ρ-parameter [55]. The tree-level ρ-parameter is defined by $\rho_0 = M_W^2/(M_1^2 \cos^2\theta_W)$, which deviates from unity for $M_1 \neq M_Z$. The deviation of the ρ-parameter $\delta\rho \equiv \rho_0 - 1$ is always positive because of $M_1 \leq M_Z$. From Eq. (3.24), $\delta\rho$ is approximately given by

$$\begin{aligned}\delta\rho &= \frac{2M_Z^2}{M_Z^2 + M_{Z'}^2 + (M_Z^2 - M_{Z'}^2)\sqrt{1+\tan^2 2\theta_Z}} - 1 \\ &\approx \frac{v_H^2}{4\left[\left(M_{Z'}^2 + \frac{1}{4}\left(g_{\rm mix} - \frac{4}{5}g_\chi\right)^2 v_H^2\right) - M_Z^2\right]}\left(g_{\rm mix} - \frac{4}{5}g_\chi\right)^2 , \end{aligned} \tag{3.28}$$

which is proportional to $\tan 2\theta_Z$. Thus, $\delta\rho$ vanishes in the limit of $\tan 2\theta_Z \to 0$, which is necessarily required.

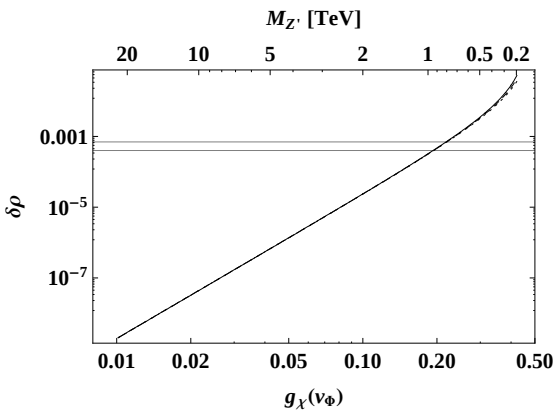

Figure 3.6: g_χ and $M_{Z'}$ dependence on $\delta\rho$. The solid, dashed, and dotted lines correspond to $N_\nu = 1$, 2, and 3, respectively. The lower and upper horizontal lines show the central value and the upper bound at 1σ, respectively.

Figure 3.6 shows g_χ (or $M_{Z'}$) dependence on $\delta\rho$, where the two horizontal lines correspond to the experimental bounds at 1σ, $\rho_0 = 1.0004^{+0.0003}_{-0.0004}$ [9]. We can see that $\delta\rho$ is almost independent of N_ν, since N_ν does not change the β functions of gauge couplings up to one-loop level. As g_χ becomes larger, or equivalently $M_{Z'}$ becomes lower, $\delta\rho$ becomes larger. The central value of ρ_0 and its upper bound at 1σ give $g_\chi \simeq 0.19$ and $g_\chi \lesssim 0.21$, or equivalently $M_{Z'} \simeq 950\,\text{GeV}$ and $M_{Z'} \gtrsim 820\,\text{GeV}$, respectively. Thus, $M_{Z'}$ should be heaver than 820 GeV.

Next, we mention Z' boson mass bounds obtained by the collider experiments. Currently, the strongest mass bounds on Z' boson has been obtained by the LHC experiments. (Experimental bounds below this sentence had been obtained by 22/04/2015. We will note the more recent results in the last of this chapter.) The most recent results are based on search for heavy neutral gauge boson decaying to e^+e^- or $\mu^+\mu^-$ pairs. The ATLAS obtains the exclusion limits at 95% C.L. as $M_{Z'} > 2.24\,\text{TeV}$ for the $U(1)_\chi$ model [111]. It has used the center-of-mass energy $\sqrt{s} = 8\,\text{TeV}$ pp collision data set collected in 2012 corresponding to an integrated luminosity of approximately 5.9 (e^+e^-) / 6.1 $(\mu^+\mu^-)$ fb^{-1}. Similarly, the CMS obtains the exclusion limits at 95% C.L. as $M_{Z'} > 2.59\,\text{TeV}$ for the sequential standard model with the SM-like couplings [112]. It has used the $\sqrt{s} = 8\,\text{TeV}$ pp collision data set and $\sqrt{s} = 7\,\text{TeV}$ dataset collected by the CMS experiment in 2011 corresponding to an integrated luminosities of up to $4.1\,\text{fb}^{-1}$.

In addition, other constraint is obtained by measurements of $e^+e^- \to f\bar{f}$, where f denotes various SM fermions, above the Z-pole at the LEP-II experiment. When $M_{Z'}$ is larger than the largest collider energy of the LEP-II, which is of about 209 GeV, one can effectively perform an expansion in $s/M_{Z'}^2$ for four fermion interactions. Then, effective four fermion interactions have been constrained by the LEP-II results. Since interaction amplitudes mediating the Z' boson are proportional to $g_{Z'}^2/M_{Z'}^2$, the experimental

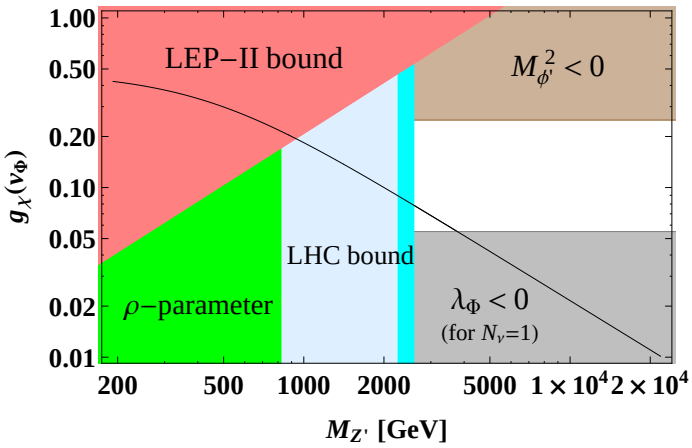

Figure 3.7: All the constraints on $M_{Z'}$ and g_χ. The black line corresponds to the flatland prediction for $N_\nu = 1$. The shaded regions show constraints obtained by Sections. 3.2 and 3.3.

bound has been obtained as the ratio $M_{Z'}/g_{Z'}$, where $g_{Z'}$ is a flavor independent Z' gauge coupling. Using the single channel estimation, the lower bound can be obtained as $M_{Z'}/g_\chi \gtrsim 3.8\,\text{TeV}$ for the $U(1)_\chi$ model [113]. In the recent parameter fitting analysis, the lower bound $M_{Z'}/g_\chi \geq 4.8\,\text{TeV}$ has been obtained at 99% C.L. [114].

We summarize all the constraints mentioned above in Fig. 3.7. In the flatland scenario, the physical quantities are uniquely determined once one free parameter is fixed. The relation between $M_{Z'}$ and g_χ are given by the black solid line. The shaded regions show constraints obtained by Sections. 3.2 and 3.3. The constraint from $\lambda_\Phi < 0$ is obtained only in $N_\nu = 1$ case, while $\lambda_\Phi < 0$ gives no constraint in $N_\nu = 2$ and 3 cases. Thus, the constraints for $N_\nu = 2$ and 3 are the same one obtained by the LHC experiments as $2.24\ (2.59)\,\text{TeV} \lesssim M_{Z'}$, where the lower bound corresponds to the ATLAS (CMS) result. On the other hand, we can find that the Z' boson mass for $N_\nu = 1$ is tightly restricted as $2.24\ (2.59)\,\text{TeV} \lesssim M_{Z'} \lesssim 3.7\,\text{TeV}$, where the upper bound is obtained by the condition of $\lambda_\Phi > 0$.

3.4 Conclusion and more recent experimental bound

We have studied the classically scale invariant model to naturally explain the origin of the Higgs mass parameter. In this chapter, we have considered $U(1)_\chi$ gauge extension with vanishing the scalar potential at the Planck scale, which is the so-called the flatland scenario. The $U(1)_\chi$ gauge symmetry is broken by the CW mechanism, and the EW symmetry is subsequently broken. When the CW mechanism successfully works as well as realizing $M_h \simeq 125\,\text{GeV}$ and $v_H \simeq 246\,\text{GeV}$, the physical quantities are uniquely determined once one free parameter is fixed.

We have investigated the vacuum stability with using the two-loop RGEs, and found that it is impossible to realize $M_h \simeq 125\,\mathrm{GeV}$ while keeping $\lambda_H > 0$, which is the same situation as in the SM. For $\lambda_\Phi > 0$, we have obtained interesting results. When the number of relevant Majorana Yukawa couplings of the right-handed neutrinos is one, i.e., $N_\nu = 1$, the lower bound of the $U(1)_\chi$ gauge coupling has been obtained by considering the decoupling effects of the Z' boson and the right-handed neutrinos. However, the condition $\lambda_\phi > 0$ does not constrain in $N_\nu = 2$ and 3 cases.

In addition, we have checked the positive definiteness of the scalar mass squared eigenvalue. The large g_χ generates the large scalar mixing, and it would make the lighter mass squared eigenvalue become negative, which induces the upper bound of g_χ. Combining the vacuum stability and the positive definiteness of the scalar mass squared eigenvalue, we have found the allowed parameter spaces for the physical quantities as in Table 3.2.

At the end of the last section, we have mentioned the experimental bounds on $M_{Z'}$, and obtained the constraints as in Fig. 3.7. In particular, the Z' boson mass for $N_\nu = 1$ is tightly restricted as $2.24\ (2.59)\,\mathrm{TeV} \lesssim M_{Z'} \lesssim 3.7\,\mathrm{TeV}$, where the lower bound corresponds to the ATLAS (CMS) result.

However, these lower bounds are not the latest data. The most recent data are collected at the LHC $\sqrt{s} = 13\,\mathrm{TeV}$ experiments in 2015 and 2016. The ATLAS experiment gives $M_{Z'} > 3.66\,\mathrm{GeV}$ for the $U(1)_\chi$ model [115], while the CMS experiment does not give the explicit bound for the $U(1)_\chi$ model.[3] Therefore, for $N_\nu = 1$, almost all parameter space have been excluded, and can be checked all parameter space near future. This fact suggests that two or three right-handed neutrinos should be degenerate in the flatland scenario, in which the baryon asymmetry of the Universe can be explained by resonant leptogenesis [117] [see Refs. [118, 119] for the $U(1)$ gauge extended model].

[3]For the sequential standard model, the ATLAS and the CMS experiments give $M_{Z'} > 4.05\,\mathrm{GeV}$ [115] and $4.0\,\mathrm{GeV}$ [116], respectively. Since these bounds are usually stronger than that of the $U(1)_\chi$ model, we do not apply these bounds.

Chapter 4

$U(1)$ gauge extended model II

In the previous chapter, we have considered the $U(1)$ gauge extended model. The model can naturally explain the origin of the Higgs mass parameter, but does not have a DM candidate. In this chapter, we extend the model to construct more phenomenologically complete theory, in which the gauge coupling unification (GCU) and the DM relic abundance can be realized by additional vector-like fermions. Unlike the previous model, the more extended model has the UV cutoff at the GCU scale, and we does not require the flatland scenario. This chapter is based on our work [71].

4.1 Extension with vector-like fermions

In addition to the $U(1)_X$ gauge extension, which we have explained in the previous chapter, we introduce three vector-like fermions ($Q_{L,R}$, $D_{L,R}$ and $N_{L,R}$), and real SM singlet scalar field (S). Charge assignments of the additional fields are shown in Table 4.1. The vector-like fermions $Q_{L,R}$, $D_{L,R}$, and $N_{L,R}$, respectively, have the same charges as the quark doublet, the down-quark singlet, and the right-handed neutrino, while only these vector-like fermions are odd under an additional Z_2 symmetry. The SM-gauge charged fermions ($Q_{L,R}$ and $D_{L,R}$) play a role for achieving the GCU [121, 122], and the SM-gauge singlet fermions ($N_{L,R}$) can become a DM candidate, whose stability is guaranteed by the Z_2 symmetry. These field contents are not an unique selection for the realization of the GCU and the DM relic abundance. We choose them for the simplest extension.[1]

The relevant Lagrangian is given by

$$\begin{aligned}\mathcal{L} = \mathcal{L}_{\rm SM} + \mathcal{L}_{\rm kin} - V(H,\Phi,S) - \big(&Y_\nu \overline{\ell_L}\tilde{H}\nu_R + \kappa_1 \overline{Q_L} H D_R + \kappa_2 \overline{D_L} H^* Q_R \\ &+ Y_M \Phi \overline{\nu_R^c}\nu_R + Y_{N_L}\Phi^* \overline{N_L} N_L^c + Y_{N_R}\Phi \overline{N_R^c} N_R \\ &+ f_Q S \overline{Q_L} Q_R + f_D S \overline{D_L} D_R + f_N S \overline{N_L} N_R + \text{h.c.}\big)\,, \end{aligned} \tag{4.1}$$

[1]The GCU can be achieved by other extra fields, but other extensions cause more degree of freedom [110]. Thus, our selection is the most economical.

	$SU(3)_C \times SU(2)_L \times U(1)_Y$	$U(1)_X$	Z_2
$Q_{L,R}$	$(\mathbf{3},\, \mathbf{2},\, 1/3)$	$(x_H+1)/3$	$-$
$D_{L,R}$	$(\mathbf{3},\, \mathbf{1},\, -2/3)$	$(-2x_H+1)/3$	$-$
$N_{L,R}$	$(\mathbf{1},\, \mathbf{1},\, 0)$	-1	$-$
S	$(\mathbf{1},\, \mathbf{1},\, 0)$	0	$+$

Table 4.1: Charge assignments of the additional fields.

where $\mathcal{L}_{\rm SM}$ is the SM Lagrangian except for the Higgs sector, $\mathcal{L}_{\rm kin}$ is kinetic terms of all fields, and $V(H,\Phi,S)$ is a scalar potential of the model. Without the Z_2 symmetry, there are additional Yukawa interactions between the SM fields and the new fields, e.g., $y_1\overline{Q_L}\tilde{H}u_R$, $y_2\overline{Q_L}Hd_R$, $y_3\overline{q_L}HD_R$, and so on. However, these coupling constants have to be very small due to constraints from the precision EW data [123]. To forbid these terms, we have imposed odd parity to only the vector-like fermions under the Z_2 symmetry.

In this model, we impose the classically scale invariance at the GCU scale, not the Planck scale. The scalar potential $V(H,\Phi,S)$ is given by

$$\begin{aligned} V(H,\Phi,S) = {} & \lambda_H(H^\dagger H)^2 + \lambda_\Phi(\Phi^\dagger\Phi)^2 + \lambda_S S^4 \\ & + \lambda_{H\Phi}(H^\dagger H)(\Phi^\dagger\Phi) + \lambda_{HS}(H^\dagger H)S^2 + \lambda_{\Phi S}(\Phi^\dagger\Phi)S^2\,, \end{aligned} \tag{4.2}$$

where there is no dimensionful parameter. As same as before, the CW mechanism can work for the complex scalar field Φ, and the $U(1)_X$ gauge symmetry is spontaneously broken by nonzero VEV of Φ. Then, the singlet scalar ϕ, the Z' boson, the right-handed neutrinos ν_R, and the vector-like fermion $N_{L,R}$ become massive. After the $U(1)_X$ gauge symmetry breaking, negative mass terms of real scalar singlet S and Higgs doublet H are generated, which induces the EW symmetry breaking. Then, the singlet scalar S, the vector-like fermions and the SM particles become massive, and typically their masses are lighter than those obtained by the $U(1)_X$ gauge symmetry breaking.

Let us explain the symmetry breaking mechanism more explicitly. As same as before, we consider the CW potential for Φ (3.4) as

$$V_\Phi(\phi) \simeq \frac{1}{4}\lambda_\Phi(v_\Phi)\,\phi^4 + \frac{1}{8\pi^2}\Big[6g_X^4 - \big({\rm tr}Y_M^4 + Y_{N_L}^4 + Y_{N_R}^4\big)\Big](v_\Phi)\,\phi^4\left(\ln\frac{\phi^2}{v_\Phi^2} - \frac{25}{6}\right)\,, \tag{4.3}$$

where there are additional terms of $Y_{N_{L,R}}$ compared with Eq. (3.5). The β function of Φ almost depends on quartic terms of g_X, Y_M and $Y_{N_{L,R}}$ for $\lambda_\Phi \simeq 0$. [β functions of the model parameters are given in App. A.4.] The CW potential (4.3) satisfies the renormalization conditions (3.6), and its stationary condition induces

$$\lambda_\Phi(v_\Phi) \simeq \frac{11}{6\pi^2}\Big[6g_X^4(v_\Phi) - \big({\rm tr}Y_M^4(v_\Phi) + Y_{N_L}^4(v_\Phi) + Y_{N_R}^4(v_\Phi)\big)\Big]\,, \tag{4.4}$$

where we have assumed that scalar quartic couplings are negligibly small in the right-hand side. When this relation is satisfied, the $U(1)_X$ gauge symmetry is broken. Since the right-hand side of Eq. (4.4) should be positive to avoid $M_\phi^2 < 0$, the quartic terms of Majorana Yukawa couplings (Y_M and $Y_{N_{L,R}}$) should be smaller than the quartic terms of g_X, and the relation $\lambda_\Phi(v_\Phi) \lesssim g_X^4(v_\Phi)$ is required. Thus, $M_\phi < M_{Z'}$ is generally expected, which are given by Eq. (3.8). For the right-handed neutrinos, there is an additional contribution from the VEV of S. We will discuss the neutrino masses in Sec. 4.2.3.

After the $U(1)_X$ gauge symmetry breaking, the effective potentials for H and S are approximately given by

$$V_H(H) = \lambda_H (H^\dagger H)^2 + m_H^2 (H^\dagger H) \qquad \text{with} \qquad m_H^2(v_\Phi) = \frac{1}{2}\lambda_{H\Phi}(v_\Phi) v_\Phi^2 \,, \tag{4.5}$$

$$V_S(S) = \lambda_S S^4 + m_S^2 S^2 \qquad \text{with} \qquad m_S^2(v_\Phi) = \frac{1}{2}\lambda_{\Phi S}(v_\Phi) v_\Phi^2 \,, \tag{4.6}$$

where we have assumed that λ_{HS} are negligibly small compared to $\lambda_{H\Phi}$ and $\lambda_{\Phi S}$. It is worth noting that, for $\kappa_{1,2} \simeq 0$, λ_{HS} is always negligibly small during the RG evolution [see Eq. (A.31)]. When $\lambda_{H\Phi}$ and $\lambda_{\Phi S}$ are negative H and S obtain the nonzero VEVs. In the unitary gauge, where $S = s/\sqrt{2}$ and $H = (0,\ h/\sqrt{2})^T$, the nonzero VEVs, $\langle s \rangle = v_S$ and $\langle h \rangle = v_H$, are obtained as

$$v_H = \sqrt{\frac{-m_H^2}{\lambda_H}} \qquad \text{and} \qquad v_S = \sqrt{\frac{-m_S^2}{\lambda_S}} \,, \tag{4.7}$$

respectively. Note that v_H and v_S are typically lower than v_Φ, because the ratios of quartic couplings, $\lambda_{\Phi S}/(2\lambda_S)$ and $\lambda_{H\Phi}/(2\lambda_H)$ should be lower than unity to avoid the vacuum instability. Then, the vector-like fermions and the SM particles become massive, while the masses of $Q_{L,R}$ and $D_{L,R}$ have to be lower than 1 TeV to realize the GCU as we will show in Sec. 4.2.1.

In the end of this section, we mention the $U(1)_X$ breaking scale v_Φ. For the $U(1)_{B-L}$ case ($x_H = 0$), $M_{Z'}/g_X > 6.9\,\text{TeV}$ is required from the LEP-II experiments [113, 124], which leads the lower bound of $v_\Phi \gtrsim 3.5\,\text{TeV}$. On the other hand, v_Φ should be not so large to avoid the hierarchy problem. A major correction to the Higgs mass is given by Z' intermediating diagrams, and one-loop and two-loop corrections are approximately given by

$$\delta m_H^2 \sim \frac{4 x_H^2 g_X^4 v_\Phi^2}{16\pi^2} \quad \text{for } x_H \neq 0 \,, \tag{4.8}$$

$$\delta m_H^2 \sim \frac{4(x_H+1)(4x_H+1)}{9} \frac{y_t^2 g_X^4 v_\Phi^2}{(16\pi^2)^2} \,, \tag{4.9}$$

respectively. When we require $\delta m_H^2 < M_h^2/2$, Eqs. (4.8) and (4.9) lead the upper bound

on v_Φ as

$$v_\Phi \lesssim \frac{1}{|x_H|}\left(\frac{0.1}{g_X}\right)^2 \times 10^5\,\text{GeV for } x_H \neq 0\,, \tag{4.10}$$

$$v_\Phi \lesssim \left(\frac{0.1}{g_X}\right)^2 \times 10^6\,\text{GeV}\,, \tag{4.11}$$

where we have taken $y_t \approx 1$. For $|x_H| < 0.1$, the two-loop correction gives stronger bound than that of the one-loop correction. In the following, we use the stronger bound for a fixed x_H. Note that the mass correction from Φ is always negligible because of the small mixing coupling $\lambda_{H\Phi}$.

4.2 Phenomenological and cosmological aspects

In this section, we will discuss phenomenological and cosmological aspects of the model: the GCU, vacuum stability and triviality, smallness of active neutrino masses, baryon asymmetry of the Universe, and dark matter. We will also restrict the model parameters from the naturalness of the Higgs mass.

4.2.1 Gauge coupling unification

First, we discuss the possibility of the GCU at a high energy scale. Since four additional vector-like fermions ($Q_{L,R}$ and $D_{L,R}$) have gauge charges under the SM-gauge groups as shown in Table 4.1, β functions of the SM-gauge couplings change, which are given by

$$\beta_{g_Y} = \frac{g_Y^3}{16\pi^2}\frac{15}{2}\,, \qquad \beta_{g_2} = \frac{g_2^3}{16\pi^2}\frac{-7}{6}\,, \qquad \beta_{g_3} = \frac{g_3^3}{16\pi^2}(-5)\,, \tag{4.12}$$

at 1-loop level. Figure 4.1 shows RG evolutions of gauge couplings $\alpha_i^{-1} \equiv 4\pi/g_i^2$, where $U(1)_Y$ gauge coupling has been normalized as $g_1 \equiv \sqrt{5/3}g_Y$. The calculation has been done for $x_H = 0$ with using 2-loop RGEs. We note that the β functions of gauge couplings are almost independent of x_H. In Fig. 4.1, the red, green, and blue lines show α_1^{-1}, α_2^{-1}, and α_3^{-1}, respectively. The dashed and solid lines correspond to the SM and our model, respectively. The left vertical line stands for a typical mass scale of vector-like fermions, which has been taken as $M_V = 800\,\text{GeV}$. For $\mu < M_V$, the β functions are the same as the SM ones, and we have taken boundary conditions for the gauge couplings such that experimental values of the Weinberg angle, the fine structure constant and the strong coupling can be reproduced [109]. The GCU can be achieved at $\Lambda_{\text{GCU}} = (2\text{–}4)\times 10^{16}\,\text{GeV}$, and the unified gauge coupling is $\alpha_{\text{GCU}}^{-1} = (35.4\text{–}35.8)$. This is the same result as shown in Ref. [121], in which only $Q_{L,R}$ and $D_{L,R}$ are added into the SM.

As the vector-like fermion masses become larger, the precision of the GCU becomes worse. Thus, the masses of $Q_{L,R}$ and $D_{L,R}$ should be lighter than 1 TeV. The lower bounds

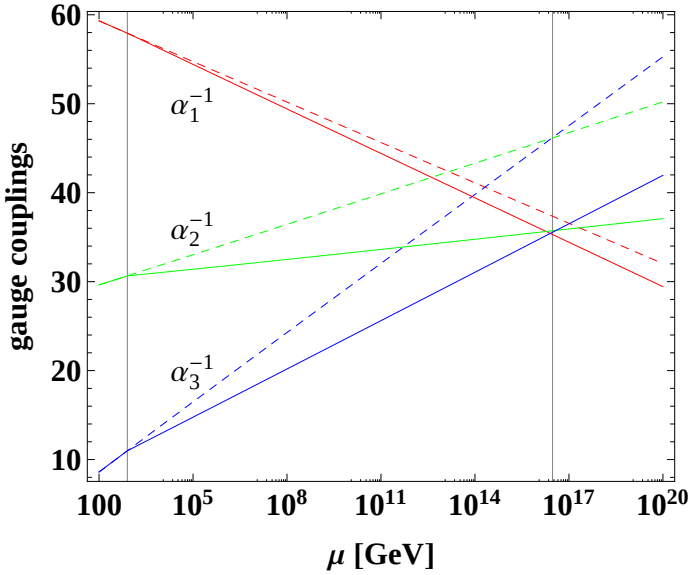

Figure 4.1: RG evolutions of gauge couplings α_i^{-1}. The dashed and solid lines correspond to the SM and our model, respectively. The vertical lines express $M_V = 800\,\mathrm{GeV}$ and $\Lambda_{\mathrm{GCU}} = 3 \times 10^{16}\,\mathrm{GeV}$.

of vector-like quarks are obtained by the LHC Run I results as $M_V \gtrsim 700$–$900\,\mathrm{GeV}$, which depend on decay modes of the vector-like quarks [125, 126, 127]. Thus, the possibility of the GCU may be testable at the future experiments. Note, however, that $Q_{L,R}$ and $D_{L,R}$ does not decay into the SM quarks due to the Z_2 symmetry. In this case, the above constraints cannot directly apply to our model, and other analyses are needed.

We mention that the proton lifetime. Above the GCU scale, we expect our model is embedded in some GUT model, e.g. $SU(5) \times U(1)_X$ or $SO(10)$. Then, the proton can decay into the lighter particles, and its lifetime is roughly derived from a four-fermion approximation for the decay channel $p \to e^+ + \pi^0$, which is given by

$$\tau_{\mathrm{p}} \sim \left(\alpha_{\mathrm{GCU}}^{-1}\right)^2 \frac{\Lambda_{\mathrm{GCU}}^4}{m_{\mathrm{p}}^5}\,, \tag{4.13}$$

where m_{p} is the proton mass. For $\Lambda_{\mathrm{GCU}} = 3 \times 10^{16}\,\mathrm{GeV}$ and $\alpha_{\mathrm{GCU}}^{-1} = 35.6$, we can estimate the lifetime as $\tau_{\mathrm{p}} \sim 10^{37}$ yrs, which is much longer than the experimental lower bound $\tau_{\mathrm{p}} > 8.2 \times 10^{33}$ yrs [9]. Thus, the model are free from the constraint on the proton decay.

4.2.2 Vacuum stability and triviality

Next, we discuss the vacuum stability. However, it is difficult to investigate exact vacuum stability conditions, since there are three scalar fields and each of them has nonzero VEV. Therefore, we simply investigate three necessary conditions: $\lambda_H > 0$, $\lambda_\Phi > 0$ and $\lambda_S > 0$.

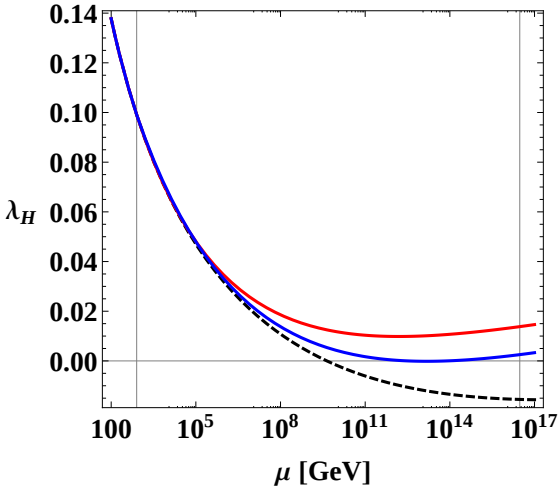

Figure 4.2: RG evolution of λ_H in the $U(1)_{B-L}$ ($x_H = 0$) case. The red and blue lines correspond to $\kappa = 0$ and $\kappa = 0.33$, respectively. The black dashed line shows the RG evolution of λ_H in the SM. The vertical lines express $M_V = 800\,\text{GeV}$ and $\Lambda_{\text{GCU}} = 3 \times 10^{16}\,\text{GeV}$.

The condition $\lambda_H > 0$ depends on additional contributions to β_{λ_H}, i.e., $\kappa_{1,2}$, g_X and scalar mixing couplings.[2] Since $Q_{L,R}$ and $D_{L,R}$ are charged under the SM gauge group, the SM-gauge couplings are larger than the SM case. Then, if the additional contributions to β_{λ_H} are negligible, λ_H becomes always positive. On the other hand, the EW vacuum does not stable for $\kappa \gtrsim 0.33$ in the $U(1)_{B-L}$ ($x_H = 0$) case, where β_{λ_H} is independent of g_X up to the one-loop level. We show the RG evolution of λ_H for $x_H = 0$ in Fig. 4.2. The red and blue lines correspond to $\kappa = 0$ and $\kappa = 0.33$, respectively. The black dashed line shows RG evolution of λ_H in the SM. Thus, $\kappa < 0.33$ is required to realize the vacuum stability.

Higgs mass corrections from $Q_{L,R}$ and $D_{L,R}$ are approximately given by

$$\delta m_H^2 \sim \frac{v_S^2}{16\pi^2}\left[(\kappa_1^2+\kappa_2^2)(f_Q^2+f_D^2)+2\kappa_1\kappa_2 f_Q f_D\right] \sim \frac{12\kappa^2 M_V^2}{16\pi^2}\,, \tag{4.14}$$

where we have taken $\kappa = \kappa_1 = \kappa_2$ in the last equality, which naturally arises from $L \leftrightarrow R$ symmetry for the vector-like fields. For simplicity, we have taken $M_V = M_Q = M_D$ ($M_Q = f_Q v_S/\sqrt{2}$ and $M_D = f_D v_S/\sqrt{2}$). Then, the naturalness condition $\delta m_H^2 < M_h^2/2$ requires $\kappa < 0.3$ for $M_V \simeq 1\,\text{TeV}$. Since the vacuum stability condition is given by $\kappa < 0.33$, the naturalness condition guarantees the vacuum stability. Note that $\kappa \simeq 0$ guarantees $\lambda_{HS} \simeq 0$ at all energy scale, which is required to justify our potential analysis for Eq. (4.6).

[2]RG evolution of λ_H also depends on mass (or Yukawa coupling) of the top quark. We will use the central value of world average, i.e., $M_t = 173.34\,\text{GeV}$ [8]. If we change this value of top quark mass, the following numerical results can slightly change.

Due to the coupling κ, vector-like fermions $Q_{L,R}$ and $D_{L,R}$ give the mass as κv_H, and the S and T parameters deviate from the SM case ($S = T = 0$). The deviations are approximately given by [128, 129]

$$S \approx \frac{43}{30\pi}\left(\frac{\kappa v_H}{M_V}\right)^2, \qquad T \approx \frac{3(\kappa v_H)^2}{10\pi \sin^2\theta_W M_W^2}\left(\frac{\kappa v_H}{M_V}\right)^2. \tag{4.15}$$

For $M_V \simeq 1\,\mathrm{GeV}$ and $\kappa < 0.3$, these values are estimated as $S < 2.5 \times 10^{-3}$ and $T < 1.9 \times 10^{-3}$, which are consistent with the precision EW data $S = 0.00 \pm 0.08$ and $T = 0.05 \pm 0.07$ [9].

The condition $\lambda_\Phi > 0$ is almost always satisfied when g_X is dominant in the right-hand side of Eq. (4.4), i.e., $\lambda_\Phi(v_\Phi) \sim g_X^4(v_\Phi) > 0$. In this case, β_{λ_Φ} is positive up to the GCU scale, and then $\lambda_\Phi(\mu)$ is larger than $\lambda_\Phi(v_\Phi)0$ for $v_\Phi < \mu < \Lambda_{\mathrm{GCU}}$. It is also possible to realize $\lambda_\Phi(\Lambda_{\mathrm{GCU}}) = 0$ as well as $\lambda_\Phi(\mu) \geq 0$, where the running of λ_Φ is curved upward as in the flatland scenario [47, 53, 55, 64]. Then, both g_X and Majorana Yukawa couplings are dominant in β_{λ_Φ}, while λ_Φ is much smaller than them.

When λ_S is negligible in its β function, solution of its RGE is approximately given by

$$\lambda_S(\mu) \approx \lambda_S(v_S) - \frac{1}{16\pi^2}\left(6f_Q^4(v_S) + 3f_D^4(v_S) + f_N^4(v_S)\right)\ln\frac{\mu^2}{v_S^2}, \tag{4.16}$$

[see Eq. (A.29)]. Once v_S is fixed, f_Q and f_D are determined to realize the GCU, while f_N remains a free parameter. To find the condition of $\lambda_S > 0$, we assume $f_N = f_Q = f_D$ at $\mu = v_S$ for simplicity. Then, we can find that λ_S is positive up to the GCU scale for $\lambda_S(v_S) \gtrsim 0.01$. This lower bound of $\lambda_S(v_S)$ is almost unchanged for different values of v_S, because v_S dependence is logarithmic.

On the other hand, when λ_S is dominant in β_{λ_S}, the Landau pole would arise, at which the theory is not valid from the viewpoint of perturbativity (triviality). The energy scale where the Landau pole appears is approximately estimated by

$$\Lambda_{\mathrm{LP}} = v_S \exp\left[\frac{4\pi^2 v_S^2}{9M_s^2}\right], \tag{4.17}$$

where $M_s = \sqrt{2\lambda_S(v_S)}v_S$ is a mass of the real singlet scalar field. Figure 4.3 shows v_S dependence on the upper (red) and lower (blue) bonds of M_s, which correspond to the Landau pole and vacuum stability conditions, respectively. Since the both bounds are almost proportional to v_S, allowed values of $\lambda_S(v_S)$ are almost unchanged for different v_S. We can find the strong constraint for λ_S as $0.01 \lesssim \lambda_S(v_S) \lesssim 0.05$.

In the same way, the Landau pole also exists when $g_X(v_\Phi)$ is sufficiently large. The energy scale where the Landau pole appears is approximately estimated by the one-loop RGE of g_X [see Eq. (A.16)] as

$$\Lambda_{\mathrm{LP}} = v_\Phi \exp\left[\frac{32\pi^2 v_\Phi^2}{(44/3 + 64/3x_H + 30x_H^2)M_{Z'}^2}\right], \tag{4.18}$$

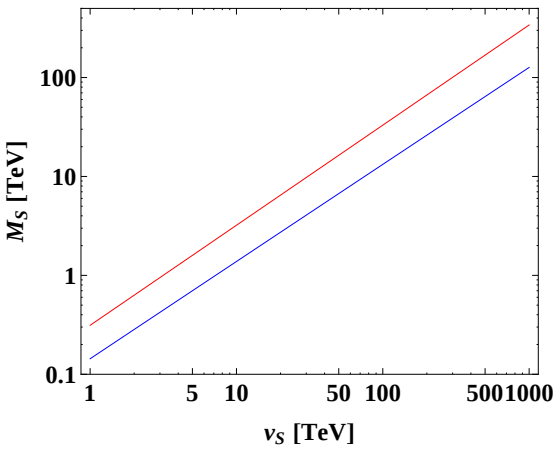

Figure 4.3: v_S dependence on the upper (red) and lower (blue) bounds of M_s, which correspond to the Landau pole and vacuum stability conditions, respectively. For the Landau pole bound, we have taken $\Lambda_{\rm LP} = \Lambda_{\rm GCU} = 3 \times 10^{16}$ GeV in Eq. (4.17).

where $M_{Z'}$ is given in Eq. (3.8). Figure 4.4 shows the upper bound of $M_{Z'}$ for fixed v_Φ, which depends on x_H. The solid lines show the maximal value of $M_{Z'}$ allowed in the model, which has been calculated by Eq. (4.18) with $\Lambda_{\rm LP} = \Lambda_{\rm GCU} = 3 \times 10^{16}$ GeV. Note that peak of the solid lines at $x_H = -16/45$ corresponds to the orthogonal basis of two $U(1)$ gauges. The dashed lines show the naturalness bound estimated by Eqs. (4.10) and (4.11). The red, green, and blue colors correspond to $v_\Phi = 10$, 100, and 1000 TeV, respectively. The shaded region ($M_{Z'} < 2.6$ TeV) is excluded by the LHC experiments [130, 131].[3]

When we define the triviality bound as $\Lambda_{\rm GCU} < \Lambda_{\rm LP}$, it prohibits the regions above the solid lines. One can see that these bounds lead $g_X(v_\Phi) \lesssim 0.5$ from Eq. (3.8), which is almost independent of v_Φ. Since the naturalness requires the stronger constraints than the triviality bound in almost all parameter space, we can say that the naturalness guarantees no Landau pole below the GCU scale. Note that the both bounds are almost the same for $v_\Phi = 10$ TeV, and they exclude $M_{Z'} > 10$ TeV.

4.2.3 Neutrino masses and baryon asymmetry of the universe

In the following, we discuss neutrino sector. From the Lagrangian (4.1), the neutrino mass matrix is given by

$$\begin{pmatrix} 0 & m_D & 0 & 0 \\ m_D^T & M_M & 0 & 0 \\ 0 & 0 & M_{N_L} & m_N \\ 0 & 0 & m_N & M_{N_R} \end{pmatrix}, \tag{4.19}$$

[3]In the recent LHC experiment at $\sqrt{s} = 13$ TeV, the strongest lower bounds are $M_{Z'} > 4.05$ TeV and 4.0 GeV given by the ATLAS [115] and the CMS [116], respectively.

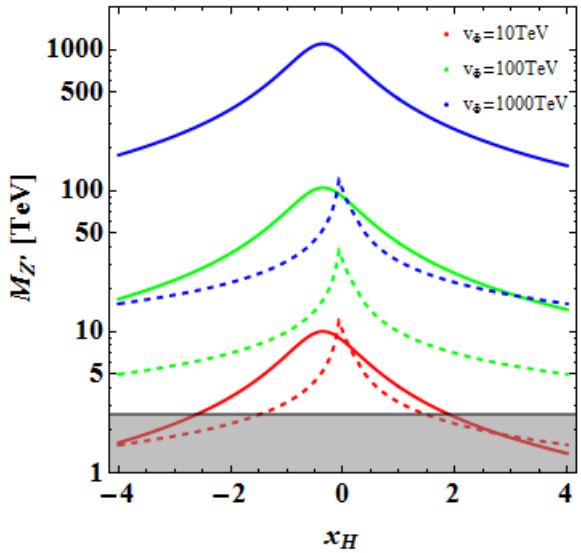

Figure 4.4: The upper bound of $M_{Z'}$ for fixed v_Φ, which depends on x_H. The solid and dashed lines show the Landau pole (4.18) and the naturalness (Eqs. (4.10) and (4.11)) bounds, respectively. For the Landau pole bound, we have taken $\Lambda_{\rm LP} = \Lambda_{\rm GCU} = 3 \times 10^{16}\,$GeV in Eq. (4.18). The shaded region ($M_{Z'} < 2.6\,$TeV) is excluded by the LHC experiments.

in the basis of $(\nu_L^i,\, \nu_R^{ic},\, N_L,\, N_R^c)^T$, where right-handed neutrino is $\nu_R = \nu_R^i = (\nu_R^1,\, \nu_R^2,\, \nu_R^3)$. The matrix components are expressed by $m_D = Y_\nu v_H/\sqrt{2}$, $M_M = Y_M v_\Phi/\sqrt{2}$, $M_{N_{L,R}} = Y_{N_{L,R}} v_\Phi/\sqrt{2}$, and $m_N = f_N v_S/\sqrt{2}$. Since there is no mixing term between $\nu_{L,R}$ and $N_{L,R}$ due to the Z_2 symmetry, the active neutrino masses can be obtained by the usual type-I seesaw mechanism [105], i.e., $m_\nu \approx m_D M_M^{-1} m_D^T$. The heavier mass eigenvalue is nearly equal to M_M, and we impose the upper bound on it from the naturalness of the Higgs mass. Neutrino one-loop diagram contributes the Higgs mass as

$$\delta m_H^2 \sim \frac{Y_\nu^2 Y_M^2 v_\Phi^2}{16\pi^2} \sim \frac{m_\nu M_M^3}{16\pi^2 v_H^2}\,, \tag{4.20}$$

where we have used the seesaw relation. For $m_\nu \sim 0.1\,$eV, the naturalness requires $M_M < 10^7\,$GeV.

Let us mention the baryon asymmetry of the Universe. In the normal thermal leptogenesis [132], there is a lower bound on the right-handed neutrino mass as $M_M \gtrsim 10^9\,$GeV [133]. However, the resonant leptogenesis can work even at the TeV scale, where two right-handed neutrino masses are well-degenerated [117]. In our model, additional $U(1)_X$ gauge interactions make the right-handed neutrinos be in thermal equilibrium with the SM particles [118]. A large efficiency factor can be easily obtained, and the sufficient baryon asymmetry of the Universe can be generated by the right-handed neutrinos with a few TeV masses. Since the neutrino Yukawa coupling Y_N and Y_M almost do not depend on other phenomenological problems which we discuss, our model can explain the baryon

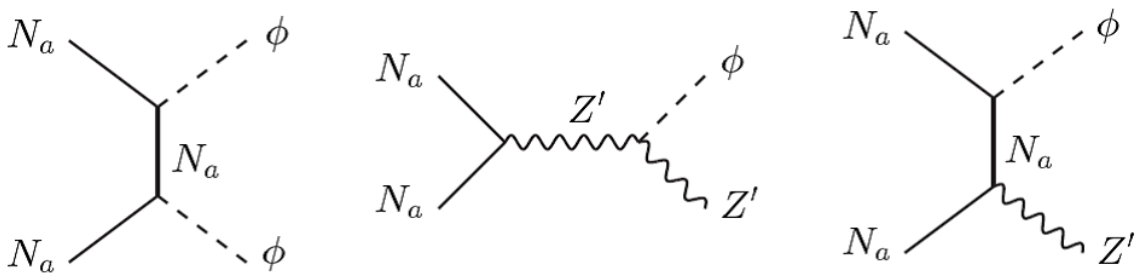

Figure 4.5: Annihilation processes of the dark matter N_a $(a = 1, 2)$.

asymmetry as shown in Ref. [118]. The detail analysis is beyond the scope of this thesis.

For the vector-like neutrinos $(N_{L,R})$, we consider $M_N = M_{N_L} = M_{N_R}$, which naturally arises from $L \leftrightarrow R$ symmetry for the vector-like fermions. Then, the mass eigenvalues are respectively $M_{N_1} = |M_N - m_N|$ and $M_{N_2} = |M_N + m_N|$ for $N_1 = (N_L^c - N_R)/\sqrt{2}$ and $N_2 = (N_L^c + N_R)/\sqrt{2}$. The lighter mass eigenstate N_1 can be a DM candidate, because its stability is guaranteed by the Z_2 symmetry. In the limit of $m_N \to 0$, N_1 and N_2 are degenerate as $M_{N_1} = M_{N_2}$, and N_2 is also effective for a calculation of the DM relic abundance. In the next subsection, we will investigate the degenerate DM case.

In our model, the $U(1)_X$ gauge symmetry breaking is successfully achieved via the CW mechanism. It requires $\lambda_\Phi(v_\Phi) > 0$ in Eq. (4.4), that is,

$$N_\nu M_M^4 + 2M_N^4 < \frac{3}{32} M_{Z'}^4 \,, \tag{4.21}$$

where N_ν is a relevant number of right-handed neutrinos, which is defined as $\mathrm{tr} M_M^4 = N_\nu M_M^4$. Thus, the Majorana masses must be lighter than the Z' boson mass. We have made sure that this constraint is always satisfied when $N_{1,2}$ explain the DM relic abundance.

4.2.4 Dark matter

To calculate the DM relic abundance, we use the same formula for the DM annihilation cross sections as in Ref. [59], where new vector-like fermion is only $N_{L,R}$ (or $N_{1,2}$), and the SM fermions do not have $U(1)_X$ charges. The annihilation processes are t-channel $N_a N_a \to \phi\phi$, t-channel $N_a N_a \to Z'\phi$, and Z' mediating s-channel $N_a N_a \to Z'\phi$. The corresponding diagrams are shown in Fig. 4.5. Although our model has other contributions to the annihilation cross sections, they are all negligible in the following setup. We consider the degenerate DM case, in which there is no vector-like mass term of $N_{L,R}$, i.e., $f_N = 0$. Thus, t-channel $N_a N_a \to ss$ process and s mediating s-channel $N_a N_a \to \nu_R \nu_R$ process does not occur at tree level. From Eq. (4.21), the relation $(2M_N)^2 < M_{Z'}^2$ is always required. Then, the annihilation cross section $\sigma(N_a N_a \to Z'^* \to f\bar{f})$, where f denotes

$U(1)_X$ charged fermions, is suppressed by $1/M_{Z'}^2$. As a result, we can use the same formula for the DM annihilation cross sections as in Ref. [59].

The spin independent cross section for the direct detection is almost dominated by t-channel exchange of scalars h and ϕ. However, our model has an additional contribution due to Z' exchange diagrams, which is given by [134]

$$\sigma_{\rm SI} = \frac{m_{\rm n}^2 M_N^2}{\pi(m_{\rm n}+M_N)^2}\frac{g_X^4}{M_{Z'}^4} = 7.75\times 10^{-42}\left(\frac{\mu_n}{1\,{\rm GeV}}\right)^2\left(\frac{1\,{\rm TeV}}{v_\Phi}\right)^4 {\rm cm}^2\,, \tag{4.22}$$

where $m_{\rm n}$ is the nucleon mass, and $\mu_n = m_n M_N/(m_n + M_N)$ is the reduced nucleon mass. For the DM with the masses of 100 GeV and 1 TeV, the small v_Φ regions such as $v_\Phi < 11\,{\rm TeV}$ and $v_\Phi < 6\,{\rm TeV}$ are excluded by the first results of the LUX experiment, respectively [135].[4] These bounds are stronger than the LEP bound, which has excluded $v_\Phi < 3.5\,{\rm TeV}$.

In the following, we concentrate on the $U(1)_{B-L}$ ($x_H = 0$) case. There are six new parameters in the model: the $U(1)_{B-L}$ gauge coupling g_X, the two Majorana Yukawa coupling Y_{N_L}, Y_{N_R}, the two quartic couplings λ_Φ and $\lambda_{H\Phi}$, and the VEV of the complex scalar field v_Φ. On the other hand, there are two conditions $Y_{N_L} = Y_{N_R} (\equiv Y_N)$ and Eq. (4.7), and we require that N_a explains the DM relic abundance $\Omega_{\rm DM}h^2 = 0.1188 \pm 0.0010$ (68% CL) [138]. Thus, we have three free parameters for the DM analysis.

Figure 4.6 shows scatter plots in (M_N, $M_{Z'}$) plane (left) and (M_ϕ, $M_{Z'}$) plane (right), which realize the DM relic abundance $\Omega_{\rm DM}h^2 = 0.1187$, and satisfy all constraints as discussed above as well as the LUX bound. (For the reference, we also show scatter plots in other parameter planes in Fig. 4.7.) The parameter space starts from the initial values $M_\phi = 100\,{\rm GeV}$, $M_N = 100\,{\rm GeV}$, and $M_{Z'} = 2.6\,{\rm TeV}$. Although both panels in Fig. 4.6 are very similar, $M_N > M_\phi$ is always satisfied. The region of $M_{Z'} < 2.6\,{\rm TeV}$ is excluded by the LHC bound [130, 131].[5] Since $g_X \lesssim 0.5$ is required to avoid the Landau pole, the upper bound on $M_{Z'}$ is given by $M_{Z'} \lesssim v_\Phi$, while, for $M_{N,\phi} \gtrsim 500\,{\rm GeV}$, the upper bound on $M_{Z'}$ is given by the naturalness (4.11). For $200\,{\rm GeV} \lesssim M_{N,\phi} \lesssim 900\,{\rm GeV}$, the lower bound on $M_{Z'}$ is given by the LUX bound. To realize the DM relic abundance, sufficiently large annihilation cross sections are required. This fact induces the lower bound on $M_{Z'}$ for $M_N \gtrsim 900\,{\rm GeV}$. From Fig. 4.6, we can see the upper bound on the DM mass as $M_N \lesssim 2.6\,{\rm TeV}$, and the bound of M_ϕ is almost the same as M_N.

[4] The newest results are reported by the LUX [136] and PandaX-II [137] Collaborations. These bounds are stronger than that in Ref. [135] by about one order magnitude, and the constraints on v_Φ becomes $v_\Phi < 14\,{\rm TeV}$ and $v_\Phi < 8\,{\rm TeV}$ for the DM with the masses of 100 GeV and 1 TeV, respectively.

[5] Actually, the latest results have excluded $M_{Z'} < 3.6\,{\rm TeV}$ for the $U(1)_{B-L}$ model [139].

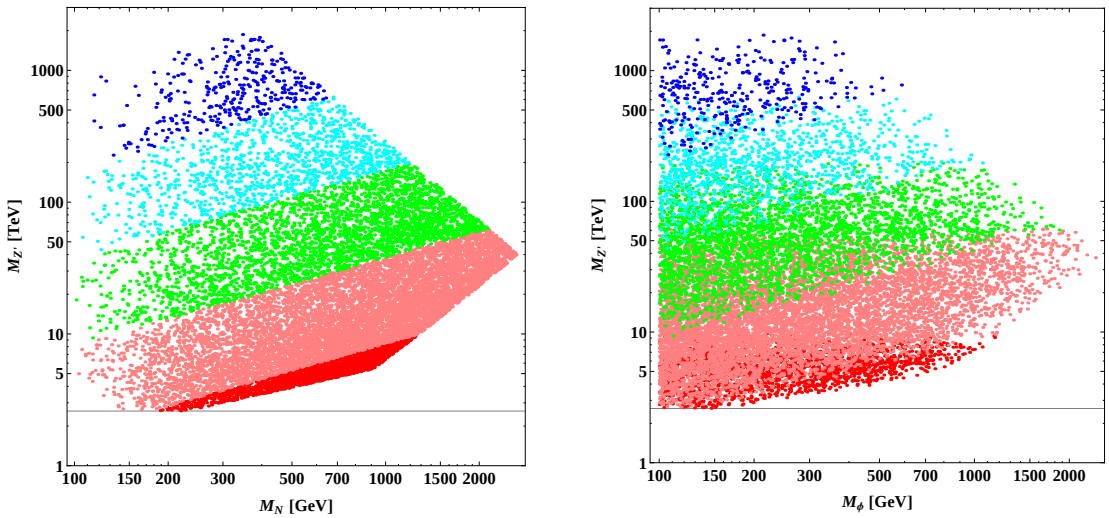

Figure 4.6: Scatter plots in (M_N, $M_{Z'}$) plane (left) and (M_ϕ, $M_{Z'}$) plane (right), which realize the DM relic abundance $\Omega_{\rm DM}h^2 = 0.1187$, and satisfy all constraints as discussed in this paper as well as the LUX bound. The horizontal line shows the lower bound on $M_{Z'}$ by the LHC experiments. The red, pink green, cyan, and blue dots correspond to $6\,\text{TeV} \leq v_\Phi < 10\,\text{TeV}$, $10\,\text{TeV} \leq v_\Phi < 100\,\text{TeV}$, $100\,\text{TeV} \leq v_\Phi < 10^3\,\text{TeV}$, $10^3\,\text{TeV} \leq v_\Phi < 10^4\,\text{TeV}$, $10^4\,\text{TeV} \leq v_\Phi < 10^5\,\text{TeV}$, respectively.

4.3 Conclusion

In the previous chapter, we have constructed the classically scale invariant model with $U(1)_X$ gauge extension. Towards the more phenomenologically appropriate model, we have introduce additional vector-like fermions, which can realize the GCU and the relic abundance of the DM. In this model, the classical scale invariance is given at the GCU scale, and it is violated around the TeV scale by the CW mechanism. The Higgs mass term can be naturally generated through the scalar mixing term as same as before. The GCU can be realized by vector-like fermions $Q_{L,R}$ and $D_{L,R}$, which have the masses lie in $800\,\text{GeV} \lesssim M_V \lesssim 1\,\text{TeV}$. They respectively have the same quantum number as the quark doublet and down-type quark singlet, but distinguished by the additional Z_2 symmetry. The GCU scale is $\Lambda_{\rm GCU} = 3 \times 10^{16}\,\text{GeV}$ with $\alpha_{\rm GCU}^{-1} = 35.6$, and the proton lifetime is estimated as $\tau_{\rm p} \sim 10^{37}$ yrs, which is much longer than the experimental lower bound $\tau_{\rm p} > 8.2 \times 10^{33}$ yrs.

In addition, we have shown that the model can explain the vacuum stability, smallness of active neutrino masses, baryon asymmetry of the Universe, and dark matter relic abundance without inducing large Higgs mass corrections. Since there are additional fermions with the SM-gauge charges, the SM-gauge couplings become larger than the SM case, which leads smaller top Yukawa couplings. Then, the β function of the Higgs self-coupling becomes larger, and hence the EW vacuum becomes stable. The smallness

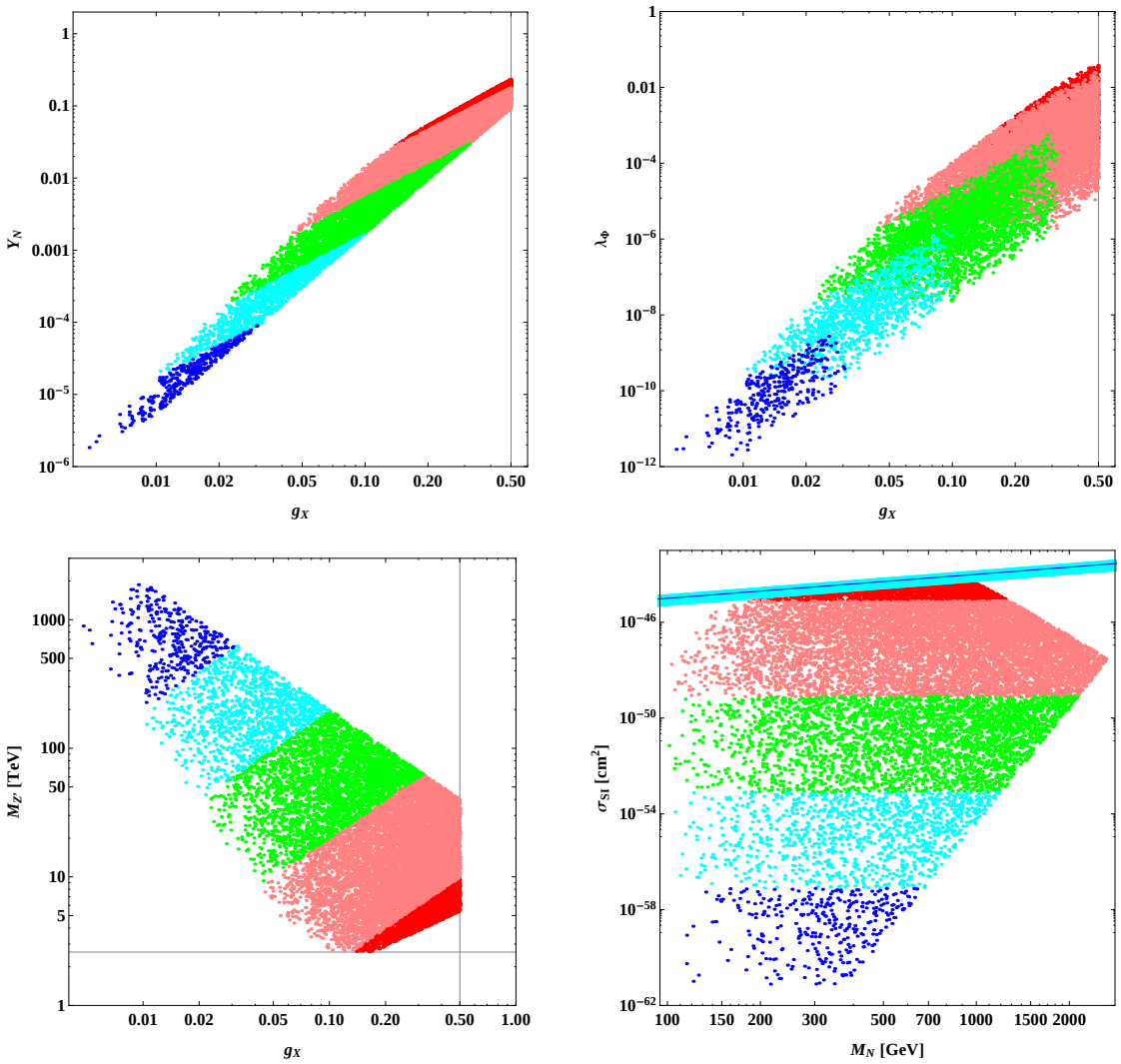

Figure 4.7: Scatter plots in (g_X, Y_N) plane (top-left), (g_X, λ_Φ) plane (top-right), (g_X, $M_{Z'}$) plane (bottom-left) and (M_N, $\sigma_{\rm SI}$) plane (bottom-right). The setup is the same as in Fig. 4.6..

of active neutrino masses and the baryon asymmetry of the Universe can be explained by the right-handed neutrinos via the type-I seesaw mechanism and resonant leptogenesis, respectively. The DM candidate is the SM-gauge singlet fermions $N_{L,R}$ or $N_{1,2}$, and stability of the DM is guaranteed by the additional Z_2 symmetry. We have analyzed the DM relic abundance in the degenerate case ($M_{N_1} = M_{N_2}$), and found the upper bound on the DM mass as $M_N \lesssim 2.6\,\text{TeV}$.

Chapter 5

Bosonic seesaw model I

We suggest the so-called bosonic seesaw mechanism in the context of classically scale invariant extension of the SM with two Higgs doublet fields. The bosonic seesaw mechanism is similar the seesaw mechanism for the neutrinos, and can naturally explain the negativeness of Higgs mass term. This chapter is based on our work [68].

5.1 Bosonic seesaw mechanism with $U(1)_{B-L}$ gauge extension

We consider the classical scale invariance with an additional $U(1)_{B-L}$ gauge symmetry. Unlike the previous models, the model includes two Higgs doublet fields. The particle contents of the model are listed in Table 5.1.[1] We impose the classical scale invariance to the model, under which the scalar potential is given by

$$\begin{aligned} V = &\lambda_1(H_1^\dagger H_1)^2 + \lambda_2(H_2^\dagger H_2)^2 + \lambda_3(H_1^\dagger H_1)(H_2^\dagger H_2) + \lambda_4(H_2^\dagger H_1)(H_1^\dagger H_2) + \lambda_\Phi(\Phi^\dagger\Phi)^2 \\ &+ \lambda_{H_1\Phi}(H_1^\dagger H_1)(\Phi^\dagger\Phi) + \lambda_{H_2\Phi}(H_2^\dagger H_2)(\Phi^\dagger\Phi) + \left(\lambda_{\rm mix}(H_2^\dagger H_1)\Phi^2 + \text{h.c.}\right) , \end{aligned} \tag{5.1}$$

where the last term plays crucial role for the bosonic seesaw mechanism. In this system, the $U(1)_{B-L}$ symmetry can be radiatively broken by the CW mechanism as same as the previous models. The CW potential for Φ (3.4) is approximately given by

$$V_\Phi(\phi) \simeq \frac{1}{4}\lambda_\Phi(v_\Phi)\phi^4 + \frac{1}{8\pi^2}\left(6g_{B-L}^4(v_\Phi) - \text{tr}Y_M^4(v_\Phi)\right)\phi^4\left(\ln\frac{\phi^2}{v_\Phi^2} - \frac{25}{6}\right) , \tag{5.2}$$

which is the same as Eq. (3.5) for $g_\chi \to g_{B-L}$. Then, the stationary condition of V_Φ approximately leads to Eq. (3.7), while we should take $g_\chi \to g_{B-L}$. Through the $U(1)_{B-L}$ symmetry breaking, the mass terms of the two Higgs doublets arise from the mixing terms

[1] The $U(1)_{B-L}$ gauge symmetry can extend an arbitrary one, if $(H_2^\dagger H_1\Phi^2 + \text{h.c.})$ is singlet under the additional $U(1)$ gauge symmetry.

	$SU(3)_C \times SU(2)_L \times U(1)_Y$	$U(1)_{B-L}$
q_L^i	$(\mathbf{3}, \mathbf{2}, 1/3)$	$1/3$
u_R^i	$(\mathbf{3}, \mathbf{1}, 4/3)$	$1/3$
d_R^i	$(\mathbf{3}, \mathbf{1}, -2/3)$	$1/3$
ℓ_L^i	$(\mathbf{1}, \mathbf{2}, -1)$	-1
e_R^i	$(\mathbf{1}, \mathbf{1}, -2)$	-1
ν_R^i	$(\mathbf{1}, \mathbf{1}, 0)$	-1
H_1	$(\mathbf{1}, \mathbf{2}, 1)$	0
H_2	$(\mathbf{1}, \mathbf{2}, 1)$	4
Φ	$(\mathbf{1}, \mathbf{1}, 0)$	2

Table 5.1: Particle contents in our model.

between $H_{1,2}$ and Φ, and the scalar mass squared matrix is read as

$$\begin{aligned} V_{\text{mass}} &= \frac{1}{2}(H_1^\dagger,\ H_2^\dagger) \begin{pmatrix} \lambda_{H_1\Phi} v_\Phi^2 & \lambda_{\text{mix}} v_\Phi^2 \\ \lambda_{\text{mix}} v_\Phi^2 & \lambda_{H_2\Phi} v_\Phi^2 \end{pmatrix} \begin{pmatrix} H_1 \\ H_2 \end{pmatrix} \\ &\approx \frac{1}{2}(H_1'^\dagger,\ H_2'^\dagger) \begin{pmatrix} \lambda_{H_1\Phi} v_\Phi^2 - \frac{\lambda_{\text{mix}}^2}{\lambda_{H_2\Phi}} v_\Phi^2 & 0 \\ 0 & \lambda_{H_2\Phi} v_\Phi^2 \end{pmatrix} \begin{pmatrix} H_1' \\ H_2' \end{pmatrix}, \end{aligned} \tag{5.3}$$

where H_1' and H_2' are mass eigenstates, and we have assumed a hierarchy among the quartic couplings as $0 \leq \lambda_{H_1\Phi} \ll \lambda_{\text{mix}} \ll \lambda_{H_2\Phi}$ at the scale $\mu = v_\Phi$.[2] In the next section, we will show that this hierarchy is dramatically reduced toward high energies in their RG evolutions. Because of this hierarchy, the mass eigenstates H_1' and H_2' are almost composed of H_1 and H_2, respectively. Hence, we approximately identify H_1' with the SM-like Higgs doublet. Note that even though all quartic couplings are positive, the SM-like Higgs doublet obtains a negative mass squared for $\lambda_{H_1\Phi} \ll \lambda_{\text{mix}}^2/\lambda_{H_2\Phi}$, and hence the electroweak symmetry is broken. This is the so-called bosonic seesaw mechanism [140, 141, 142].

In more precise analysis for the electroweak symmetry breaking, we take into account a scalar one-loop diagram through the quartic couplings, λ_3 and λ_4, shown in Fig. 5.1, and the SM-like Higgs doublet mass is given by

$$\begin{aligned} -m_H^2 &\simeq -\frac{\lambda_{H_1\Phi}}{2} v_\Phi^2 + \frac{\lambda_{\text{mix}}^2}{2\lambda_{H_2\Phi}} v_\Phi^2 + \frac{\lambda_{H_2\Phi}}{16\pi^2}(2\lambda_3 + \lambda_4) v_\Phi^2 \\ &\simeq \lambda_{H_2\Phi} v_\Phi^2 \left[\frac{1}{2}\left(\frac{\lambda_{\text{mix}}}{\lambda_{H_2\Phi}}\right)^2 + \frac{2\lambda_3 + \lambda_4}{16\pi^2} \right], \end{aligned} \tag{5.4}$$

where we have omitted the $\lambda_{H_1\Phi}$ term in the second line, and the observed Higgs boson mass $M_h = 125$ GeV is given by $M_h^2 = -2m_H^2$.

In addition to the scalar one-loop diagram, one may consider other Higgs mass corrections coming from a neutrino one-loop diagram and two-loop diagrams mediating the

[2] In our analyses, we will take boundary conditions as $\lambda_1(v_\Phi) = \lambda_2(v_\Phi) = \lambda_H(v_\Phi)$, for simplicity, where λ_H is the Higgs self-coupling in the SM.

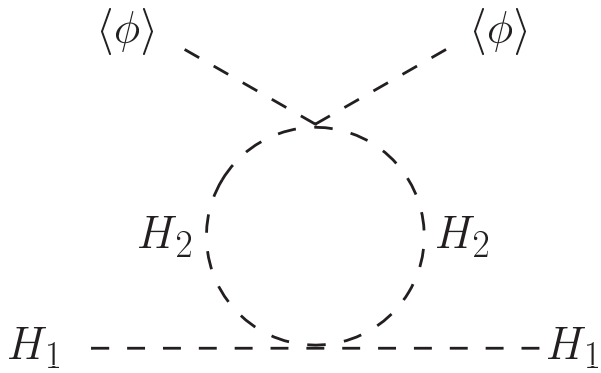

Figure 5.1: Scalar one-loop diagram which contributes to the SM-like Higgs doublet mass.

v_Φ	10 TeV	100 TeV
1-loop with scalar	$\sim (50\,\mathrm{GeV})^2$	$\sim (50\,\mathrm{GeV})^2$
2-loop with Z'	$(\mathcal{O}(1)\,\mathrm{GeV})^2$	$(\mathcal{O}(10)\,\mathrm{GeV})^2$
1-loop with neutrino	$(\mathcal{O}(10^{-3})\,\mathrm{GeV})^2$	$(\mathcal{O}(10^{-3})\,\mathrm{GeV})^2$

Table 5.2: Typical orders of magnitude of the quantum corrections to the SM-like Higgs doublet mass.

$U(1)_{B-L}$ gauge boson (Z') and the top quark, which are, respectively, found to be [42]

$$\delta m_H^2 \sim \frac{Y_\nu^2 Y_M^2 v_\Phi^2}{16\pi^2}\,, \qquad \delta m_H^2 \sim \frac{y_t^2 g_{B-L}^4 v_\Phi^2}{(16\pi^2)^2}\,, \tag{5.5}$$

where they are the same as Eqs. (4.9) and (4.20), respectively. It turns out that these contributions are negligibly small compared to the scalar one-loop correction in Eq. (5.4). As we will discuss in the next section, the quartic couplings λ_3 and λ_4 should be sizable as $\lambda_{3,4} \gtrsim 0.15$ in order to stabilize the EW vacuum. The neutrino one-loop correction is roughly proportional to the active neutrino mass by using the seesaw relation, and it is highly suppressed by the smallness of the active neutrino mass. The two-loop corrections with the Z' boson is suppressed by the two-loop factor $1/(16\pi^2)^2$. Unless g_{B-L} is sufficiently large, the two-loop corrections are smaller than the scalar one-loop correction. In Table 5.2, we summarize typical orders of magnitude for the three corrections for $v_\Phi = 10$ and 100 TeV. For the active neutrino mass, we have adopted the seesaw relation, $m_\nu \sim (Y_\nu v_H)^2/(Y_M v_\Phi) \sim 0.1\,\mathrm{eV}$. For both $v_\Phi = 10$ and 100 TeV, we have fixed $\lambda_3 = \lambda_4 = 0.15$, $g_{B-L} = 0.15$ and $Y_\nu = 2.0 \times 10^{-6}$, while we have used $\lambda_{H2\Phi} = 0.01$ (10^{-4}) and $Y_M = 0.23$ (0.023) for $v_\Phi = 10$ (100) TeV.

The other scalar masses are approximately given by

$$\begin{aligned} M_\phi^2 &= \frac{6}{11}\lambda_\Phi v_\Phi^2\,, \\ M_H^2 &= M_A^2 = \lambda_{H_2\Phi} v_\Phi^2 + (\lambda_3 + \lambda_4) v_H^2\,, \\ M_{H^\pm}^2 &= \lambda_{H_2\Phi} v_\Phi^2 + \lambda_3 v_H^2\,, \end{aligned} \tag{5.6}$$

where M_ϕ is the mass of the SM singlet scalar, M_H (M_A) is the mass of CP-even (CP-odd) neutral Higgs boson, and $M_{H\pm}$ is the mass of charged Higgs boson. The extra heavy Higgs bosons are almost degenerate. The masses of the Z' boson and the right-handed neutrinos are given by

$$\begin{aligned} M_{Z'} &= 2g_{B-L}v_\Phi \,, \\ M_N &= \sqrt{2}y_M v_\Phi \simeq \left[\frac{3}{2N_\nu}\left(1-\frac{\pi^2\lambda_\Phi}{11g_{B-L}^4}\right)\right]^{1/4} M_{Z'} \,, \end{aligned} \tag{5.7}$$

where we have used $\mathrm{tr}Y_M = N_\nu y_M$, for simplicity, and N_ν stands for the number of relevant Majorana couplings. In the following analysis, we will take $N_\nu = 1$ because our final results are almost insensitive to N_ν. In the last equality in Eq. (5.7), we have used Eq. (3.7).

5.2 Numerical results

Before presenting our numerical results, we first discuss constraints on the model parameters from the perturbativity and the vacuum stability in the RG evolutions. In our analysis, all values of couplings are given at $\mu = v_\Phi$. For v_Φ at the TeV scale, we find the constraint $g_{B-L} \lesssim 0.3$ to avoid the Landau pole of the $U(1)_{B-L}$ gauge coupling below the Planck scale, while a more severe constraint $g_{B-L} \lesssim 0.2$ is obtained to avoid a blowup of the quartic coupling λ_2 below the Planck scale. From $g_{B-L} \lesssim 0.2$ and the experimental bound $M_{Z'} > 2.9\,\mathrm{TeV}$ on the Z' boson mass [130, 131], we find $v_\Phi > 7.25\,\mathrm{TeV}$.[3] The EW vacuum stability, in other words, $\lambda_H(\mu) > 0$ at all scales between the EW scale and the Planck scale, can be realized by sufficiently large λ_3 and/or λ_4 as $\lambda_3 = \lambda_4 \gtrsim 0.15$. To keep their perturbativity below the Planck scale, $\lambda_3 = \lambda_4 \lesssim 0.48$ must be satisfied, while we will find that the naturalness of the EW scale leads to a more severe upper bound.

To realize the hierarchy $\lambda_{H_1\Phi} \ll \lambda_{\mathrm{mix}} \ll \lambda_{H_2\Phi}$, we take $\lambda_{H_1\Phi} = 0$, for simplicity. When we consider λ_{mix} in the range of $0 < \lambda_{\mathrm{mix}} < 0.1 \times \lambda_{H_2\Phi}$, the relation between v_Φ and $\lambda_{H_2\Phi}$ obtained by Eq. (5.4) is shown in the left panel of Fig. 5.2. Here, we have taken $\lambda_3 = \lambda_4 = 0.15$ as reference values. The red and blue lines correspond to the lowest value $\lambda_{\mathrm{mix}} = 0$ and the highest value $\lambda_{\mathrm{mix}} = 0.1 \times \lambda_{H_2\Phi}$, respectively.[4] Note that $\lambda_{H_2\Phi}v_\Phi^2$ is almost constant. Since all heavy Higgs boson masses are approximately determined by $\lambda_{H_2\Phi}v_\Phi^2$, they are almost independent of v_Φ, as shown in the right panel of Fig. 5.2. We can find that the heavy Higgs boson masses lie in the range between 1 TeV and 1.7 TeV, which can be tested at the LHC in the near future.

[3] Using the latest bound $M_{Z'} > 3.6\,\mathrm{TeV}$ [139], we find more strong constraint as $v_\Phi > 9\,\mathrm{TeV}$.

[4] Although the bosonic seesaw mechanism does not work for $\lambda_{\mathrm{mix}} = 0$, the EW symmetry can be radiatively broken through the scalar loop correction shown in Fig. 5.1.

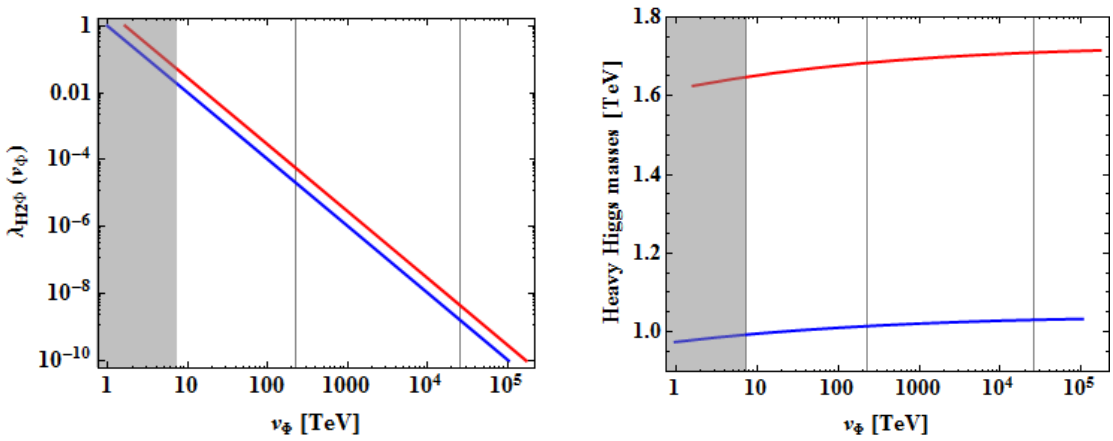

Figure 5.2: The relation between v_Φ and $\lambda_{H_2\Phi}$ through Eq. (5.4) (left panel), and the corresponding heavy Higgs boson mass $\simeq \sqrt{\lambda_{H_2\Phi}} v_\Phi$ (right panel). The red and blue lines correspond to $\lambda_{\rm mix} = 0$ and $\lambda_{\rm mix} = 0.1 \times \lambda_{H_2\Phi}$, respectively. The shaded region shows the perturbativity bound $v_\Phi > 7.25\,$TeV. The vertical lines show the upper bound on v_Φ, at which Higgs mass corrections from the two loop diagrams with the $U(1)_{B-L}$ gauge boson, which is calculated by the latter of Eq. (5.5), become $(10\,{\rm GeV})^2$ for $g_{B-L} = 0.1$ (left) and $g_{B-L} = 0.01$ (right), respectively.

In Eq. (5.4), it may be natural for the first term from the tree-level couplings dominates over the second term from the 1-loop correction. This naturalness leads to the constraint of $\lambda_3 = \lambda_4 < 0.26$, which is more severe than the perturbativity bound $\lambda_3 = \lambda_4 \lesssim 0.48$ as discussed above. This condition is equivalent to the fact that the origin of the negative mass term mainly comes from the diagonalization of the scalar mass squared matrix in Eq. (5.3), namely, the bosonic seesaw mechanism.

We show the RG evolutions of the quartic couplings in Fig. 5.3. Here, we have taken $\lambda_{H_1\Phi} = 0$, and $\lambda_{H_2\Phi} = 10^{-2}$ and 10^{-4} for $v_\Phi = 10\,$TeV (left panel) and $100\,$TeV (right panel), respectively. The red, green, and blue lines correspond to the RG evolutions of $\lambda_{H_1\Phi}$, $\lambda_{H_2\Phi}$, and $\lambda_{\rm mix}$, respectively. In this plot, other input parameters have been set as $g_{B-L} = 0.17$ and $\lambda_3 = \lambda_4 = 0.17$ to realize the EW vacuum stability without the Landau pole, and $\lambda_\Phi = 10^{-3}$. The value of $\lambda_1 = \lambda_2 = \lambda_H$ at $\mu = v_\Phi$ has been evaluated by extrapolating the SM Higgs self-coupling from the EW scale to v_Φ. For this parameter choice, the Z' boson and the right-handed neutrinos have the masses of the same order of magnitude as $M_{Z'} = 3.4\ (34)\,$TeV and $M_N = 2.0\ (20)\,$TeV for $v_\Phi = 10\ (100)\,$TeV, while the $B-L$ Higgs boson mass is calculated as $M_\phi = 0.23\ (2.3)\,$TeV. As is well-known, $M_\phi \ll M_{Z'}$ is a typical prediction of the CW mechanism. The masses of the heavy Higgs bosons are roughly $1\,$TeV for both $v_\Phi = 10\,$TeV and $100\,$TeV.

In order for the bosonic seesaw mechanism to successfully work, we have assumed the hierarchy among the quartic couplings as $\lambda_{H_1\Phi} \ll \lambda_{\rm mix} \ll \lambda_{H_2\Phi}$ at the scale $\mu = v_\Phi$.

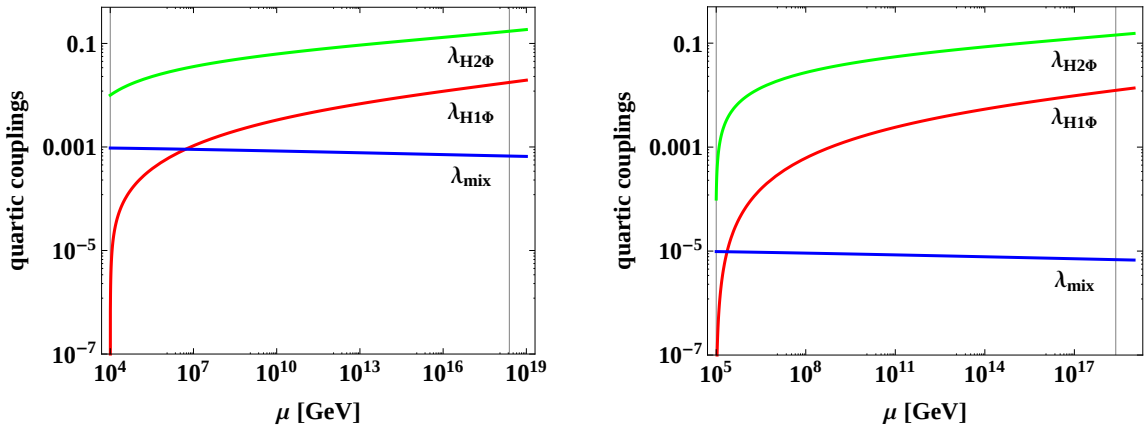

Figure 5.3: RG evolutions of the quartic couplings for $v_\Phi = 10\,\text{TeV}$ (left) and $100\,\text{TeV}$ (right). The red, green, and blue lines correspond to $\lambda_{H_1\Phi}$, $\lambda_{H_2\Phi}$, and λ_{mix}, respectively. The rightmost vertical line shows the reduced Planck scale.

	$SU(3)_C \times SU(2)_L \times U(1)_Y$	$U(1)_{B-L}$
$S_{L,R}$	$(\mathbf{1},\, \mathbf{1},\, 0)$	x
$S'_{L,R}$	$(\mathbf{1},\, \mathbf{1},\, 0)$	$x-2$
$D_{L,R}$	$(\mathbf{1},\, \mathbf{2},\, 1)$	x
$D'_{L,R}$	$(\mathbf{1},\, \mathbf{2},\, 1)$	$x+2$

Table 5.3: Additional vector-like fermions. x is an arbitrary real number.

One may think it unnatural to introduce this large hierarchy by hand. However, we find from Fig. 5.3 that the large hierarchy between $\lambda_{H_1\Phi}$ and $\lambda_{H_2\Phi}$ tends to disappear toward high energies. This is because the β functions of the small couplings $\beta_{\lambda_{H_1\Phi}}$ and $\beta_{\lambda_{H_2\Phi}}$ are not simply proportional to themselves, but include terms given by other sizable couplings [see Appendix for the explicit formulas of their β functions]. This behavior of reducing the large hierarchy in the RG evolutions is independent of the choice of the boundary conditions for g_{B-L}, λ_3, λ_4 and λ_Φ. Therefore, Fig. 5.3 indicates that once our model is defined at some high energy, e.g., the Planck scale, the large hierarchy among the quartic couplings, which is crucial for the bosonic seesaw mechanism to work, is naturally achieved from a mild hierarchy at the high energy.

We have seen in Fig. 5.3 that λ_{mix} is almost unchanged. This is because its β function is proportional to itself, which is given Eq. (A.45) in Appendix. Hence, the hierarchy between λ_{mix} and other quartic couplings gets enlarged toward high energies. To avoid this situation and make our model more natural, one may introduce additional vector-like fermions listed in Table 5.3, for example.[5] Although x is an arbitrary real number, we assume $x \neq \pm 1$ to distinguish the new fermions from the charged leptons and the

[5] As another possibility, one may think that some symmetry forbids the λ_{mix} term and it is generated via a small breaking of the symmetry.

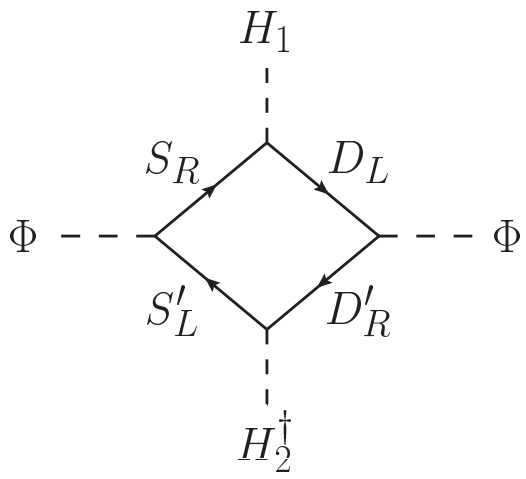

Figure 5.4: One-loop diagram due to the additional fermions, which is relevant to $\beta_{\lambda_{\rm mix}}$.

right-handed neutrinos. These fermions have Yukawa couplings as

$$\begin{aligned}-\mathcal{L}_V = & Y_{SS}\overline{S_L}\Phi S'_R + Y_{SD}\overline{S'_R}H_2^\dagger D'_L + Y_{DD}\overline{D'_L}\Phi D_R + Y_{DS}\overline{D_R}H_1 S_L \\ & + Y'_{SS}\overline{S_R}\Phi S'_L + Y'_{SD}\overline{S'_L}H_2^\dagger D'_R + Y'_{DD}\overline{D'_R}\Phi D_L + Y'_{DS}\overline{D_L}H_1 S_R + \text{h.c.}\,, \end{aligned} \tag{5.8}$$

so that $\beta_{\lambda_{\rm mix}}$ includes terms of $Y_{SS}Y_{SD}Y_{DD}Y_{DS}$ and $Y'_{SS}Y'_{SD}Y'_{DD}Y'_{DS}$, which are not proportional to $\lambda_{\rm mix}$. These terms originate from the diagram shown in Fig. 5.4. Accordingly, the stationary condition of V_Φ is modified to

$$\lambda_\Phi \simeq \frac{11}{6\pi^2}\left[6g_{B-L}^4 - {\rm tr}Y_M^4 - \frac{1}{8}\left(Y_{SS}^4 + Y_{SS}'^4 + 2Y_{DD}^4 + 2Y_{DD}'^4\right)\right]. \tag{5.9}$$

From the vacuum stability condition $\lambda_\Phi > 0$ and perturbativity condition $g_{B-L} < 0.2$, the additional Yukawa contribution should satisfy $Y_{SS}^4 + Y_{SS}'^4 + 2Y_{DD}^4 + 2Y_{DD}'^4 \lesssim 3\times(0.4)^4$. Note that masses of vector-like fermions are dominantly generated by v_Φ, and they can be sufficiently heavy to avoid the current experimental bounds.

Figure 5.5 shows the RG evolution of the quartic couplings for $v_\Phi = 100$ TeV with the additional vector-like fermions. The input parameters are the same as in Fig. 5.3, while we have taken the Yukawa couplings as $Y_{SS} = Y_{SD} = Y_{DD} = Y_{DS} = 0.2$ and $Y'_{SS} = Y'_{SD} = Y'_{DD} = Y'_{DS} = 0.1$ at $\mu = v_\Phi$, as reference values. Toward high energies, $|\lambda_{\rm mix}|$ becomes larger, and the hierarchy with other quartic couplings becomes milder. We can see that $\lambda_{H_1\Phi}$ is negative below $\mu \simeq 10^8$ GeV, because the contribution of additional Yukawa couplings dominates over $\beta_{\lambda_{H_1\Phi}}$ below $\mu \simeq 10^8$ GeV. Above this scale, the contribution of $U(1)_{B-L}$ gauge couplings becomes dominant, and then $\lambda_{H_1\Phi}$ becomes positive. As a result, the large hierarchy at the $U(1)_{B-L}$ gauge symmetry breaking scale can be realized with the mild hierarchy at some high energy, e.g., the Planck scale. We expect that a UV complete theory, which provides the origin of the classical scale invariance, takes place at the high energy.

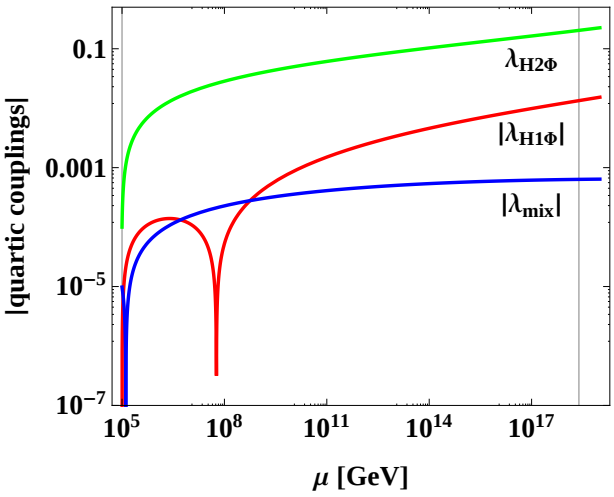

Figure 5.5: RG evolution of the quartic couplings for $v_\Phi = 100\,\text{TeV}$ with the additional vector-like fermions. The input parameters are the same as in Fig. 5.3.

5.3 Conclusion

We have investigated the classically scale invariant $U(1)_{B-L}$ model with two Higgs doublet fields. Through the Coleman-Weinberg mechanism, the $U(1)_{B-L}$ gauge symmetry is radiatively broken. This symmetry breaking leads breaking of the scale invariance, and is the sole origin of all dimensionful parameters in the model. The mass terms of the two Higgs doublet fields are generated through their quartic couplings with the $B-L$ Higgs field. All generated masses are set to be positive but, nevertheless, the EW symmetry breaking can be realized by the bosonic seesaw mechanism. In order for the bosonic seesaw mechanism to successfully work, we need a large hierarchy among the quartic couplings of two Higgs doublet fields. Although it seems unnatural to introduce the large hierarchy by hand at the $U(1)_{B-L}$ gauge symmetry breaking scale, we have found through analysis of the RG evolutions of the quartic couplings that this hierarchy is dramatically reduced toward high energies. Therefore, once our model is defined at some high energy, e.g., the Planck scale, in other words, the origin of the classical scale invariance is provided by some UV complete theory at the Planck scale, the bosonic seesaw mechanism is naturally realized with a mild hierarchy among the quartic couplings. The requirements for the perturbativity of the running couplings and the EW vacuum stability in the RG analysis as well as for the naturalness of the EW scale, we have identified the regions of model parameters such as $g_{B-L}(v_\Phi) \lesssim 0.2$, $0.15 \lesssim \lambda_3(v_\Phi) = \lambda_4(v_\Phi) \lesssim 0.23$, and $v_\Phi \lesssim 100\,\text{TeV}$. We have also found that all heavy Higgs boson masses are almost independent of v_Φ, and lie in the range between 1 TeV and 1.7 TeV, which can be tested at the LHC in the near future.

Chapter 6

Bosonic seesaw model II

In the previous chapter, we have developed the bosonic seesaw model in the perturbative scheme, which is based on the CW mechanism. In this chapter, we consider strong-coupling dynamics in an additional $SU(N_{\rm HC})$ sector, namely, hypercolor (HC) sector. The HC dynamics is similar to the QCD, and a condensate of additional vector-like fermions breaks the classical scale invariance. We will see that the non-perturbative effect of the $SU(N_{\rm HC})$ sector can dynamically realize the bosonic seesaw mechanism. This chapter is based on our works [95, 96].

6.1 Bosonic seesaw mechanism with $SU(N_{\rm HC})$ gauge extension

The model we employ is based on the classically scale invariant SM with a strongly coupled HC dynamics at the TeV scale. The HC sector is described by the HC-gluon $\mathcal{G}_\mu = \mathcal{G}^a_\mu \lambda^a/2$ with a gauge coupling $g_{\rm HC}$ and three vector-like fermion triplets, $F_{L,R} = (\chi_i,\ \psi)^T_{L,R}$, which are shown in Table 6.1. Without the EW symmetry, the HC theory possesses the chiral $U(3)_L \times U(3)_R$ symmetry as well as the classically scale invariance. The Lagrangian is given by

$$\mathcal{L} = \mathcal{L}_{\rm SM}|_{m_H^2=0} + \Delta\mathcal{L} + \bar{F} i\gamma^\mu D_\mu F - \frac{1}{2}{\rm tr}[\mathcal{G}^2_{\mu\nu}] - V\,, \tag{6.1}$$

with

$$D_\mu = \partial_\mu - i g_{\rm HC}\mathcal{G}_\mu\,, \qquad \mathcal{G}_{\mu\nu} = \partial_\mu \mathcal{G}_\nu - \partial_\nu \mathcal{G}_\mu - i g_{\rm HC}[\mathcal{G}_\mu, \mathcal{G}_\nu]\,, \tag{6.2}$$

where the EW gauges have been switched off momentarily. The chiral symmetry is assumed to be explicitly broken due to the soft breaking terms:

$$\begin{aligned} \Delta\mathcal{L} &= \mathcal{L}_y + \mathcal{L}_S\,, \\ \mathcal{L}_y &= -y\,\overline{F_L}\begin{pmatrix} 0 & H \\ H^\dagger & 0 \end{pmatrix} F_R + {\rm h.c.}\,, \qquad (6.3) \\ \mathcal{L}_S &= i g_S\left(\overline{F_L}F_R - \overline{F_R}F_L\right) S\,, \qquad (6.4) \end{aligned}$$

	$SU(3)_C \times SU(2)_L \times U(1)_Y$	$SU(N_{\rm HC})$
$\chi_{L,R}$	$(\mathbf{1},\, \mathbf{2},\, 1)$	$\mathbf{N}_{\rm HC}$
$\psi_{L,R}$	$(\mathbf{1},\, \mathbf{1},\, 0)$	$\mathbf{N}_{\rm HC}$

Table 6.1: Charge assignments of vector-like fermions.

where the Yukawa couplings y and g_S are assumed to be real and much smaller than unity in order to realize the chiral symmetry approximately. There are two elementary scalar fields: H denotes the elementary Higgs doublet field, and S is a pseudoscalar field having no gauge charges. The potential term V in Eq. (6.1) includes the H and S as

$$V = \lambda_H (H^\dagger H)^2 + \lambda_S S^4 + \kappa_H S^2 (H^\dagger H)\,. \tag{6.5}$$

We will see that the mixing coupling κ_H should be small from the stationary condition of V.

We expect the HC dynamics causes chiral condensate $\langle \bar{F} F \rangle = \langle \bar{\chi}_i \chi_i \rangle = \langle \bar{\psi} \psi \rangle \neq 0$. Here, let us mention the NG bosons. Due to the classically scale invariance, the vector-like fermion masses are forbidden. The chiral symmetry in the HC sector $U(3)_L \times U(3)_R$ is rewritten by

$$SU(3)_V \times SU(3)_A \times U(1)_V \times U(1)_A\,, \tag{6.6}$$

where $U(1)_V$ is similar to the baryon number symmetry. This vector-like symmetry is expected to be unbroken by the strong-coupling dynamics due to the Vafa-Witten's theorem [143]. It guarantees the stability of the lightest HC-baryon, which can be a candidate of the dark matter as will be seen in the next chapter 7.4 [100]. On the other hand, it is well known that $U(1)_A$ is explicitly broken by anomaly [144]. The chiral condensate should occur as preserving $SU(2)_L \times U(1)_Y$ symmetry, and then we expect $\langle \bar{\chi} \psi \rangle = \langle \bar{\psi} \chi \rangle = 0$, while $\langle \bar{\chi} \chi \rangle \neq 0$ and $\langle \bar{\psi} \psi \rangle \neq 0$. The condensate of vector-like fermions cause chiral symmetry breaking to

$$SU(3)_V \times U(1)_V\,. \tag{6.7}$$

Thus, there are eight NG bosons plus heavy η' corresponding to the $U(1)_A$ anomaly. The η' mass can be calculated by the Witten-Veneziano formula [145, 146]. Actually, the chiral symmetry is explicitly broken by the EW gauge symmetry, $SU(2)_L \times U(1)_Y$, and the remaining symmetry is

$$SU(2)_{\chi V} \times U(1)_{\chi V} \times U(1)_{\psi V}\,. \tag{6.8}$$

This breaking generates mass splitting for the NG boson masses.

At $\mu = \Lambda_{\rm HC}$, $SU(N_{\rm HC})$ gauge coupling becomes large as 4π, and the vector-like fermions are confined by non-perturbative effects. Then, the composite HC Higgs fields $\sim \bar{F}_i F_j/\Lambda_{\rm HC}^2$ are generated, in which $1/\Lambda_{\rm HC}^2$ is expected by a naive dimensional analysis. Among them, the component $\Theta \sim \bar{\psi}\chi/\Lambda_{\rm HC}^2$ has the same quantum number as that of the elementary Higgs doublet H. Taking into account the Yukawa term $\mathcal{L}_y$ in Eq. (6.3) and generation of the Θ mass term, one can write the effective Lagrangian at $\Lambda_{\rm HC}$ to quadratic order in fields as

$$\mathcal{L}_{\rm eff} = -y\Lambda_{\rm HC}^2 \left[\Theta^\dagger H + {\rm h.c.}\right] - M_\Theta^2 \Theta^\dagger \Theta \,. \tag{6.9}$$

This leads to the seesaw type mass matrix for the Higgs doublet H and the composite Higgs doublet Θ, and it is diagonalized by expanding terms in powers of $y \ll 1$ to be

$$\begin{aligned}
& \begin{pmatrix} H \\ \Theta \end{pmatrix}^\dagger \begin{pmatrix} 0 & y\Lambda_{\rm HC}^2 \\ y\Lambda_{\rm HC}^2 & M_\Theta^2 \end{pmatrix} \begin{pmatrix} H \\ \Theta \end{pmatrix} \\
\approx & \begin{pmatrix} H_1 \\ H_2 \end{pmatrix}^\dagger \begin{pmatrix} -y^2 \frac{\Lambda_{\rm HC}^4}{M_\Theta^2} & 0 \\ 0 & M_\Theta^2 \left(1 + \frac{y^2 \Lambda_{\rm HC}^2}{M_\Theta^2}\right) \end{pmatrix} \begin{pmatrix} H_1 \\ H_2 \end{pmatrix} \\
\equiv & \begin{pmatrix} H_1 \\ H_2 \end{pmatrix}^\dagger \begin{pmatrix} -m_{H_1}^2 & 0 \\ 0 & m_{H_2}^2 \end{pmatrix} \begin{pmatrix} H_1 \\ H_2 \end{pmatrix} .
\end{aligned} \tag{6.10}$$

The eigenstates in this matrix (H_1, H_2) are given by

$$\begin{aligned}
\begin{pmatrix} H_1 \\ H_2 \end{pmatrix} &= \begin{pmatrix} \cos\theta_H & -\sin\theta_H \\ \sin\theta_H & \cos\theta_H \end{pmatrix} \begin{pmatrix} H \\ \Theta \end{pmatrix} \\
&\simeq \begin{pmatrix} 1 - \frac{y^2}{2} + \mathcal{O}(y^4) & -y(1 - \frac{3}{2}y^2) + \mathcal{O}(y^5) \\ y(1 - \frac{3}{2}y^2) + \mathcal{O}(y^5) & 1 - \frac{y^2}{2} + \mathcal{O}(y^4) \end{pmatrix} \begin{pmatrix} H \\ \Theta \end{pmatrix} ,
\end{aligned} \tag{6.11}$$

where we have taken $M_\Theta \simeq \Lambda_{\rm HC}$. Since y is much smaller than unity, the lighter (heavier) mass eigenstate H_1 (H_2) is almost composed of H (Θ). Note that the classical scale invariance is broken by the HC dynamics, and the negative sign of the lower eigenvalue $(-m_{H_1}^2)$ is dynamically generated by the bosonic seesaw mechanism.

The η' gets the mass from the $U(1)_A$ anomaly as in the case of the ordinary QCD. The size of the mass can be roughly estimated by scaling from the QCD to be

$$M_{\eta'} \sim \mathcal{O}(1{\rm GeV}) \times \left(\frac{\Lambda_{\rm HC}}{\Lambda_{\rm QCD}}\right) \times \sqrt{\frac{3}{N_{\rm HC}}} \,, \tag{6.12}$$

where $N_{\rm HC}$ dependence is explicitly shown. One should note that the η' couples to the $U(1)_A$ current, $J_\mu^0 = \frac{1}{\sqrt{6}} \bar{F}\gamma_\mu\gamma_5 \cdot \mathbf{1}_{3\times 3} \cdot F$. Hence, by taking into account the η' mass generation from the anomaly, the g_S term in Eq. (6.4) becomes

$$\mathcal{L}_S \approx g_S \Lambda_{\rm HC}^2 \eta' S - \frac{1}{2} M_{\eta'}^2 (\eta')^2 \,. \tag{6.13}$$

Again, the form of Eq. (6.13) leads the seesaw type mass matrix, so one can readily see that the lower eigenvalue, corresponding to the S-mass squared, is negative:

$$\begin{aligned}
\mathcal{L}_S &\approx -\frac{1}{2}\begin{pmatrix} S \\ \eta' \end{pmatrix}^T \begin{pmatrix} 0 & -g_S\Lambda_{\rm HC}^2 \\ -g_S\Lambda_{\rm HC}^2 & M_{\eta'}^2 \end{pmatrix}\begin{pmatrix} S \\ \eta' \end{pmatrix} \\
&\approx -\frac{1}{2}\begin{pmatrix} \mathcal{S} \\ \eta^0 \end{pmatrix}^T \begin{pmatrix} -g_S^2\frac{\Lambda_{\rm HC}^4}{M_{\eta'}^2} & 0 \\ 0 & M_{\eta'}^2\left(1+\frac{g_S^2\Lambda_{\rm HC}^2}{M_{\eta'}^2}\right) \end{pmatrix}\begin{pmatrix} \mathcal{S} \\ \eta^0 \end{pmatrix} \\
&\equiv -\frac{1}{2}\begin{pmatrix} \mathcal{S} \\ \eta^0 \end{pmatrix}^T \begin{pmatrix} -m_{\mathcal{S}}^2 & 0 \\ 0 & m_{\eta^0}^2 \end{pmatrix}\begin{pmatrix} \mathcal{S} \\ \eta^0 \end{pmatrix} . \qquad (6.14)
\end{aligned}$$

The eigenstates in this matrix $(\mathcal{S}, \eta^0)$ are given by

$$\begin{aligned}
\begin{pmatrix} \mathcal{S} \\ \eta^0 \end{pmatrix} &= \begin{pmatrix} \cos\theta_S & \sin\theta_S \\ -\sin\theta_S & \cos\theta_S \end{pmatrix}\begin{pmatrix} S \\ \eta' \end{pmatrix} \\
&\simeq \begin{pmatrix} 1-\frac{g_S^2}{2}+\mathcal{O}(g_S^4) & g_S(1-\frac{3}{2}g_S^2)+\mathcal{O}(g_S^5) \\ -g_S(1-\frac{3}{2}g_S^2)+\mathcal{O}(g_S^5) & 1-\frac{g_S^2}{2}+\mathcal{O}(g_S^4) \end{pmatrix}\begin{pmatrix} S \\ \eta' \end{pmatrix} , \qquad (6.15)
\end{aligned}$$

to the nontrivial order of expansion in $g_S \ll 1$, where we have taken $M_{\eta'} \simeq \Lambda_{\rm HC}$. Thus, the pseudoscalar $\mathcal{S}$ obtains the nonzero VEV, which play the significant role to give the pseudo-NG boson (HC-pion) masses, as will be clearly seen in the next section.

6.2 Mass spectrum

Including the dynamically generated terms, we thus see that the potential (6.5) is modified at the scale $\Lambda_{\rm HC}$ as follows:

$$\begin{aligned}
V &= \lambda_H(H^\dagger H)^2 + \lambda_S S^4 + \kappa_H S^2(H^\dagger H) + \lambda_\Theta(\Theta^\dagger\Theta)^2 \\
&\quad -\begin{pmatrix} H \\ \Theta \end{pmatrix}^\dagger \begin{pmatrix} 0 & y\Lambda_{\rm HC}^2 \\ y\Lambda_{\rm HC}^2 & M_\Theta^2 \end{pmatrix}\begin{pmatrix} H \\ \Theta \end{pmatrix} - \frac{1}{2}\begin{pmatrix} S \\ \eta' \end{pmatrix}^T \begin{pmatrix} 0 & g_S\Lambda_{\rm HC}^2 \\ g_S\Lambda_{\rm HC}^2 & M_{\eta'}^2 \end{pmatrix}\begin{pmatrix} S \\ \eta' \end{pmatrix} \\
&= \lambda_H\Big((H_1^\dagger c_H + H_2^\dagger s_H)(H_1 c_H + H_2 s_H)\Big)^2 + \lambda_S(\mathcal{S}c_S - \eta^0 s_S)^4 \\
&\quad +\kappa_H(\mathcal{S}c_S - \eta^0 s_S)^2\Big((H_1^\dagger c_H + H_2^\dagger s_H)(H_1 c_H + H_2 s_H)\Big) \\
&\quad +\lambda_\Theta\Big((-H_1^\dagger s_H + H_2^\dagger c_H)(-H_1 s_H + H_2 c_H)\Big)^2 \\
&\quad -m_{H_1}^2(H_1^\dagger H_1) + m_{H_2}^2(H_2^\dagger H_2) - \frac{1}{2}m_{\mathcal{S}}^2\mathcal{S}^2 + \frac{1}{2}m_{\eta^0}^2(\eta^0)^2 , \qquad (6.16)
\end{aligned}$$

where we have used $c_{H,S} = \cos\theta_{H,S}$ and $s_{H,S} = \sin\theta_{H,S}$, and added the self-coupling of Θ, which can generically be induced from the underlying HC dynamics, and is expected to be $\gtrsim \mathcal{O}(10)$. Based on this potential, we discuss the realization of the EW symmetry breaking.

We now parametrize the scalar and pseudoscalar fields with their VEVs for the (approximate) mass eigenstate fields (H_1, H_2) and ($\mathcal{S}$, η^0) in Eqs. (6.11) and (6.15):

$$\begin{aligned} H_1 &= \begin{pmatrix} \varphi_1^+ \\ \frac{1}{\sqrt{2}}(v_1 + h_1 + i\varphi_1^0) \end{pmatrix}, \qquad H_2 = \begin{pmatrix} \varphi_2^+ \\ \frac{1}{\sqrt{2}}(v_2 + h_2 + i\varphi_2^0) \end{pmatrix}, \\ \mathcal{S} &= v_S + s\,, \qquad \eta^0 = v_\eta + e_0\,. \end{aligned} \tag{6.17}$$

where $\varphi_{1,2}^+$ have electromagnetic charge $+1$, while charge conjugate fields $\varphi_{1,2}^-$ have electromagnetic charge -1. The stationary conditions of the potential (6.16) leads

$$\begin{aligned} m_{H_1}^2 v_1 &= \kappa_H c_H (v_1 c_H + v_2 s_H)(v_S c_S - v_\eta s_S)^2 + \lambda_H c_H (v_1 c_H + v_2 s_H)^3 \\ &\quad + \lambda_\Theta s_H (v_1 s_H - v_2 c_H)^3\,, \\ m_{H_2}^2 v_2 &= -\kappa_H s_H (v_1 c_H + v_2 s_H)(v_S c_S - v_\eta s_S)^2 - \lambda_H s_H (v_1 c_H + v_2 s_H)^3 \\ &\quad + \lambda_\Theta c_H (v_1 s_H - v_2 c_H)^3\,, \\ m_{\mathcal{S}}^2 v_S &= \kappa_H c_S (v_1 c_H + v_2 s_H)^2 (v_S c_S - v_\eta s_S) + 4\lambda_S c_S (v_S c_S - v_\eta s_S)^3\,, \\ m_{\eta^0}^2 v_\eta &= \kappa_H s_S (v_1 c_H + v_2 s_H)^2 (v_S c_S - v_\eta s_S) + 4\lambda_S s_S (v_S c_S - v_\eta s_S)^3\,. \end{aligned} \tag{6.18}$$

Form the latter two equations, we find

$$\tan\theta_S = \frac{m_{\eta_0}^2 v_\eta}{m_{\mathcal{S}}^2 v_S}\,. \tag{6.19}$$

Since θ_S has nonzero and finite value, both v_S and v_η should be nonzero. The stationary condition for v_2 includes the trivial solution $v_2 = 0$, in which φ_1^0 and $\varphi_1^\pm$ become massless NG bosons eaten by the Z and $W^\pm$ bosons. For simplicity, we take $v_2 = 0$ in the following analysis. Taking $v_2 = 0$, the stationary conditions induce by expanding terms in powers of y and g_S as

$$\begin{aligned} m_{H_1}^2 &= \lambda_\Theta v_1^2 s_H^2 = y^2 \lambda_\Theta v_1^2 + \cdots \ (\simeq y^2 \Lambda_{\rm HC}^2)\,, \\ \kappa_H &= -\frac{(\lambda_H c_H^2 - \lambda_\Theta s_H^2) v_1^2}{(v_S c_S - v_\eta s_S)^2} = -\frac{v_1^2}{v_S^2}\lambda_H + \cdots\,, \\ m_{\mathcal{S}}^2 &= 4\lambda_S v_S^2 + \cdots \ (\simeq g_S^2 \Lambda_{\rm HC}^2)\,, \\ m_{\eta^0}^2 &= 4\lambda_S g_S \frac{v_S^3}{v_\eta} + \cdots \ (\simeq \Lambda_{\rm HC}^2)\,, \end{aligned} \tag{6.20}$$

where the second equation has come from imposing $v_2 = 0$, and the ellipses denote terms suppressed by higher orders in expansion with respect to y and g_S. The expressions in the parenthesis correspond to the seesaw-induced formulae [see Eqs. (6.10) and (6.14)].

For the approximate mass eigenstates (h_1, h_2, s, e_0), the square of masses are calculated by second derivatives of the potential (6.16), and given, at the leading order level, as

$$\begin{pmatrix} 2\lambda_H v_1^2 & 0 & -\frac{2\lambda_H v_1^3}{v_S} & 0 \\ 0 & m_{H_2}^2 & 0 & 0 \\ -\frac{2\lambda_H v_1^3}{v_S} & 0 & 12\lambda_S v_S^2 - m_S^2 - \frac{\lambda_H v_1^4}{v_S^2} & 0 \\ 0 & 0 & 0 & m_{\eta^0}^2 \end{pmatrix}, \tag{6.21}$$

where we have used the former two exact relations in Eq. (6.20). For $v_S \gg v_1$, there is almost no mixing between h_1 and s, and then, the fields (h_1, h_2, s, e_0) can regard as the exact mass eigenstates with the following mass eigenvalues:[1]

$$\begin{aligned} m_{h_1}^2 &\simeq 2\lambda_H v_1^2 \,, \\ m_{h_2}^2 &\simeq m_{H_2}^2 \simeq \Lambda_{\rm HC}^2 \,, \\ m_s^2 &\simeq 8\lambda_S v_S^2 \simeq 2g_S^2 \Lambda_{\rm HC}^2 \,, \\ m_{e_0}^2 &\simeq m_{\eta^0}^2 \simeq \Lambda_{\rm HC}^2 \,, \end{aligned} \tag{6.22}$$

where the seesaw-induced formulae have been used at the last approximate expressions in the latter three lines, and h_1 is identified as the 125 GeV Higgs boson. By adjusting parameters to satisfy the stationary conditions (6.20), the VEV of h_1 can realize the EW scale as $v_1 = 246\,\text{GeV}$ with the H self-coupling $\lambda_H > 0$, hence $\kappa_H < 0$. This statement is valid even for $\kappa_H = 0$ case, in which $\tan^2\theta_H = \lambda_H/\lambda_\Theta$ is satisfied. From this fact, we can say that the EW symmetry is broken purely by the bosonic seesaw mechanism, not by the scalar-mixing term (or κ_H term) as in the $U(1)$ gauge extended model which we have discussed before. The masses of other heavy Higgs bosons (φ_2^0, $\varphi_2^\pm$) are $m_{H_1}^2 + m_{H_2}^2$, which is approximately given by $\simeq \Lambda_{HC}^2$. It is worth noting that, in addition to particles with the $\mathcal{O}(\Lambda_{\rm HC})$ mass on the natural scale of HC dynamics, the present model predicts a light pseudoscalar s with mass of $\mathcal{O}(g_S\Lambda_{\rm HC})$ ($\ll \Lambda_{\rm HC}$), as the consequence of the bosonic seesaw mechanism.

As has been clarified in Eq. (6.22), the square of masses for fluctuating fields (h_1^0, h_2^0, s, e_0) are properly positive-definite at the chosen stationary space (v_1, v_2, v_S, v_η) satisfying the stationary conditions Eq. (6.20) with $v_2 = 0$. This implies that the vacuum has safely been aligned to where the EW symmetry is broken with extra nonzero CP-odd VEVs (v_S, v_η). By taking some reference values for the potential parameters, we have numerically checked that the EW-broken vacuum indeed locates at the global minimum. Actually, the alignment problem should be argued by taking into account all the possible vacuums including nonzero VEVs for other composite HC Higgs fields like $\bar{\chi}\chi$, $\bar{\psi}\psi$, and so forth. However, due to the presence of the chiral symmetry in the underlying HC theory, one can be allowed to rotate the composite HC Higgs fields to be aligned to the desired direction, where the potential is minimized at the EW-broken vacuum. More rigorous proof is to be beyond scope of the present study, which will be argued elsewhere.

Since the Yukawa terms in Eqs. (6.3) and (6.4) explicitly break the chiral $SU(3)_L \times SU(3)_R$ symmetry, the eight NG bosons become pseudo's (HC-pions Π^a) through those

[1] If there is non-negligible mixing between h_1 and s, the Higgs phenomena would deviate from the SM case, and they could be evidence of the beyond the SM. However, they are strictly constrained by the results of collider experiments, so we do not consider such a situation in this work.

interactions. Using the current algebra technique and expanding things in powers of y and g_S, we can evaluate the HC-pion masses and find that they are almost degenerate to be

$$m_\Pi \simeq 2(g_S v_S)\frac{\Lambda_{\rm HC}}{f} \qquad \text{with} \quad f = \frac{f_\Pi}{\sqrt{N_{\rm HC}/3}}\,, \tag{6.23}$$

where f_Π is the HC-pion decay constant. The detail of the derivation for this formula is presented in the next section. For $f \sim \Lambda_{\rm HC}/(4\pi)$, the HC-pion masses depend on $(g_S v_S)$, while it is expected to be $\mathcal{O}(\Lambda_{\rm HC})$ as same as the QCD-pions. Thus, the small g_S ($\ll 1$) predicts relatively large v_S, which is typically much larger than $\Lambda_{\rm HC}$.

The scale $\Lambda_{\rm HC}$ can be set by considering the bosonic seesaw relation derived so as to realize the EW symmetry breaking, $\lambda_\Theta v_1^2 \simeq \Lambda_{\rm HC}^2$ [see Eq. (6.20)], with $v_1 = 246\,\text{GeV}$. Here, the self-coupling of the composite Higgs doublet Θ, λ_Θ, can be estimated, in a way analogous to the linear sigma model of QCD, to be $\lambda_\Theta = \mathcal{O}(10^{2\text{-}3})$.[2] Hence, $\Lambda_{\rm HC}$ is expected to be of $\mathcal{O}(1)\,\text{TeV}$, and then, new particles masses are $\mathcal{O}(1)\,\text{TeV}$ except for the s mass which is given by $\mathcal{O}(g_S)\,\text{TeV}$.

As a reference value, we may set the HC-pion mass to be $750\,\text{GeV}$ [3] so that the combination $(g_S v_S)$ can be fixed as

$$(g_S v_S) \simeq 30\,\text{GeV} \times \left(\frac{m_\Pi}{750\,\text{GeV}}\right)\left(\frac{4\pi f}{\Lambda_{\rm HC}}\right)\,. \tag{6.24}$$

Then, we may take $\Lambda_{\rm HC} \sim 4\pi f$ to get the formula for the coupling g_S,

$$g_S \simeq \frac{30\,\text{GeV}}{v_S} \times \left(\frac{m_\Pi}{750\,\text{GeV}}\right) \ll 1\,, \tag{6.25}$$

which implies $v_S \gtrsim \mathcal{O}(1\,\text{TeV})$. Actually, if we consider s as an invisible axion-like DM as discussed in the next chapter, v_S is much larger than the TeV scale as $\sim 10^{13}\,\text{GeV}$, in which g_S is much smaller than unity as $\sim 10^{-12}$.

6.3 Computation of HC-pion masses

In this Appendix we shall calculate the HC-pion masses arising from the Yukawa terms in Eqs. (6.3) and (6.4).

[2] Recall the QCD sigma meson mass, on the order of GeV, is expressed by the linear sigma model as $m_\sigma \sim \sqrt{\lambda_\sigma} f_\pi$ with the QCD pion decay constant $f_\pi \sim 100$ MeV and the quartic coupling λ_σ. From this relation we find $\lambda_\sigma \sim 100$.

[3] Actually, this value was motivated by the LHC diphoton excess at around $750\,\text{GeV}$ providing in Refs. [147, 148]. However, the diphoton excess already has disappeared in the recent analyses [149, 150]. Nevertheless, the following technique of numerical calculation for the collider physics can be useful to search new physics.

6.3.1 Masses from the g_S-term

First of all, one should note that the nonzero VEV of S, v_S, is required in the present model, which provides masses for the eight HC-pions (Π^a) via the g_S-term in Eq. (6.4). The HC-pion masses can be evaluated according to the standard current algebra, which turn out to show up at the second order of perturbation in g_S:

$$(m_\Pi^2)^{ab}\Big|_{g_S} = -\frac{i}{2} g_S^2 v_S^2 \int d^4x \langle \Pi^a | T(J_P(x) J_P(0)) | \Pi^b \rangle \,, \tag{6.26}$$

where $J_P(x) = i\bar{F}(x)\gamma_5 F(x)$, and the symbol T stands for the time-ordered product. We use the partially-conserved axialvector current (PCAC) relations and the current algebra,

$$\begin{aligned} &\partial^\mu J^a_{\mu 5}(x) = -f_\Pi m_\Pi^2 \, \Pi^a(x) \,, \\ &[iQ^a_5, \, \mathcal{O}(x)] = \delta^a_5 \mathcal{O}(x) \,, \qquad Q^a_5 = \int d^3x J^0_5(x) \,, \end{aligned} \tag{6.27}$$

where the current $J^a_{\mu 5}$ is defined as $J^a_{\mu 5} = \bar{F}\gamma_\mu\gamma_5(\lambda^a/2)F$ with the Gell-Mann matrix λ^a ($a = 1, \cdots, 8$); f_Π is the Π-decay constant, defined as $\langle 0 | J^a_\mu(0) | \Pi^b(p) \rangle = -ip_\mu f_\Pi \delta^{ab}$; the $\mathcal{O}$ denotes an arbitrary Heisenberg operator, and δ^a_5 denotes the infinitesimal-chiral transformation, which acts on the F-fermion as $\delta^a_5 F = -i\gamma_5(\lambda^a/2)F$. Using these together with the reduction formula, one thus evaluates Eq. (6.26) to arrive at

$$\begin{aligned} (m_\Pi^2)^{ab}\Big|_{g_S} &= m_\Pi^2 = -4i\frac{g_S^2 v_S^2}{f_\Pi^2}\,\delta^{ab} \int d^4x \left(\langle 0 | T(J^a_S(x) J^b_S(0)) | 0 \rangle - \langle 0 | T(J_{\eta'}(x) J_{\eta'}(0)) | 0 \rangle \delta^{ab} \right) \\ &= 4\frac{g_S^2 v_S^2}{f_\Pi^2}\,\delta^{ab}\,\left[\Pi_S(0) - \Pi_{\eta'}(0)\right] \,, \end{aligned} \tag{6.28}$$

where $J^a_S(x) = \bar{F}(x)(\lambda^a/2)F(x)$, $J_{\eta'}(x) = \frac{1}{\sqrt{6}}\bar{F}(x)i\gamma_5 F(x)$, and we have defined the current correlators $\Pi_{S,\eta'}$ as

$$\begin{aligned} &\int d^4x e^{ipx} \langle 0 | T(J^a_S(x) J^b_S(0)) | 0 \rangle \equiv i\Pi_S(p^2)\delta^{ab} \,, \\ &\int d^4x e^{ipx} \langle 0 | T(J_{\eta'}(x) J_{\eta'}(0)) | 0 \rangle \equiv i\Pi_{\eta'}(p^2) \,. \end{aligned} \tag{6.29}$$

We may expand the correlators by assuming the resonances pole saturation,

$$\begin{aligned} \Pi_S(p^2) &= \sum_{n=1}^{\infty} \frac{F^2_{S_n} m^2_{S_n}}{m^2_{S_n} - p^2} \,, \\ \Pi_{\eta'}(p^2) &= \sum_{n=1}^{\infty} \frac{F^2_{\eta'_n} m^2_{\eta'_n}}{m^2_{\eta'_n} - p^2} \,, \end{aligned} \tag{6.30}$$

with the masses (m_{S_n}, $m_{\eta'_n}$) and the decay constants (F_{S_n}, $F_{\eta'_n}$). Then, the HC-pion mass formula in Eq. (6.28) is rewritten as a sum rule to be

$$m_\Pi^2\Big|_{g_S} = 4\frac{g_S^2 v_S^2}{f_\Pi^2} \sum_n \left[F^2_{S_n} - F^2_{\eta'_n} \right] \,. \tag{6.31}$$

Analogously to the QCD case, the $\eta' \equiv \eta'_{(n=1)}$ decay constant $F_{\eta'_1}$ is expected to be of order of the pion decay constant [151], $f_\Pi \sim \mathcal{O}(\frac{\Lambda_{\rm HC}}{4\pi})$, and the higher resonance contributions could numerically be canceled each other in the sum over the scalar and pseudoscalar sectors, namely, by $F_{S_n} \simeq F_{\eta'_n} \simeq \mathcal{O}(\Lambda_{\rm HC})$ for $n \geq 2$. Thus, we may evaluate the sum rule just by keeping the lowest resonance contribution:

$$\begin{aligned} m_\Pi^2\Big|_{g_S} &\simeq 4\frac{g_S^2 v_S^2}{f_\Pi^2}\left(F_{S_1}^2 - F_{\eta'_1}^2\right) \\ &\simeq 4\frac{g_S^2 v_S^2}{f_\Pi^2/(N_{\rm HC}/3)}\Lambda_{\rm HC}^2\,, \end{aligned} \tag{6.32}$$

where in the last line we have clarified that the mass is independent of the number of HC, $N_{\rm HC}$.

6.3.2 Masses from the y-term

Similarly to the g_S-term, the y-Yukawa term ($\mathcal{L}_y$) in Eq. (6.3) gives masses to the HC-pions via the H-Higgs VEV $v_1 \simeq 246\,\text{GeV}$. Again, the estimate of the mass can be done by using the current algebra technique:

$$\begin{aligned} (m_\Pi^2)^{ab}\Big|_y &= -\frac{1}{f_\Pi^2}\langle 0|[iQ_5^a,\,[iQ_5^b,\,\mathcal{L}_y]]|0\rangle \\ &= -\frac{yv_1}{\sqrt{2}f_\Pi^2}\langle 0|[iQ_5^a,\,[iQ_5^b,\,\bar{\chi}_2\psi + \bar{\psi}\chi_2]]|0\rangle\,. \end{aligned} \tag{6.33}$$

The nonzero elements for the mass matrix are thus found be

$$\begin{aligned} (m_\Pi^2)^{14}\Big|_y &= (m_\Pi^2)^{14}\Big|_y = -\frac{yv_1}{f_\Pi^2}\langle\bar{F}F\rangle\,, \\ (m_\Pi^2)^{25}\Big|_y &= (m_\Pi^2)^{52}\Big|_y = -\frac{yv_1}{f_\Pi^2}\langle\bar{F}F\rangle\,, \\ (m_\Pi^2)^{36}\Big|_y &= (m_\Pi^2)^{63}\Big|_y = \frac{yv_1}{f_\Pi^2}\langle\bar{F}F\rangle\,, \\ (m_\Pi^2)^{68}\Big|_y &= (m_\Pi^2)^{86}\Big|_y = \sqrt{3}\frac{yv_1}{f_\Pi^2}\langle\bar{F}F\rangle\,, \end{aligned} \tag{6.34}$$

where $\langle\bar{F}F\rangle$ denotes the chiral condensate per flavors, i.e., $\langle\bar{F}F\rangle = \langle\bar{\chi}_1\chi_1\rangle = \langle\bar{\chi}_2\chi_2\rangle = \langle\bar{\psi}\psi\rangle$.

6.3.3 Diagonalization of the HC-pion sector

Combining Eq. (6.32) with Eq. (6.34). one finds the HC-pion mass matrix acting on the current-eigenstate vector $(\Pi^1, \cdots, \Pi^8)^T$:

$$\left(\begin{array}{c|c|c|c|c|c|c|c}
m_{gS}^2 & 0 & 0 & (m_y^2)^{14} & 0 & 0 & 0 & 0 \\ \hline
0 & m_{gS}^2 & 0 & 0 & (m_y^2)^{25} & 0 & 0 & 0 \\ \hline
0 & 0 & m_{gS}^2 & 0 & 0 & (m_y^2)^{36} & 0 & 0 \\ \hline
(m_y^2)^{41} & 0 & 0 & m_{gS}^2 & 0 & 0 & 0 & 0 \\ \hline
0 & (m_y^2)^{52} & 0 & 0 & m_{gS}^2 & 0 & 0 & 0 \\ \hline
0 & 0 & (m_y^2)^{63} & 0 & 0 & m_{gS}^2 & 0 & (m_y^2)^{68} \\ \hline
0 & 0 & 0 & 0 & 0 & 0 & m_{gS}^2 & 0 \\ \hline
0 & 0 & 0 & 0 & 0 & (m_y^2)^{86} & 0 & m_{gS}^2
\end{array}\right), \tag{6.35}$$

where m_{gS}^2 and $(m_y^2)^{ab}$ respectively stand for the masses in Eqs. (6.32) and (6.34). The mass matrix can easily be diagonalized by an orthogonal rotation, which relates the current eigenstates $\{\Pi\}$ with the mass eigenstates $\{\tilde{\Pi}\}$ as

$$\begin{aligned}
\begin{pmatrix} \tilde{\Pi}^1 \\ \tilde{\Pi}^4 \end{pmatrix} &= \begin{pmatrix} -\frac{1}{\sqrt{2}} & \frac{1}{\sqrt{2}} \\ \frac{1}{\sqrt{2}} & \frac{1}{\sqrt{2}} \end{pmatrix} \begin{pmatrix} \Pi^1 \\ \Pi^4 \end{pmatrix}, \\
\begin{pmatrix} \tilde{\Pi}^2 \\ \tilde{\Pi}^5 \end{pmatrix} &= \begin{pmatrix} -\frac{1}{\sqrt{2}} & \frac{1}{\sqrt{2}} \\ \frac{1}{\sqrt{2}} & \frac{1}{\sqrt{2}} \end{pmatrix} \begin{pmatrix} \Pi^2 \\ \Pi^5 \end{pmatrix}, \\
\begin{pmatrix} \tilde{\Pi}^3 \\ \tilde{\Pi}^6 \\ \tilde{\Pi}^8 \end{pmatrix} &= \begin{pmatrix} -\frac{\sqrt{3}}{\sqrt{2}} & 0 & \frac{1}{2} \\ \frac{1}{2\sqrt{2}} & -\frac{1}{\sqrt{2}} & \frac{1}{2}\sqrt{\frac{3}{2}} \\ \frac{1}{2\sqrt{2}} & \frac{1}{\sqrt{2}} & \frac{1}{2}\sqrt{\frac{3}{2}} \end{pmatrix} \begin{pmatrix} \Pi^3 \\ \Pi^6 \\ \Pi^8 \end{pmatrix}, \\
\tilde{\Pi}^7 &= \Pi^7 ,
\end{aligned} \tag{6.36}$$

with the mass eigenvalues,

$$\begin{aligned}
& m_{\tilde{\Pi}^1}^2 = m_{\tilde{\Pi}^2}^2 \simeq m_{gS}^2 + \frac{y v_1 \langle \bar{F} F \rangle}{\sqrt{2} f_\Pi^2} , \\
& m_{\tilde{\Pi}^3}^2 \simeq m_{gS}^2 , \\
& m_{\tilde{\Pi}^4}^2 = m_{\tilde{\Pi}^5}^2 \simeq m_{gS}^2 - \frac{y v_1 \langle \bar{F} F \rangle}{\sqrt{2} f_\Pi^2} , \\
& m_{\tilde{\Pi}^6}^2 \simeq m_{gS}^2 - \frac{\sqrt{2} y v_1 \langle \bar{F} F \rangle}{f_\Pi^2} , \\
& m_{\tilde{\Pi}^7}^2 \simeq m_{gS}^2 , \\
& m_{\tilde{\Pi}^8}^2 \simeq m_{gS}^2 + \frac{\sqrt{2} y v_1 \langle \bar{F} F \rangle}{f_\Pi^2} ,
\end{aligned} \tag{6.37}$$

where terms of $\mathcal{O}(y^2)$ have been neglected.

By tuning y to be $\ll 1$, we can neglect the y-corrections to the HC-pion masses. Note that, even if those off-diagonal corrections are numerically neglected, the HC-pions significantly mix independently of the y as in Eq. (6.36): this is the reflection of degenerate perturbation theory well-known in the quantum mechanics. Such a "non-decoupling" mixing will thus affect the HC-pion phenomenology as described in the next sections.

6.4 Effective chiral Lagrangian

In this Appendix we present the effective chiral Lagrangian for the HC-pions and derive interaction terms relevant to study the LHC phenomenology.

The low-energy effective theory of the present model can be described by the HC-pion fields Π, by the nonlinear realization of the underlying flavor chiral $SU(3)_L \times SU(3)_R$ symmetry associated with the flavor condensate of F-fermions $F_{L,R} = (\chi_i,\, \psi)_{L,R}$ $(i = 1, 2)$, $\langle \bar{\chi}_i \chi_i \rangle = \langle \bar{\psi}\psi \rangle \neq 0$. The basic variable to construct the effective model is the chiral field U, which transforms under the global chiral symmetry as $U \to g_L \cdot U \cdot g_R^\dagger$, where $g_{L,R}$ belong to the chiral $SU(3)_{L,R}$ groups, respectively. When the SM gauges are turned on, the global chiral symmetry is partially localized according to the SM-gauge embedding as in Ref. [95]. Then, the effective gauged-chiral Lagrangian invariant under the chiral $SU(3)_L \times SU(3)_R$ and $U(1)_V$ symmetries is written as

$$\begin{aligned}
\mathcal{L}_{\rm eff} &= \mathcal{L}_{\rm kin} + \mathcal{L}_{\rm mass} + \cdots\,, \\
\mathcal{L}_{\rm kin} &= \frac{f_\Pi^2}{4}\,{\rm tr}[|D_\mu U|^2]\,, \\
\mathcal{L}_{\rm mass} &= b\,{\rm tr}[U\mathcal{M}^\dagger + {\rm h.c.}]\,,
\end{aligned} \tag{6.38}$$

where

$$\begin{aligned}
U &= \exp\left(\frac{2i\Pi}{f_\Pi}\right) = \exp\left(\frac{2i\sum_{a=1}^{8}\Pi^a\frac{\lambda^a}{2}}{f_\Pi}\right)\,, \\
D_\mu U &= \partial_\mu U - i[\mathcal{V}_\mu,\, U]\,, \\
\mathcal{V}_\mu &= g_2 W_\mu + g_Y \frac{Y_F}{2} B_\mu = g_W \sum_{a=1}^{3} \frac{\lambda^a}{2} W_\mu^a + g_Y \frac{Y_F}{2} B_\mu\,, \\
Y_F &= \frac{\sqrt{3}}{6}\lambda_8 + \frac{1}{\sqrt{6}}\lambda_0 = \begin{pmatrix} 1 & & \\ & 1 & \\ & & 0 \end{pmatrix}\,, \qquad \lambda_0 = \frac{2}{\sqrt{6}}\mathbf{1}_{3\times 3}\,,
\end{aligned} \tag{6.39}$$

with the EW gauge fields $(W_\mu^a,\, B_\mu)$. The chiral field U parametrizes the HC-pion fields regarding to the spontaneous breaking of the chiral $SU(3)_L \times SU(3)_R$ symmetry down to the diagonal subgroup $SU(3)_V$, just like the ordinary QCD, with the associated HC-pion decay constant f_Π. The electroweak charges of U have come from the underlying

F-fermion fields and its vector-like condensate [95]. In Eq. (6.38), the spurion field $\mathcal{M}$ has been introduced, in which $\mathcal{M}$ transforms under the chiral symmetry as same as U, i.e., $\mathcal{M} \to g_L \cdot \mathcal{M} \cdot g_R^\dagger$. The spurion field is assumed to get the vacuum expectation value, $\langle \mathcal{M} \rangle = \mathbf{1}_{3\times 3}$, leading to the explicit breaking of the chiral symmetry. Then, the $\mathcal{L}_{\rm mass}$ term can be matched to the underlying explicit breaking term, as discussed in the previous section, to determine the parameter b in front of it. The explicit relation between the parameter b and those explicit breaking coefficients will be irrelevant for the present study, so will not be specified here.

In addition to the Lagrangian in Eq. (6.38), the HC sector yields anomalous vertices related to the chiral $SU(3)_L \times SU(3)_R$ anomaly with the SM charges gauged, *a la* Wess-Zumino-Witten term [152]. Such terms give significant contributions to HC-pion decays to dibosons involving photons. Taking into account the fact that only vectorial symmetry has been gauged at present, one easily finds that only the following term is relevant for the diboson processes:

$$\mathcal{L}_{\rm WZW} = -\frac{N_{\rm HC}}{4\pi^2 f_\Pi} \epsilon^{\mu\nu\rho\sigma} {\rm tr}[\partial_\mu \mathcal{V}_\nu \partial_\rho \mathcal{V}_\sigma \Pi] \,. \tag{6.40}$$

In terms of the mass-eigenstate gauge fields ($W_\mu^\pm$, A_μ, Z_μ) as given in Sec. 2.1, the external gauge field $\mathcal{V}_\mu$ is expressed as

$$\mathcal{V}_\mu = \frac{e}{\sqrt{2} s_W} \left(W_\mu^+ I^+ + W_\mu^- I^- \right) + e Q_{\rm em}^F A_\mu + \frac{e}{s_W c_W} \left(I^3 - s_W^2 Q_{\rm em}^F \right) Z_\mu \,, \tag{6.41}$$

with

$$I^3 = \frac{\lambda^3}{2} \,, \qquad I^\pm = \frac{\lambda^1 \pm i\lambda^2}{2} \,, \qquad Q_{\rm em}^F = I^3 + \frac{Y_F}{2} = \begin{pmatrix} 1 & & \\ & 0 & \\ & & 0 \end{pmatrix} \,, \tag{6.42}$$

Expanding the Π field parametrized as in Eq. (6.39) in terms of the component fields Π^a, and using Eq. (6.41), one readily finds that the couplings to neutral Π's arise as follows:

$$\begin{aligned}
\mathcal{L}_{\rm WZW}^{\rm NC} = & -\frac{N_{\rm HC}}{4\pi^2 f_\Pi} \sum_{a=3,6,8} \Bigg[{\rm tr}[I^a \{I^+,\, I^-\}] \cdot \frac{e^2}{2 s_W^2} dW^+ dW^- \Pi^a \\
& + {\rm tr}[I^a \{Q_{\rm em}^F,\, I^3 - s_W^2 Q_{\rm em}^F\}] \cdot \frac{e^2}{s_W c_W} dA dZ \Pi^a \\
& + {\rm tr}[I^a Q_{\rm em}^F Q_{\rm em}^F] \cdot e^2 dA dA \Pi^a - {\rm tr}[I^a \left(\{I^3,\, Q_{\rm em}^F\} - s_W^2 Q_{\rm em}^F Q_{\rm em}^F \right)] \cdot \frac{e^2}{c_W^2} dZ dZ \Pi^a \Bigg] \\
= & -\frac{N_{\rm HC}}{4\pi^2 f_\Pi} \left[\frac{e^2}{2} dA dA + \frac{e^2 (c_W^2 - s_W^2)}{2 s_W c_W} dA dZ - \frac{e^2}{2} dZ dZ \right] \left(\Pi^3 + \frac{\Pi^8}{\sqrt{3}} \right) \\
& - \frac{N_{\rm HC}}{4\pi^2 f_\Pi} \left[\frac{e^2}{2 s_W^2} dW^+ dW^- \right] \left(\frac{\Pi^8}{\sqrt{3}} \right) \,,
\end{aligned} \tag{6.43}$$

where $dV_1 dV_2 \equiv \epsilon^{\mu\nu\rho\sigma}\partial_\mu V_{1\nu}\partial_\rho V_{2\sigma}$, and $I^a = \lambda^a/2$. In terms of the mass-eigenstate pions $\{\tilde{\Pi}\}$ in Eq. (6.36), the WZW interaction terms for the neutral pions are expressed as

$$\begin{aligned}\mathcal{L}^{\rm NC}_{\rm WZW} = & -\frac{N_{\rm HC}}{4\pi^2 f_\Pi}\left[\left(-\frac{e^2}{2}dAdA + \frac{7e^2}{16s_W^2}dW^+dW^- - \frac{e^2(c_W^2-s_W^2)}{2s_Wc_W}dAdZ + \frac{e^2}{2}dZdZ\right)\frac{\tilde{\Pi}^3}{\sqrt{3}}\right.\\ & \left. + \left(\frac{e^2}{2}dAdA + \frac{3e^2}{16s_W^2}dW^+dW^- + \frac{e^2(c_W^2-s_W^2)}{2s_Wc_W}dAdZ - \frac{e^2}{2}dZdZ\right)\frac{\tilde{\Pi}^6+\tilde{\Pi}^8}{\sqrt{2}}\right].\end{aligned} \tag{6.44}$$

The LHC phenomenology will closely be studied in the next section.

On the other hand, the charged current couplings to the current-eigenstate pions $\{\Pi\}$ are

$$\begin{aligned}\mathcal{L}^{\rm CC}_{\rm WZW} = & -\frac{N_{\rm HC}}{4\pi^2 f_\Pi}\sum_a\left[{\rm tr}[\{I^\pm,\, Q^F_{\rm em}\}I^a]\frac{e^2}{\sqrt{2}s_W}dW^\pm dA\Pi^a\right.\\ & \left. - {\rm tr}[\{I^\pm,\, Q^F_{\rm em}\}I^a]\frac{e^2}{\sqrt{2}c_W}dW^\pm dZ\Pi^a\right]\\ = & -\frac{N_{\rm HC}}{4\pi^2 f_\Pi}\left[\frac{e^2}{2s_W}dW^\pm dA\Pi^\mp - \frac{e^2}{2c_W}dW^\pm dZ\Pi^\mp\right],\end{aligned} \tag{6.45}$$

where the charged pions are defined as

$$\Pi^\pm \equiv \frac{\Pi^1 \mp i\Pi^2}{\sqrt{2}}. \tag{6.46}$$

Writing things in terms of the mass-eigenstates $\{\tilde{\Pi}\}$ with use of Eq. (6.36), one gets the charged-current interaction terms,

$$\mathcal{L}^{\rm CC}_{\rm WZW} = -\frac{N_{\rm HC}}{4\pi^2 f_\Pi}\left[-\frac{e^2}{2\sqrt{2}s_W}dW^\pm dA(\tilde{\Pi}^\mp - \tilde{\Pi}'^\mp) + \frac{e^2}{2\sqrt{2}c_W}dW^\pm dZ(\tilde{\Pi}^\mp - \tilde{\Pi}'^\mp)\right], \tag{6.47}$$

where the mass-eigenstates of charged pions are defined as

$$\tilde{\Pi}^\pm \equiv \frac{\tilde{\Pi}^1 \mp i\tilde{\Pi}^2}{\sqrt{2}}, \qquad \tilde{\Pi}'^\pm \equiv \frac{\tilde{\Pi}^4 \mp i\tilde{\Pi}^5}{\sqrt{2}}. \tag{6.48}$$

In addition to the eight HC-pions, one may write down the WZW term for η' coupled to the associate current $J^0_{\mu 5} = \frac{1}{\sqrt{6}}\bar{F}i\gamma_5 F$, in a way similar to Π's:

$$\mathcal{L}^{\eta'}_{\rm WZW} = -\frac{N_{\rm HC}}{4\pi^2 f_\Pi}\left[e^2 dAdA + \frac{e^2(c_W^2-s_W^2)}{s_Wc_W}dAdZ - e^2 dZdZ\right]\frac{\eta'}{\sqrt{6}}. \tag{6.49}$$

Since the η' mixes with the pseudoscalar S through Eq. (6.15), in terms of the mass-eigenstates $(s,\, e_0)$ the WZW term for the η' now looks like

$$\mathcal{L}^{\eta'}_{\rm WZW} \simeq -\frac{N_{\rm HC}}{4\pi^2 f_\Pi}\left[e^2 dAdA + \frac{e^2(c_W^2-s_W^2)}{s_Wc_W}dAdZ - e^2 dZdZ\right]\frac{(g_S s + e_0)}{\sqrt{6}}, \tag{6.50}$$

up to terms suppressed by $\mathcal{O}(g_S^2)$. Here, we have omitted the CP-violating terms like $dAdA$, $dAdZ$ and $dWdW$, since they can be washed out due to the fact that the $SU(2)_L \times U(1)_Y$ groups themselves are topologically trivial.

6.5 HC-pions at the LHC

In this section, we shall present quantities relevant for the HC-pion phenomenologies at the LHC and calculate the HC-pion production cross sections.

6.5.1 The decay properties

From Eq. (6.44), one can easily calculate the partial decay rates for the neutral HC-pions $\tilde{\Pi}^{3,6,8}$ to find

$$\begin{aligned}
\Gamma(\tilde{\Pi}^3 \to \gamma\gamma) &= \left(\frac{N_{\rm HC}\alpha_{\rm em}}{2\sqrt{3}\pi f_\Pi}\right)^2 \frac{m_\Pi^3}{16\pi}\,, \\
\Gamma(\tilde{\Pi}^3 \to WW) &= \left(\frac{7N_{\rm HC}\alpha_{\rm em}}{16\sqrt{3}\pi f_\Pi s_W^2}\right)^2 \frac{m_\Pi^3}{32\pi}\left(1-\frac{4m_W^2}{m_\Pi^2}\right)^{3/2}\,, \\
\Gamma(\tilde{\Pi}^3 \to ZZ) &= \left(\frac{N_{\rm HC}\alpha_{\rm em}}{2\sqrt{3}\pi f_\Pi}\right)^2 \frac{m_\Pi^3}{16\pi}\left(1-\frac{4m_Z^2}{m_\Pi^2}\right)^{3/2}\,, \\
\Gamma(\tilde{\Pi}^3 \to Z\gamma) &= \left(\frac{N_{\rm HC}\alpha_{\rm em}}{2\sqrt{3}\pi f_\Pi}\frac{c_W^2-s_W^2}{s_W c_W}\right)^2 \frac{m_\Pi^3}{32\pi}\left(1-\frac{m_Z^2}{m_\Pi^2}\right)^{3}\,,
\end{aligned} \tag{6.51}$$

and

$$\begin{aligned}
\Gamma(\tilde{\Pi}^{6,8} \to \gamma\gamma) &= \left(\frac{N_{\rm HC}\alpha_{\rm em}}{2\sqrt{2}\pi f_\Pi}\right)^2 \frac{m_\Pi^3}{16\pi}\,, \\
\Gamma(\tilde{\Pi}^{6,8} \to WW) &= \left(\frac{3N_{\rm HC}\alpha_{\rm em}}{16\sqrt{2}\pi f_\Pi s_W^2}\right)^2 \frac{m_\Pi^3}{32\pi}\left(1-\frac{4m_W^2}{m_\Pi^2}\right)^{3/2}\,, \\
\Gamma(\tilde{\Pi}^{6,8} \to ZZ) &= \left(\frac{N_{\rm HC}\alpha_{\rm em}}{2\sqrt{2}\pi f_\Pi}\right)^2 \frac{m_\Pi^3}{16\pi}\left(1-\frac{4m_Z^2}{m_\Pi^2}\right)^{3/2}\,, \\
\Gamma(\tilde{\Pi}^{6,8} \to Z\gamma) &= \left(\frac{N_{\rm HC}\alpha_{\rm em}}{2\sqrt{2}\pi f_\Pi}\frac{c_W^2-s_W^2}{s_W c_W}\right)^2 \frac{m_\Pi^3}{32\pi}\left(1-\frac{m_Z^2}{m_\Pi^2}\right)^{3}\,,
\end{aligned} \tag{6.52}$$

where $\alpha_{\rm em} = e^2/(4\pi)$. We will hereafter take the mass to be $m_\Pi = 750\,\text{GeV}$ as a reference value. Note that the branching fractions of $\tilde{\Pi}^{3,6,8}$ are completely determined independently of $N_{\rm HC}$ and f_Π, once the masses and the weak mixing angle are fixed. Thus, one gets

$$\begin{aligned}
{\rm Br}(\tilde{\Pi}^3 \to \gamma\gamma) &\simeq 0.10\,, \\
{\rm Br}(\tilde{\Pi}^3 \to WW) &\simeq 0.72\,, \\
{\rm Br}(\tilde{\Pi}^3 \to ZZ) &\simeq 0.091\,, \\
{\rm Br}(\tilde{\Pi}^3 \to Z\gamma) &\simeq 0.085\,,
\end{aligned} \tag{6.53}$$

and

$$\begin{aligned}
\mathrm{Br}(\tilde{\Pi}^{6,8} \to \gamma\gamma) &\simeq 0.24\,, \\
\mathrm{Br}(\tilde{\Pi}^{6,8} \to WW) &\simeq 0.32\,, \\
\mathrm{Br}(\tilde{\Pi}^{6,8} \to ZZ) &\simeq 0.22\,, \\
\mathrm{Br}(\tilde{\Pi}^{6,8} \to Z\gamma) &\simeq 0.21\,.
\end{aligned} \tag{6.54}$$

The total width is calculated as a function of $N_{\rm HC}$ and $f \equiv f_\Pi/\sqrt{N_{\rm HC}/3}$. For $f = 92\,\mathrm{GeV}$ (or equivalently $\Lambda_{\rm HC} \sim 1.2\,\mathrm{TeV}$), we have

$N_{\rm HC}$	$\Gamma_{\rm tot}(\tilde{\Pi}^3)$ [MeV]	$\Gamma_{\rm tot}(\tilde{\Pi}^{6,8})$ [MeV]
3	46	28
4	61	38
5	76	47

. (6.55)

The partial decay widths for the charged HC-pions ($\tilde{\Pi}^\pm$, $\tilde{\Pi}'^\pm$) are calculated from Eq. (6.47) as

$$\begin{aligned}
\Gamma(\tilde{\Pi}^{(\prime)\pm} \to W^\pm\gamma) &= \left(\frac{N_{\rm HC}\alpha_{\rm em}}{2\sqrt{2}\pi f_\Pi s_W}\right)^2 \frac{m_\Pi^3}{32\pi}\left(1 - \frac{m_W^2}{m_\Pi^2}\right)^3\,, \\
\Gamma(\tilde{\Pi}^{(\prime)\pm} \to W^\pm Z) &= \left(\frac{N_{\rm HC}\alpha_{\rm em}}{2\sqrt{2}\pi f_\Pi c_W}\right)^2 \frac{m_\Pi^3}{32\pi}\left[1 - \frac{(m_W+m_Z)^2}{m_\Pi^2}\right]^{3/2}\left[1 - \frac{(m_W-m_Z)^2}{m_\Pi^2}\right]^{3/2}\,.
\end{aligned} \tag{6.56}$$

Again, the mass has been set to $\simeq 750\,\mathrm{GeV}$. The branching ratios are computed independently of f_Π and $N_{\rm HC}$ to be

$$\begin{aligned}
\mathrm{Br}[\tilde{\Pi}^{(\prime)\pm} \to W^\pm\gamma] &\simeq 0.79\,, \\
\mathrm{Br}[\tilde{\Pi}^{(\prime)\pm} \to W^\pm Z] &\simeq 0.21\,.
\end{aligned} \tag{6.57}$$

For $f = 92$ GeV, the total widths are

$N_{\rm HC}$	$\Gamma_{\rm tot}(\tilde{\Pi}^{(\prime)\pm})$ [MeV]
3	19
4	25
5	32

. (6.58)

The neutral $\tilde{\Pi}^7$ does not couple in the WZW term as seen from Eq. (6.44). They may be searched through the multi-body cascade-decay processes like $\tilde{\Pi}^7 \to Z^*/\gamma^* + \tilde{\Pi}^{3,6,8} \to l^+l^- + \gamma\gamma$, $\tilde{\Pi}^7 \to Z^*/\gamma^* + \tilde{\Pi}^{3,6,8} \to jj + \gamma\gamma$.

6.5.2 The LHC productions and signals

The neutral HC-pions ($\tilde{\Pi}^{3,6,8}$) can dominantly be produced through the photon-photon fusion ($\gamma\gamma$F) process. The 750 GeV resonance production through the $\gamma\gamma$F has been

studied in Refs. [153]-[160]. We may quote the numerical number estimated in Ref. [155] to evaluate the $\gamma\gamma$F production of pseudoscalar $\tilde{\Pi}$ with the mass $m_{\tilde{\Pi}} = 750\,\mathrm{GeV}$ at $\sqrt{s} = 13\ (8)\,\mathrm{TeV}$:

$$\sigma_{\gamma\gamma\mathrm{F}}(pp \to \tilde{\Pi} \to XY) \simeq 10.8\ (5.5)\,\mathrm{pb} \times \left(\frac{\Gamma_{\mathrm{tot}}(\tilde{\Pi})}{45\,\mathrm{GeV}}\right) \times \mathrm{Br}[\tilde{\Pi} \to \gamma\gamma]\,\mathrm{Br}[\tilde{\Pi} \to XY]\,, \quad (6.59)$$

where X and Y denote particles produced via the $\tilde{\Pi}$ decays. Then, the energy scale of the cross section is approximately given by

$$\sigma_{\gamma\gamma\mathrm{F}} \propto \frac{N_{\mathrm{HC}}^2}{f_\Pi^2} \sim \frac{N_{\mathrm{HC}}}{f^2}\,, \quad (6.60)$$

where we have used $f_\Pi = f\sqrt{N_{\mathrm{HC}}/3}$. Since all neutral HC-pions $\tilde{\Pi}^{3,6,8}$ contribute to the diphoton cross section, the referenced formula in Eq. (6.59) should be appropriately modified.

First of all, consider the photon-photon scattering amplitudes mediated by $\tilde{\Pi}^{3,6,8}$ and write it as $(i\mathcal{M}_3) + (i\mathcal{M}_6) + (i\mathcal{M}_8)$. Taking into account the coupling properties of the neutral HC-pions in Eq. (6.44), we then evaluate the square of the combined scattering amplitude by factoring the Π_3 coupling as

$$\Big|(i\mathcal{M}_3) + (i\mathcal{M}_6) + (i\mathcal{M}_8)\Big|^2 \sim \Gamma^2(\tilde{\Pi}^3 \to \gamma\gamma)\Big|D_3 + 2\cdot\frac{3}{2}\,D_6\Big|^2\,, \quad (6.61)$$

where $D_i = 1/[(M_{\gamma\gamma}^2 - m_\Pi^2) + i m_\Pi \Gamma_i]$ with the total widths Γ_i for $i = 3, 6, 8$, in which $\Gamma_6 = \Gamma_8$ [see Eq. (6.55)]. Using the narrow width approximation,

$$|D_i|^2 \approx \frac{\pi}{m_\Pi \Gamma_i}\delta(M_{\gamma\gamma}^2 - m_\Pi^2)\,, \quad (6.62)$$

one can easily rewrite the right hand side of Eq. (6.61) as follows:

$$\Big|(i\mathcal{M}_3) + (i\mathcal{M}_6) + (i\mathcal{M}_8)\Big|^2 \sim \frac{\pi}{m_\Pi \Gamma_3}\delta(M_{\gamma\gamma}^2 - m_\Pi^2)\left[1 + \frac{9\Gamma_3}{\Gamma_6} + \frac{12\Gamma_3}{\Gamma_6 + \Gamma_3}\right]\Gamma^2(\tilde{\Pi}^3 \to \gamma\gamma)\,. \quad (6.63)$$

Then, the $\gamma\gamma F$ cross section at the center of mass energy $\sqrt{s}$, in which the resonance $\tilde{\Pi}^0$ decays to diphoton, is evaluated as

$$\begin{aligned}\sigma_{\gamma\gamma F}^{\gamma\gamma} = \frac{8\pi}{s}\int d\eta \int dM_{\gamma\gamma}^2 \frac{M_{\gamma\gamma}^2}{m_\Pi^2} f_{\gamma/p}\left(\frac{M_{\gamma\gamma}}{\sqrt{s}}e^{\eta}\right)\cdot f_{\gamma/p}\left(\frac{M_{\gamma\gamma}}{\sqrt{s}}e^{-\eta}\right) \\ \times \frac{\pi}{m_\Pi \Gamma_3}\delta(M_{\gamma\gamma}^2 - m_\Pi^2)\left[1 + \frac{9\Gamma_3}{\Gamma_6} + \frac{12\Gamma_3}{\Gamma_6 + \Gamma_3}\right]\Gamma^2(\tilde{\Pi}^3 \to \gamma\gamma)\,, \end{aligned} \quad (6.64)$$

with the photon luminosity function $f_{\gamma/p}$. From the referenced formula in Eq. (6.59), for $\sqrt{s} = 13\ (8)\,\mathrm{TeV}$ we read off

$$\frac{8\pi^2}{s}\frac{1}{m_\Pi}\int d\eta f_{\gamma/p}\cdot f_{\gamma/p} = 10.8\ (5.5)\,\mathrm{pb}/(45\,\mathrm{GeV})\,, \quad (6.65)$$

so that Eq. (6.64) is expressed to be

$$\sigma_{\gamma\gamma F}^{\sqrt{s}=13(8)\,\mathrm{TeV},\gamma\gamma} = 10.8\ (5.5)\,\mathrm{pb} \times \left(\frac{\Gamma_3}{45\,\mathrm{GeV}}\right) \times \frac{2}{3}\left[1 + \frac{9\Gamma_6}{\Gamma_3} + \frac{12\Gamma_6}{\Gamma_6+\Gamma_3}\right] \times \mathrm{Br}[\tilde{\Pi}^6 \to \gamma\gamma]\,\mathrm{Br}[\tilde{\Pi}^3 \to \gamma\gamma]\,, \tag{6.66}$$

where we have used $\Gamma(\tilde{\Pi}^3 \to \gamma\gamma) = 2/3\Gamma(\tilde{\Pi}^6 \to \gamma\gamma)$ read off from Eqs. (6.51) and (6.52).

Similarly, one can easily reach the results for the ZZ and $Z\gamma$ channels:

$$\sigma_{\gamma\gamma F}^{\sqrt{s}=13(8)\,\mathrm{TeV},ZZ/Z\gamma} = 10.8\ (5.5)\,\mathrm{pb} \times \left(\frac{\Gamma_3}{45\,\mathrm{GeV}}\right) \times \frac{2}{3}\left[1 + \frac{9\Gamma_6}{\Gamma_3} + \frac{12\Gamma_6}{\Gamma_6+\Gamma_3}\right] \times \mathrm{Br}[\tilde{\Pi}^6 \to \gamma\gamma]\,\mathrm{Br}[\tilde{\Pi}^3 \to ZZ/Z\gamma]\,, \tag{6.67}$$

and for the WW channel:

$$\sigma_{\gamma\gamma F}^{\sqrt{s}=13(8)\,\mathrm{TeV},WW} = 10.8\ (5.5)\,\mathrm{pb} \times \left(\frac{\Gamma_3}{45\,\mathrm{GeV}}\right) \times \frac{2}{3}\left[\frac{81}{49} + \frac{\Gamma_6}{\Gamma_3} + \frac{36}{7}\frac{\Gamma_6}{\Gamma_6+\Gamma_3}\right] \times \mathrm{Br}[\tilde{\Pi}^6 \to \gamma\gamma]\,\mathrm{Br}[\tilde{\Pi}^3 \to WW]\,, \tag{6.68}$$

where use has been made of $\Gamma(\tilde{\Pi}^3 \to ZZ/Z\gamma) = (2/3)\Gamma(\tilde{\Pi}^6 \to ZZ/Z\gamma)$ and $\Gamma(\tilde{\Pi}^3 \to WW) = (98/27)\Gamma(\tilde{\Pi}^6 \to WW)$ read off from Eqs. (6.51) and (6.52).

Taking $f = 92\,\mathrm{GeV}$ as a reference value, we give lists of the estimated cross sections for the HC-pions as below:

N_{HC}	$\sigma_{\gamma\gamma F}^{8\mathrm{TeV}}(pp \to \tilde{\Pi}^0 \to \gamma\gamma)$ [fb]	$\sigma_{\gamma\gamma F}^{13\mathrm{TeV}}(pp \to \tilde{\Pi}^0 \to \gamma\gamma)$ [fb]
3	1.3	2.5
4	1.7	3.4
5	2.2	4.3

, (6.69)

N_{HC}	$\sigma_{\gamma\gamma F}^{8\mathrm{TeV}}(pp \to \tilde{\Pi}^0 \to Z\gamma)$ [fb]	$\sigma_{\gamma\gamma F}^{13\mathrm{TeV}}(pp \to \tilde{\Pi}^0 \to Z\gamma)$ [fb]
3	1.1	2.2
4	1.5	2.9
5	1.8	3.6

, (6.70)

N_{HC}	$\sigma_{\gamma\gamma F}^{8\mathrm{TeV}}(pp \to \tilde{\Pi}^0 \to ZZ)$ [fb]	$\sigma_{\gamma\gamma F}^{13\mathrm{TeV}}(pp \to \tilde{\Pi}^0 \to ZZ)$ [fb]
3	1.2	2.3
4	1.6	3.1
5	2.0	3.9

, (6.71)

N_{HC}	$\sigma_{\gamma\gamma F}^{8\mathrm{TeV}}(pp \to \tilde{\Pi}^0 \to WW)$ [fb]	$\sigma_{\gamma\gamma F}^{13\mathrm{TeV}}(pp \to \tilde{\Pi}^0 \to WW)$ [fb]
3	2.8	5.5
4	3.7	7.3
5	4.7	9.1

,(6.72)

where $\tilde{\Pi}^0$ denotes the sum of $\tilde{\Pi}^{3,6,8}$.

The $\sqrt{s} = 8\,\text{TeV}$ 95% C.L. limits on 750 GeV scalars decaying to $\gamma\gamma$, $Z\gamma$, ZZ and WW have been placed as follows [161]-[166]:

$$\begin{aligned}
\sigma_{\gamma\gamma}^{8\,\text{TeV}}|_{\text{exp}} &\lesssim 2.3\,\text{fb}\,, \\
\sigma_{Z\gamma}^{8\,\text{TeV}}|_{\text{exp}} &\lesssim 4.0\,\text{fb}\,, \\
\sigma_{ZZ}^{8\,\text{TeV}}|_{\text{exp}} &\lesssim 12\,\text{fb}\,, \\
\sigma_{WW}^{8\,\text{TeV}}|_{\text{exp}} &\lesssim 40\,\text{fb}\,.
\end{aligned} \tag{6.73}$$

Thus, all the predicted signal strengths of $\tilde{\Pi}^{3,6,8}$ are consistent with the 8 TeV bounds.

As to the HC η', e_0, with the mass $= \mathcal{O}(1)\,\text{TeV}$, the prefactors (10.8 and 5.5) in Eq. (6.59) are changed almost according to the scaling law for the effective photon approximation as

$$\frac{\sigma_{\gamma\gamma\text{F}}(m_{e_0})}{\sigma_{\gamma\gamma\text{F}}(m_{\tilde{\Pi}} = 750\,\text{GeV})} \approx \left[\frac{\log(m_{e_0}/\sqrt{s})}{\log(750\,\text{GeV}/\sqrt{s})}\right]^3 \simeq 0.73\ (0.68)\,, \tag{6.74}$$

with the center of mass energy $\sqrt{s} = 13\ (8)\,\text{TeV}$. Thus the e_0 cross sections are evaluated as

$$\sigma_{\gamma\gamma\text{F}}(pp \to e_0 \to XY) \simeq 7.8\ (3.7)\,\text{pb} \times \left(\frac{\Gamma_{\text{tot}}(e_0)}{45\,\text{GeV}}\right) \times \text{Br}[e_0 \to \gamma\gamma]\,\text{Br}[e_0 \to XY]\,. \tag{6.75}$$

The partial decay rates are evaluated from Eq. (6.50) as

$$\Gamma\left(e_0 \to \gamma\gamma\right) = \left(\frac{N_{\text{HC}}\alpha_{\text{em}}}{\sqrt{6}\pi f_\Pi}\right)^2 \frac{m_{e_0}^3}{16\pi}\,, \tag{6.76}$$

$$\Gamma\left(e_0 \to ZZ\right) = \left(\frac{N_{\text{HC}}\alpha_{\text{em}}}{\sqrt{6}\pi f_\Pi}\right)^2 \frac{m_{e_0}^3}{16\pi}\left(1 - \frac{4m_Z^2}{m_{e_0}^2}\right)^{\frac{3}{2}}\,, \tag{6.77}$$

$$\Gamma\left(e_0 \to WW\right) = \left(\frac{N_{\text{HC}}\alpha_{\text{em}}}{\sqrt{6}\pi f_\Pi s_W^2}\right)^2 \frac{m_{e_0}^3}{32\pi}\left(1 - \frac{4m_W^2}{m_{\eta^0}^2}\right)^{\frac{3}{2}}\,, \tag{6.78}$$

$$\Gamma\left(e_0 \to Z\gamma\right) = \left(\frac{N_{\text{HC}}\alpha_{\text{em}}}{\sqrt{6}\pi f_\Pi}\frac{c_W^2 - s_W^2}{s_W c_W}\right)^2 \frac{m_{e_0}^3}{32\pi}\left(1 - \frac{m_Z^2}{m_{e_0}^2}\right)^3\,, \tag{6.79}$$

and

$$\Gamma\left(s \to \gamma\gamma\right) = \left(\frac{g_S N_{\text{HC}}\alpha_{\text{em}}}{\sqrt{6}\pi f_\Pi}\right)^2 \frac{m_s^3}{16\pi}\,. \tag{6.80}$$

The branching ratios for e_0 are computed independently of f_Π and N_{HC} as

$$\begin{aligned}
\text{Br}[e_0 \to \gamma\gamma] &\simeq 0.080\,, \\
\text{Br}[e_0 \to WW] &\simeq 0.77\,, \\
\text{Br}[e_0 \to ZZ] &\simeq 0.076\,, \\
\text{Br}[e_0 \to Z\gamma] &\simeq 0.069\,.
\end{aligned} \tag{6.81}$$

Taking $m_{e_0} = 1\,\text{TeV}$ as a reference value and $f = f_\Pi/\sqrt{N_{\rm HC}/3} = 92\,\text{GeV}$ as well, we may calculate the total width:

$N_{\rm HC}$	$\Gamma_{\rm tot}(e_0)$ [MeV]
3	273
4	364
5	455

. (6.82)

and the LHC signal strengths of e_0 produced via the $\gamma\gamma F$ process:

$N_{\rm HC}$	$\sigma^{8\text{TeV}}_{\gamma\gamma F}(pp \to e_0 \to \gamma\gamma)$ [fb]	$\sigma^{13\text{TeV}}_{\gamma\gamma F}(pp \to e_0 \to \gamma\gamma)$ [fb]
3	0.14	0.30
4	0.19	0.40
5	0.24	0.51

. (6.83)

The $\sqrt{s} = 8\,\text{TeV}$ 95% C.L. limits on 1 TeV scalars decaying to $\gamma\gamma$, $Z\gamma$, ZZ and WW have been placed as follows [161]-[166]:

$$\begin{aligned}
\sigma^{8\,\text{TeV}}_{\gamma\gamma}|_{\rm exp} &\lesssim 1.0\,\text{fb}\,,\\
\sigma^{8\,\text{TeV}}_{Z\gamma}|_{\rm exp} &\lesssim 1.5\,\text{fb}\,,\\
\sigma^{8\,\text{TeV}}_{ZZ}|_{\rm exp} &\lesssim 10\,\text{fb}\,,\\
\sigma^{8\,\text{TeV}}_{WW}|_{\rm exp} &\lesssim 35\,\text{fb}\,,
\end{aligned} \tag{6.84}$$

which are far above all the predicted signals of the e_0, to be tested at the LHC 13 TeV in the near future.

With more precise analysis on the $\gamma\gamma$ fusion as done in Ref. [167], the production cross section can be made larger by about factor of 2 than the numbers in Eq. (6.59). Then, the optimal value of the decay constant f would be made larger by about $\sqrt{2}$, i.e., $f \simeq 130\,\text{GeV}$. In that case, we would have the $\Lambda_{\rm HC} \simeq 4\pi f \simeq 1.6\,\text{TeV}$, where $m_\Pi/\Lambda_{\rm HC} \simeq 0.5$, so the chiral perturbation with respect to the HC-pion can be more plausible than the present case with $m_\Pi/\Lambda_{\rm HC} \simeq 0.7$.

6.6 Conclusion

The origin of the EW symmetry breaking has been not established yet, although the SM-like Higgs boson has been discovered. In this chapter, we have investigated the dynamical origin of the EW symmetry breaking via the bosonic seesaw mechanism in the classically scale invariant $SU(N_{\rm HC})$ extended model. The classical scale invariance is broken by the HC-fermion condensate, which is induced by strong-coupling HC dynamics. After the phase transition at $\mu = \Lambda_{\rm HC}$, there are the elementary and composite Higgs doublets, and the EW symmetry breaking dynamically occur via the bosonic seesaw mechanism. We have introduced the real pseudo-scalar singlet field to make the NG bosons become

massive. It is an interesting feature that the mass of this pseudoscalar can be much lighter than other extra particles which lie in $\mathcal{O}(\Lambda_{\rm HC})$. Thus, this pseudoscalar can be a smoking-gun of the model and will be identified as the dark matter candidate, as will be discussed in the next chapter.

Other signals characteristic to the present model involve not only HC-pions, but also the HC-η' and HC composite scalar states, both of which are expected to have the mass on the order of $\Lambda_{\rm HC}$. As briefly studied in Sec. 6.5, the HC-η' can be produced at the LHC, via the photon-photon fusion process as well as the HC-pions. The discovery channels will be similar to the HC-pions: WW, ZZ, $Z\gamma$ and $\gamma\gamma$ modes. Since the production cross section decreases as the resonance mass grows, the photon-photon fusion cross section for the HC-η' significantly gets smaller than that of the HC-pions, so it may be challenging to search at the LHC.

As to the HC composite scalars, the couplings to the SM particles are controlled by the tiny Yukawa coupling y ($\ll 1$) through the mixing with the SM Higgs. It would be worth investigating how much large the y coupling is allowed to be consistent with the currently reported heavy Higgs search data, and to discuss the LHC discovery potential, while such those topics are deserved to the future study. In the latter part of next chapter, we will see the tiny coupling of y is required for the HC-baryon to realize the DM relic abundance.

Chapter 7

Dark matter in the bosonic seesaw model II

As the consequence of the bosonic seesaw, the fluctuating mode of S, which we call s, develops tiny couplings to the SM particles and is predicted to be very light. The s predominantly decays to diphoton and can behave as an invisible axion-like DM. The mass of the s-DM is constrained by currently available cosmological and astrophysical limits to be $10^{-4}\,\mathrm{eV} \lesssim m_s \lesssim 1\,\mathrm{eV}$. We find that the sufficient amount of relic abundance for the s-DM can be accumulated via the coherent oscillation.

For other DM candidate, we propose a new type of Higgs-portal DM production mechanism, called bosonic-seesaw portal scenario. The composite HC-baryon is stable by the residual HC-baryon number symmetry, and can be a DM candidate. It significantly couples to the SM-like Higgs boson via the bosonic seesaw, and can be produced from the thermal plasma below the decoupling temperature around the new strong coupling scale, to account for the observed relic abundance of the dark matter.

The former and the latter part of this chapter are based on our works [96] and [100], respectively.

7.1 The light pseudoscalar s as a dark matter candidate

As noted in the previous chapter, the present model predicts the light pseudoscalar s as the direct consequence of the bosonic seesaw. In the present study, we shall try to identify the s as a DM candidate and this section devotes ourselves to discuss several cosmological and astrophysical limits on the s-DM.

7.1.1 Lifetime

We first evaluate the s mass, decay property, and its lifetime. The s mass is related to the HC-pion masses through Eqs. (6.22) and (6.25) as

$$m_s \simeq \sqrt{2} g_S \Lambda_{\rm HC} \simeq 42\,{\rm GeV} \times \left(\frac{m_\Pi}{750\,{\rm GeV}}\right)\left(\frac{\Lambda_{\rm HC}}{1\,{\rm TeV}}\right)\left(\frac{1\,{\rm TeV}}{v_S}\right) . \tag{7.1}$$

The s couplings to the SM particles arise from mixing with the HC-η' coupled to the SM gauge bosons, WW, ZZ, $Z\gamma$ and $\gamma\gamma$, along with the tiny factor $g_S \ll 1$ [see Sec. 6.4]. Taking into account the size of the s mass in Eq. (7.1), we thus find that the decay channel of s is only the diphoton mode through the vertex:

$$\mathcal{L}_{s\gamma\gamma} = -\frac{1}{4} g_{s\gamma\gamma}\, s\, F_{\mu\nu}\tilde{F}^{\mu\nu} , \qquad \tilde{F}^{\mu\nu} \equiv \frac{1}{2}\epsilon^{\mu\nu\rho\sigma} F_{\rho\sigma} , \tag{7.2}$$

with $F_{\mu\nu} = \partial_\mu A_\nu - \partial_\nu A_\mu$ and

$$g_{s\gamma\gamma} = \frac{4\sqrt{2}}{\pi}\sqrt{N_{\rm HC}}\frac{g_S \alpha_{\rm em}}{f} \simeq 16\sqrt{N_{\rm HC}}\alpha_{\rm em}\frac{m_s}{\Lambda_{\rm HC}^2} , \tag{7.3}$$

where we have used $m_s \simeq g_S \Lambda_{\rm HC}$ and $f = \Lambda_{\rm HC}/(4\pi)$. The lifetime of s is calculated by $\tau = \Gamma_s^{-1}$ with

$$\Gamma_s/N_{\rm HC} = \frac{g_{s\gamma\gamma}^2}{4096\pi} m_s^3/N_{\rm HC} \simeq 275\,{\rm meV} \times \left(\frac{m_s}{42\,{\rm GeV}}\right)^5 \left(\frac{1\,{\rm TeV}}{\Lambda_{\rm HC}}\right)^4 . \tag{7.4}$$

If s is a DM candidate, its lifetime has to be longer than the age of the universe at present time, which requires $\tau \gtrsim 4 \times 10^{17}$ sec. From Eq. (7.4), the s mass is thus constrained as

$$m_s \lesssim 12\,{\rm keV} \times \left(\frac{3}{N_{\rm HC}}\right)^{1/5} \left(\frac{\Lambda_{\rm HC}}{1\,{\rm TeV}}\right)^{4/5} . \tag{7.5}$$

7.1.2 Astrophysical and cosmological limits

Line emission observations

The s-DM dominantly decays to photon, which is expected to affect several line emission observations such as gamma-ray, X-ray, and cosmic ray, so the mass of s can be severely constrained as in the case for other DM candidates [168, 169]. In addition, the mass-independent limit on the coupling to the photon, $g_{s\gamma\gamma}$, can be placed by the observations of the horizontal branch stars for a lower mass range $m_s \lesssim 0.1\,{\rm keV}$ [170]. Figure 7.1 shows the lifetime of s ($\tau \times N_{\rm HC}$) as a function of the mass m_s. The figure implies the upper bound on the s as

$$m_s \lesssim 1\,{\rm keV} \quad \text{with} \quad \tau \times N_{\rm HC} \simeq 3.1 \times 10^{23}\,{\rm sec} \times \left(\frac{1\,{\rm keV}}{m_s}\right)^5 \left(\frac{\Lambda_{\rm HC}}{1\,{\rm TeV}}\right)^4 , \tag{7.6}$$

which is given by the line emission limits.

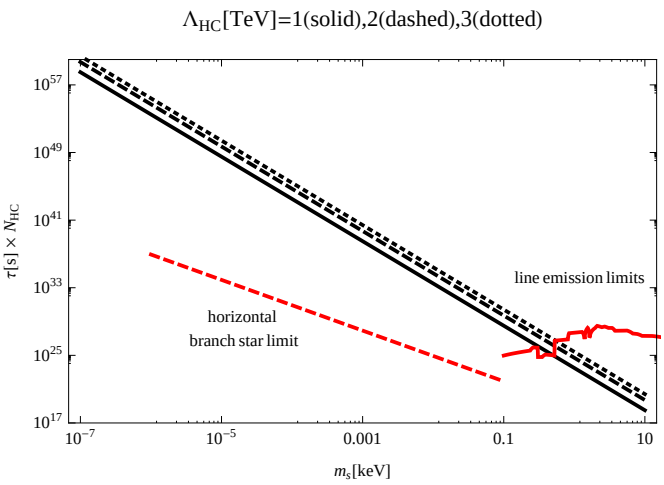

Figure 7.1: The line emission and horizontal branch star observation limits on the s mass. The region below the red-solid and -dashed lines are excluded. The data have been quoted from Refs. [168, 169, 170].

Constraints on the thermal dark matter

The s-DM can be thermally produced by the scattering with the photon, $s + \gamma \leftrightarrow s + \gamma$, through the interaction in Eq. (7.2) with the coupling $g_{s\gamma\gamma}$ (7.3) in the early universe. The reaction rate $R(T)$ can roughly be estimated as

$$R(T) = n(T)\langle \sigma v \rangle \approx g_{s\gamma\gamma}^4 T^5 \,. \tag{7.7}$$

The decoupling temperature of the s, T_D, can be evaluated by equating $R(T)$ with the Hubble parameter

$$H(T) = \sqrt{\frac{\rho}{3M_{\rm Pl}^2}}\,, \qquad \text{with} \quad \rho = \frac{\pi^2}{30} g_*(T) T^4 \,, \tag{7.8}$$

where $M_{\rm Pl} = 2.44 \times 10^{18}$ GeV is the reduced Planck mass and $g_*(T)$ is effective degrees of freedom for relativistic particles. The value of $g_*(T_D)$ is estimated by combining the SM, the HC sector and the pseudoscalar s as $g_*(T_D) = g_*^{\rm SM} + g_*^s + g_*^{\rm HC}$, where $g_*^{\rm SM} = 106.75$ and $g_*^s = 1$. The value of $g_*^{\rm HC}$ is calculated as

$$\begin{aligned} g_*^{\rm HC} &= \left[2 \times (N_{\rm HC}^2 - 1)\right]_{\mathcal{G}_{\rm HC}} + \frac{7}{8} N_{\rm HC} \left[(2 \times 2 \times 2)_\chi + (2 \times 2)_\psi\right] \\ &= 2(N_{\rm HC}^2 - 1) + \frac{21}{2} N_{\rm HC} \,. \end{aligned} \tag{7.9}$$

For $N_{\rm HC} = (3,\ 4,\ 5)$, we have

$$g_*(T_D) = (155.25,\ 179.75,\ 208.25)\,. \tag{7.10}$$

Thus, we find

$$T_D \approx 10^{11}\,\mathrm{GeV} \times \left(\frac{3}{N_{\mathrm{HC}}}\right)^{2/3} \left(\frac{1\,\mathrm{keV}}{m_s}\right)^{4/3} \left(\frac{\Lambda_{\mathrm{HC}}}{1\,\mathrm{TeV}}\right)^{8/3} \left(\frac{g_*(T_D)}{200}\right)^{1/6}, \tag{7.11}$$

where Eq. (7.3) have been used.

Even after decoupling from the thermal equilibrium, s (with mass $\lesssim 1\,\mathrm{keV}$ as in Eq. (7.6)) can be still relativistic at present, which is constrained by the null observation of dark radiation [171]. Although the total entropy in a comoving volume is conserved, the entropy does not flow in s after its decoupling, and thus, the present temperature of s is different from that of photon, $T_0 = 2.7\,\mathrm{K} \simeq 2.3 \times 10^{-4}\,\mathrm{eV}$. the present temperature of the s is estimated as

$$T_0(s) \simeq \left(\frac{g_{*S}(T_0)}{g_{*S}(T_D)}\right)^{1/3} T_0 \simeq 6 \times 10^{-5}\,\mathrm{eV}\,, \tag{7.12}$$

where $g_{*S}(T)$ is effective degrees of freedom for relativistic particles in entropy, and we have used $g_{*S}(T_D) = g_*(T_D)$ and $g_{*S}(T_0) = 43/11$. Then, the dark radiation is estimated by

$$\Delta N_{\mathrm{eff}} = \left(\frac{T_0(s)}{T_0(\nu)}\right)^3 \simeq (0.07,\ 0.06,\ 0.05) \quad \text{for } N_{\mathrm{HC}} = (3,\ 4,\ 5)\,, \tag{7.13}$$

with the neutrino temperature $T_0(\nu) = (4/11)^{1/3} T_0$. These values are consistent with the current dark radiation constraint $\Delta N_{\mathrm{eff}} < 0.1$ [171]. However, if there is no dark radiation, the s mass may be required to be

$$m_s \gtrsim T_0(s) \simeq 6 \times 10^{-5}\,\mathrm{eV}\,. \tag{7.14}$$

If s decouples from the photon after inflation with the reheating temperature T_R, the temperature of s is heated up to the same as the photon temperature, so that s would be a warm or hot dark matter-like particle. Currently such a light warm matter has been severely constrained by the cosmic microwave background spectrum. This situation can be avoided by imposing $T_D > T_R$. The present model may follow a typical Higgs inflation scenario, as discussed in Ref. [172, 173, 174], in which $T_R \simeq 10^{14}$ GeV. Taking this value as a reference and using Eq. (7.11), we thus find

$$m_s \lesssim 6\,\mathrm{eV} \times \left(\frac{3}{N_{\mathrm{HC}}}\right)^{1/2} \left(\frac{\Lambda_{\mathrm{HC}}}{1\,\mathrm{TeV}}\right)^{2} \left(\frac{g_*(T_D)}{200}\right)^{1/8}. \tag{7.15}$$

From Eqs. (7.6), (7.14) and (7.15), the s mass is constrained as

$$6 \times 10^{-5}\,\mathrm{eV} \lesssim m_s \lesssim 6\,\mathrm{eV}\,. \tag{7.16}$$

7.2 Cosmological productions and detection of the s-dark matter

In this section, we closely explore the possibility for the s as a DM to account for the relic abundance at the present time.

7.2.1 Thermal production

Though the s-DM decouples from the thermal equilibrium in the early universe at $T_D \approx 10^{15}\,\text{GeV} \times (1\,\text{eV}/m_s)^{4/3} (> T_R)$, there might exist the chance to thermally accumulate the number density by production cross sections interacting with the HC sector until the HC sector decouples from the thermal equilibrium at around $T = \Lambda_{\text{HC}} = \mathcal{O}(\text{TeV})$. The relevant production processes involve only a single s in the final state, which is scattered off from the HC sector-fermion $F = (\chi,\ \psi)$ such as $F + \bar{F} \to \gamma/Z + s$, through the s-γ-γ vertex in Eq. (7.2) and the s-Z-γ, s-Z-Z vertices listed in Sec. 6.4.[1] The production cross section roughly goes like

$$\sigma(F + \bar{F} \to \gamma/Z + s) \sim \alpha_{\text{em}} N_{\text{HC}} \left(\frac{\sqrt{N_{\text{HC}}} g_S \alpha_{\text{em}}}{\Lambda_{\text{HC}}} \right)^2 \simeq 10^{-31} \times \frac{N_{\text{HC}}^2}{\Lambda_{\text{HC}}^2} \left(\frac{m_s}{1\,\text{eV}} \right)^2 \left(\frac{1\,\text{TeV}}{\Lambda_{\text{HC}}} \right)^2 , \tag{7.17}$$

where in the second equality we have used the first relationship in Eq. (7.1).

The corresponding number density per entropy density at present time ($Y_s(T_0) = n_s(T_0)/s(T_0)$) can be estimated by integrating the Boltzmann equation with the above production cross section over the temperature from the reheating temperature $T_R \approx 10^{14}$ GeV down to the freeze-out temperature $T_F = \Lambda_{\text{HC}}$. Following the formula given in Ref. [175] we evaluate $Y_s(T_0)$ as

$$\begin{aligned} Y_s(T_0) &= \int_{\Lambda_{\text{HC}}}^{T_R} dT \frac{\langle \sigma(F + \bar{F} \to \gamma/Z + s) v \rangle n_F n_{\bar{F}}}{s(T) H(T) T} \\ &= \frac{135\sqrt{10} M_P}{2\pi^3} \int_{\Lambda_{\text{HC}}}^{T_R} dT \frac{\langle \sigma(F + \bar{F} \to \gamma/Z + s) v \rangle n_F n_{\bar{F}}}{g_*^{3/2}(T) T^6} , \end{aligned} \tag{7.18}$$

where in the last line we have used $s(T) = g_{*s}(T) \frac{2\pi^2}{45} T^3$ with $g_*(T) = g_{*s}(T)$. The thermal averaged cross section is expressed to be

$$\langle \sigma(F + \bar{F} \to s + \gamma/Z) v \rangle n_F n_{\bar{F}} = \zeta^2(3) \eta_F \eta_{\bar{F}} \frac{g_F g_{\bar{F}}}{16\pi^4} T^6 \int_0^\infty dx x^4 K_1(x) \sigma(x^2) , \tag{7.19}$$

[1] When the temperature is significantly higher than Λ_{HC}, the s-coupling to diphoton may arise from the HC fermion loops. Even if the universe is in such a symmetric phase by taking into account the thermal effect, the vertex is anyhow generated with the magnitude of the order of $g_{s\gamma\gamma}$, which is given by Eq. (7.3).

where $\zeta(3) \simeq 1.202$ and $K_1(x)$ stands for the modified Bessel function of the first kind, $\sigma(x^2) = \sigma(s/T^2)$ and $g_{F(\bar{F})}$ is the internal spin degree of freedom for the HC fermion (anti-fermion) F; $\eta_{F(\bar{F})}$ is a number density factor associated with the initial state particle assigned as $\eta_{F(\bar{F})} = 3/4$ for fermions (anti-fermion). Using these values, we can calculate $Y_s(T_0)$ to get

$$\begin{aligned} Y_s(T_0) &\approx \frac{135\sqrt{10}}{32\pi^6} \frac{M_P T_R}{g_*^{3/2}(T_R)\Lambda_{\rm HC}^2} \times 10^{-31} \times N_{\rm HC}^2 \left(\frac{m_s}{1\,{\rm eV}}\right)^2 \left(\frac{1\,{\rm TeV}}{\Lambda_{\rm HC}}\right)^2 \\ &\approx 10^{-10} \times N_{\rm HC}^2 \left(\frac{m_s}{1\,{\rm eV}}\right)^2 \left(\frac{1\,{\rm TeV}}{\Lambda_{\rm HC}}\right)^4 \left(\frac{200}{g_*(T_R)}\right)^{3/2} , \end{aligned} \tag{7.20}$$

where use has been made of $g_*(T_R) = g_*(\Lambda_{\rm HC})$. Thus, it turns out that the thermal relic is too small to explain the present DM abundance. This result is essentially caused by the tiny coupling of g_S, which leads to the extremely small cross section with the HC sector in Eq. (7.17).

7.2.2 Non-thermal production

Analogously to the case of axion dark matter [168], the s-DM population can be accumulated by "misalignment" of the classical s field and the coherent oscillation. Assuming the initial position at which the oscillation starts to be the vicinity of the vacuum $s = 0$ with the VEV v_S, we write the equation of motion for s under the Friedmann-Robertson-Walker metric to be

$$\frac{d^2 s}{dt^2} + 3H(T)\frac{ds}{dt} + m_s^2\, s \approx 0\,. \tag{7.21}$$

This describes the damping harmonic oscillation in which the oscillation takes place at $T = T_{\rm osc}$ where $3H(T) \approx m_s$, i.e.,

$$T_{\rm osc} \simeq 13\,{\rm TeV} \times \left(\frac{m_s}{1\,{\rm eV}}\right)^{1/2} \left(\frac{200}{g_*(T_{\rm osc})}\right)^{1/4} . \tag{7.22}$$

This implies $130\,{\rm GeV} \lesssim T_{\rm osc} \lesssim 13\,{\rm TeV}$ for $10^{-4}\,{\rm eV} \lesssim m_s \lesssim 1\,{\rm eV}$. Since the s mass is generated through the bosonic seesaw mechanism at $T \simeq \Lambda_{\rm HC} = \mathcal{O}(1)\,{\rm TeV}$, we find that the temperature at which the coherent oscillation starts, what we call T_S, depend on m_s as

$$\begin{aligned} T_S &\simeq \Lambda_{\rm HC} \quad \text{for} \quad 6\times 10^{-3}\,{\rm eV}\left(\frac{\Lambda_{\rm HC}}{1\,{\rm TeV}}\right)^2 \lesssim m_s < 1\,{\rm eV}\,, \\ T_S &\simeq T_{\rm osc} \quad \text{for} \quad 10^{-4}\,{\rm eV} \lesssim m_s \lesssim 6\times 10^{-3}\,{\rm eV}\left(\frac{\Lambda_{\rm HC}}{1\,{\rm TeV}}\right)^2 . \end{aligned} \tag{7.23}$$

The energy density of the classical s field is thus accumulated by the coherent oscillation starting from the temperature T_S in Eq. (7.23), cooling down to the present temperature T_0.

At the $T = T_S$ the energy density of s corresponds to the vacuum energy defined as

$$\rho_s(T_S) = V(\theta) - V(\theta = 0)\,, \tag{7.24}$$

where the θ is defined as the amount of the shift from the original S field at the VEV v_S to be $S = v_S(1+\theta)$ with $\theta \ll 1$, and the potential $V(\theta)$ is read off as

$$V(\theta) = V(\theta = 0) + \frac{1}{2} m_s^2 v_s^2 \theta^2 + \mathcal{O}(\theta^3)\,. \tag{7.25}$$

One can easily see that, during the coherent oscillation, the number density per comoving volume is conserved and the s behaves just like a non-relativistic particle satisfying $\rho_s \propto R^{-3}$ with the expansion rate R. Hence, we estimate the present DM abundance

$$\frac{\rho_s(T_S)}{\rho_s(T_0)} = \frac{m_s n_s(T_S)}{m_s n_s(T_0)} = \frac{s(T_S)}{s(T_0)}\,, \quad \text{i.e.,} \;\; \rho_s(T_0) = \frac{s(T_0)}{s(T_S)} \rho_s(T_S)\,, \tag{7.26}$$

and obtain

$$\rho_s(T_0) \simeq (4200\ \text{GeV})^4\, \theta^2 \left(\frac{T_0}{T_S}\right)^3 \frac{g_{*S}(T_0)}{g_{*S}(T_S)} \left(\frac{m_\Pi}{750\ \text{GeV}}\right)^2 \left(\frac{\Lambda_{\text{HC}}}{1\ \text{TeV}}\right)\,, \tag{7.27}$$

by using Eq. (7.1). This relation shows that s can explain the relic DM abundance with an appropriate value of θ.

From Eqs. (7.23), (7.25) and (7.26), and using the second equality in Eq. (7.1), we can calculate the s-DM relic density, $\Omega_s h^2 = \rho_s(T_0)/(\rho_{\text{cr}}/h^2)$ with $\rho_{\text{cr}}/h^2 = 0.8 \times 10^{-46}\,\text{GeV}^4$. We show the contour plot on the (m_s, θ) plane with the observed dark matter relic density $\Omega_{\text{DM}} h^2 \simeq 0.118$ [9] in Fig. 7.2. Here, we have used $s(T_0) = \frac{2\pi^2}{45} g_{*s}(T_0) T_0^3$ with $g_{*s}(T_0) = 43/11$ and $T_0 \simeq 2.3 \times 10^{-4}\,\text{eV}$, $g_{*s}(\Lambda_{\text{HC}}) = 200$ as a reference value, and assumed $g_{*s}(T_S < \Lambda_{\text{HC}}) = g_*^{\text{SM}} = 106.75$. From the figure, we find that the relic density of the s, with the mass in a range of $10^{-4}\,\text{eV} \lesssim m_s \lesssim 1\,\text{eV}$, can be accumulated enough to account for the present DM abundance.

7.2.3 Detection possibility in experiments

As has so far been seen in this chapter, the s-DM has the lifetime much longer than the age of the universe and has extremely tiny couplings to the SM particles, and hence the detection at collider experiments is unlikely to be possible.

As in the case of invisible axion-like DM detection [176, 177, 178], cosmic pseudoscalar s, left over from the big bang, may be detected by microwave cavity haloscopes. In that facility, a strong static magnetic field is provided to make the s drift through the microwave

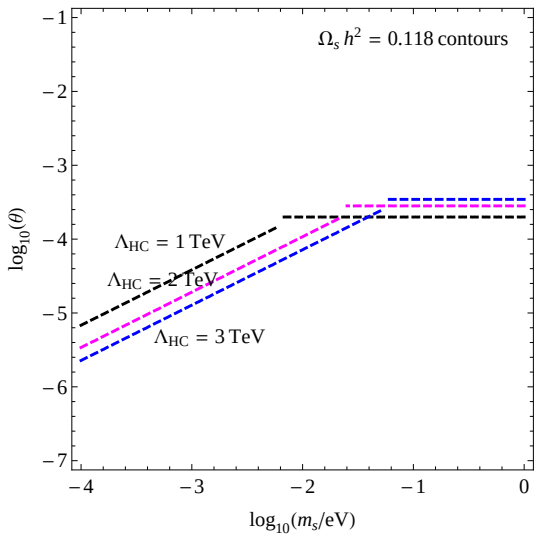

Figure 7.2: The contour plots on the $(m_s,\, \theta)$ plane realizing the observed present dark matter density $\Omega_{\rm DM}h^2 = 0.118$ [9]. The bumps, which show up when T_S gets lower than $\Lambda_{\rm HC}$, are due to the discontinuity of the effective degrees of freedom g_{*s} around the $T_S = \Lambda_{\rm HC}$ as described in the text.

cavity, resonantly converted to microwave photons according to the s-γ-γ interaction in Eq. (7.2). The conversion power P is given by [176, 177, 178]

$$P = \frac{1}{8} g_{s\gamma\gamma}^2 \rho_s(T_0) B_0^2 L_x V \,, \tag{7.28}$$

where $\rho_s(T^0)$ is the local s energy density, B_0 the magnetic strength scale, V the volume of the cavity, and L_x the size of the x direction. Taking a typical experimental setup currently employed [179], $B_0 = 10\,\text{Tesla}$, $L_x = 1\,\text{m}$, $V = 1\,\text{m}^3$ and the local halo density $\rho_{\rm halo} \simeq 0.3\,\text{GeV/cm}^3$, we estimate the detection power

$$P/N_{\rm HC} \simeq 10^{-34}\,\text{Watt} \times \left(\frac{1\,\text{TeV}}{\Lambda_{\rm HC}}\right)^2 \left(\frac{m_s}{10^{-4}\,\text{eV}}\right)^2 \left(\frac{\rho_s(T_0)}{\rho_{\rm halo}}\right) \,, \tag{7.29}$$

where we have used Eq. (7.3). The power for $m_s \sim 1\,\text{eV}$ is comparable with the axion detection potential [179], so the s can be hunted at the same level of the sensitivity as the axion by the microwave cavity experiments.

7.3 Discussions for the s-dark matter

The crucial deference between the s-DM and the axion-like DM can be seen by no evidence for observations probing couplings to matters, such as the test of gravitational inverse-square law and energy loss in stars like neutron star cooling. The s coupling to matters can be generated at loop levels by the g_S and κ_H couplings. As seen from Eqs. (6.20) and (6.22), however, those couplings are extremely small, suppressed by $(m_s/\Lambda_{\rm HC}) \ll 1$

or $(v_1/v_s) \ll 1$ [see also Eq. (6.25)]. Hence, one can conclude that there is no chance to detect the s-DM through the couplings to matters, in contrast to the axion case. Thus, there are no evidence for observations with the matter-portal, but some signals identical among s and the axion in the line shapes, and microwave cavity experiments would be a clear hint to distinguish them. (Note that a dilaton-like DM signal in the microwave cavity is clearly different from those of s and the axion, due to the different type of the coupling to photons: $E \cdot B$ for pseudoscalars, while $E \cdot E$ or $B \cdot B$ for scalars.)

As discussed in previous sections, we have assumed that the reheating epoch is associated with the Higgs inflation scenario. It might be the case, however, that one needs somewhat large non-minimal couplings between the SM Higgs and the scalar curvature. In that case, the reheating epoch would be shifted, so the upper bound on the mass of s, as estimated in Eq. (7.15), could be affected. Detailed study closely connected with inflation scenarios is to be performed in the future literature.

It should be noted that s as a candidate of the DM is intact even if the HC-pion mass is not set to the present reference value. This is because that it is solely tied with realization of the EW symmetry breaking via the bosonic seesaw: the s mass has to be much smaller than $\Lambda_{\rm HC}$, which is controlled by the small coupling g_S ($\ll 1$) in Eq. (6.22); the s couplings to the SM particles, mainly to photons, necessarily becomes tiny by the same g_S coupling strength as the consequence of the bosonic seesaw, which would suggest to regard the s as a DM candidate; the s mass is then inevitably constrained by cosmological bounds, to be order of eV, as discussed above.

Actually, the couplings of the s-dark matter are required to be extremely small: the coupling to HC-fermions, $g_S \sim 10^{-12}$, from Eq. (7.1) for $m_s \sim 1\,\text{eV}$ (which is coincidentally as small as the Yukawa coupling for neutrino in Dirac neutrino models); the quartic coupling $\lambda_S \sim 10^{-44}$ from Eq. (6.22) with $v_S \sim 10^{13}\,\text{GeV}$ estimated from Eq. (6.25) with $m_s \sim 1\,\text{eV}$ and $g_S \sim 10^{-12}$; the coupling to the 125 GeV Higgs boson, $\kappa_H \sim 10^{-22}$, estimated from Eq. (6.22) with $v_S \sim 10^{13}\,\text{GeV}$. The origin of these extremely small couplings could be explained by the underlying Planck scale physics, which is, however, beyond the scope of the present study, to be pursued elsewhere. Note that the realization of the EW symmetry breaking has theoretically nothing to do with the smallness of those couplings, which are only related to the physics of the light s including the mass generation of HC-pions and the property as the invisible DM.

We have so far focused on the possibility for the predicted light pseudoscalar s to be a DM candidate. Actually, another scenario can be made: with the s mass around GeV scale, the s could be just a long-lived particle having the lifetime much shorter than the age of the present universe. That sort of a light long-lived particle could be accessible at the LHC. This interesting another possibility will be pursued in another publication. In

the next section, we will investigate another DM scenario, in which the s mass is not so light as eV scale, while we do not discuss the phenomenology for s.

7.4 Bosonic-seesaw portal dark mater

We now suppose that the HC sector possesses $N_{\rm HC} = 4$, i.e. the $SU(4)_{\rm HC}$. The HC-baryon can be realized as a complex scalar, having the HC scalar-baryon charge. Our argument is substantially unchanged even if we employ the case other than the $SU(4)_{\rm HC}$ in which fermionic HC-baryons can be present. Among them, the EW-singlet HC scalar-baryon, $\varphi \sim \psi\psi\psi\psi$ can be another DM candidate which is stabilized by the HC-baryon conserved charge. The mass is expected to be on the order of $\mathcal{O}(N_{\rm HC}\Lambda_{\rm HC})$.[2] From the bosonic seesaw mechanism, $\Lambda_{\rm HC}$ is naturally expected to be of $\mathcal{O}(1)$ TeV as mentioned in Sec. 6.2. Thus, the mass of HC-baryon DM should be $\mathcal{O}(1)$ TeV.

The EW-singlet complex scalar baryon, φ, strongly and minimally couples to the composite HC Higgs doublet, Θ, like

$$a \cdot \varphi^\dagger \varphi \Theta^\dagger \Theta \,, \tag{7.30}$$

with the order one (or larger) coefficient a. By the bosonic seesaw mechanism, the Θ starts to mix with the elementary Higgs doublet H below the scale $\Lambda_{\rm HC}$. This dynamically generates, so-called, a Higgs portal coupling between the dark matter φ and the SM-like Higgs H_1:

$$\kappa_{\varphi H} \cdot \varphi^\dagger \varphi H_1^\dagger H_1 \,, \quad \text{with} \;\; \kappa_{\varphi H} = a y^2 \,, \tag{7.31}$$

where the factor y^2 has come from the bosonic-seesaw mixing strength y ($\Theta \approx y H_1 + H_2$, which can be understood by diagonalizing the mass matrix Eq. (6.10)) between the SM-like Higgs H_1 and heavy Higgs H_2. The mixing strength y is supposed to be much smaller than $\mathcal{O}(1)$, so that the Higgs portal coupling $\kappa_{\varphi H}$ can naturally be small to be consistent with the present relic abundance of the DM, as will be clarified later on.

In the thermal history, the HC scalar-baryon φ was decoupled from the thermal equilibrium at the temperature around $\Lambda_{\rm HC}$ because of the decoupling of the HC-pions and HC-fermions. It is, however, crucial to note that, since the φ has the Higgs portal coupling in Eq. (7.31) dynamically induced from the bosonic seesaw, the φ can still be thermally produced via the SM sector below the decoupling temperature $T = \Lambda_{\rm HC}$, *a la* "freeze-in" scenarios.

Let us evaluate the thermal production cross sections arising from the bosonic-seesaw portal coupling in Eq. (7.31). Below $T = \Lambda_{\rm HC}$, the relevant processes are: hh, WW, ZZ,

[2] In the Refs. [180, 181, 182], a similar composite dark baryon as the DM candidate, so-called stealth DM, has been discussed in a context different than the bosonic seesaw.

$t\bar{t} \to \varphi^\dagger\varphi$. Those cross sections are computed at the tree-level of the perturbation in couplings to be

$$\begin{aligned}
\sigma(hh \to \varphi^\dagger\varphi) &= \frac{\kappa_{\varphi H}^2}{16\pi}\frac{s}{(s-m_h^2)^2}\left(1-\frac{4m_\varphi^2}{s}\right)^{5/2}, \\
\sigma(WW \to \varphi^\dagger\varphi) &= \frac{9\kappa_{\varphi H}^2}{64\pi}\frac{s}{(s-m_h^2)^2}\left(1-\frac{4m_\varphi^2}{s}\right)^{1/2}\left(\frac{m_W^2}{s}\right)^2\left[2+\left(1-\frac{s}{2m_W^2}\right)^2\right], \\
\sigma(ZZ \to \varphi^\dagger\varphi) &= \frac{9\kappa_{\varphi H}^2}{64\pi}\frac{s}{(s-m_h^2)^2}\left(1-\frac{4m_\varphi^2}{s}\right)^{1/2}\left(\frac{m_Z^2}{s}\right)^2\left[2+\left(1-\frac{s}{2m_Z^2}\right)^2\right], \\
\sigma(t\bar{t} \to \varphi^\dagger\varphi) &= \frac{3\kappa_{\varphi H}^2}{32\pi}\frac{s}{(s-m_h^2)^2}\left(1-\frac{4m_\varphi^2}{s}\right)^{1/2}\left(\frac{m_t^2}{s}\right)\left[1-\frac{4m_t^2}{s}\right],
\end{aligned} \tag{7.32}$$

with $\sqrt{s}$ being the center of mass energy. The number density per entropy density today, $Y(T_0) = n(T_0)/s(T_0)$, can be calculated by integrating the Boltzman equation with the production cross sections $\sigma(ij \to \varphi^\dagger\varphi)$ to be

$$Y(T_0) = \frac{135\sqrt{10}M_{\rm Pl}\zeta^2(3)}{32\pi^7}\int_{T_0}^{\Lambda_{\rm HC}} dT \sum_{i,j}\frac{g_i g_j \eta_i \eta_j}{[g_*(T)]^{3/2}}\int_0^\infty dx x^4 K_1(x)\sigma(ij \to \varphi^\dagger\varphi), \tag{7.33}$$

where $g_i = 2$ (1) and $\eta_i = 3/4$ (1) for fermions (bosons), and $x \equiv \sqrt{s}/T$.

The thermal-relic abundance, $\Omega_\varphi h^2 = Y(T_0)\cdot m_\varphi s(T_0)/(\rho_{\rm cr}h^{-2})$, turns out to actually be almost independent of the φ mass. The bosonic-seesaw portal coupling $\kappa_{\varphi H}$ is then constrained by the presently observed DM abundance $\simeq 0.1$. Figure 7.3 shows the constraint plot on the portal coupling, which shows us

$$\kappa_{\varphi H} \lesssim 10^{-10}, \qquad \text{or} \qquad y \lesssim 10^{-5}\times(1.0/a)^{1/2}, \tag{7.34}$$

where $g_*(T)$ in Eq. (7.33) has been taken to be $\simeq 100$. The smallness of the portal coupling is consistent with the bosonic seesaw mechanism: the small portal couping, required by the relic abundance, can naturally be encoded in the bosonic seesaw scenario. Note also that the tiny $\kappa_{\varphi H}$ or y in Eq. (7.34) is consistent with the bosonic seesaw paradigm.

Having the Higgs portal coupling, the HC-baryon DM can be detected by the direct detection experiments such as the LUX [136], PandaX-II [136], and upcoming XENON1T and LZ [183]. The spin-independent (SI) cross section is computed as

$$\sigma_{\rm SI}(\varphi N \to \varphi N) \simeq \frac{\kappa_{\varphi H}^2}{16\pi m_h^4} m_*^2(N,\varphi) g_{hNN}^2, \tag{7.35}$$

where $g_{hNN} \simeq 0.25\,\text{GeV}/v$ [184, 185, 186] and $m_*(N,\varphi) = m_N m_\varphi/(m_N + m_\varphi)$ is the reduced mass with $m_N \simeq 940\,\text{MeV}$. Using the upper bound on the portal coupling $\kappa_{\varphi H}$ given in Eq. (7.34) and taking the DM mass 1-5 TeV for the reference value, we find the

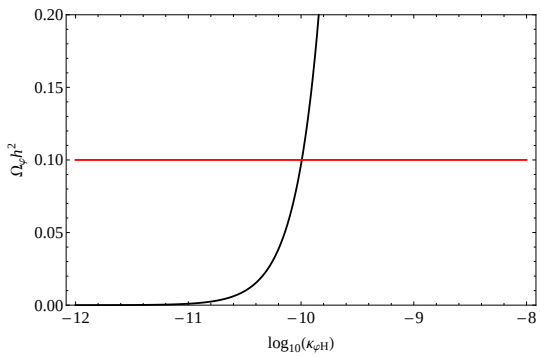

Figure 7.3: The constraint on the bosonic-seesaw portal coupling $\kappa_{\varphi H}$ from the presently observed relic abundance ($\simeq 0.1$ drawn as red-horizontal line in the plot). The DM mass dependence is almost negligible in evaluating the relic abundance. The plot has been shown by taking the mass to be 1 TeV.

upper bound on the SI cross section, $\sigma_{\rm SI} \lesssim 10^{-63}\,{\rm cm}^2$. This value is far below the current limit most stringently set by the LUX2016, $\sigma_{\rm SI} \leq 10^{-45}\,{\rm cm}^2$ at the TeV range [136], and the sensitivity in the future-prospected XENON1T or LZ, $\sigma_{\rm SI} \leq 10^{-47}\,{\rm cm}^2$ [183], which will actually be overlapped with the expected neutrino background [187].

7.5 Conclusion

We have investigated the DM physics in the bosonic seesaw model constructed in the previous chapter. From the bosonic seesaw mechanism, the scale invariance breaking occur at $\Lambda_{\rm HC}$ by the strong-coupling HC dynamics, and it subsequently leads the EW symmetry breaking. The breaking scale naturally expected to be of $\mathcal{O}(1)$ TeV, and the mass of new particles exist at $\mathcal{O}(1)$ TeV except for the pseudoscalar s (fluctuating mode of S). This S plays the crucial role to realize the EW bosonic seesaw, as well as to give masses for the composite NG bosons (HC-pions): in this sense, the S acts like another "Higgs" in the theory. Thus, discovering the fluctuating mode of S, called s, is the smoking-gun of the present model.

There are two different DM candidates: one is the invisible axion-like pseudoscalar s with eV scale mass; another is the EW-singlet lightest HC-baryon φ with TeV scale mass. These have completely different property of the DM, but both origin are strongly related with the strong-coupling HC dynamics. In the former case, the smallness of the s mass and coupling to the SM particles correspond to the smallness of the chiral symmetry breaking in the HC sector. In the latter case, the stability of φ is guaranteed by the residual HC-baryon number symmetry, and the smallness of φ to the SM particles is given by the same reason as that for s.

Because of the classical-scale invariance, the pseudoscalar S originally couples only to

the SM-like Higgs and HC-fermions. After the dynamical scale breaking and triggering the EW bosonic seesaw, the s thus develops vanishingly small couplings to the SM particles, which arise only through the tiny mixing with the HC-η'. In addition, it turned out that in relation to the HC-pion masses, the s mass is predicted to be very light and to predominantly decay to diphoton, so we have identified the s as a DM candidate. The s mass was then severely constrained by several cosmological observations, such as line emissions of X-ray, gamma-ray and cosmic-ray, no evidence for dark radiations, and a typical Higgs inflation scenario. The s mass was thus bounded to be $10^{-4}\text{eV} \lesssim m_s \lesssim 1\text{eV}$.

We have examined the possibility of the cosmological productions of the s. It was shown that the s is unlikely to be thermally produced essentially due to its tiny couplings to the HC sector in the thermal equilibrium. We have then found that the sufficient amount of relic abundance of s as the cold DM can be accumulated via the coherent oscillation.

The detection potential in microwave cavity experiments was also addressed so that the s with mass around 1 eV can have the same level of the detection sensibility as that of the axion in the currently equipped experimental setup, so the s can be hunted by the microwave cavity experiments.

In the bosonic-seesaw portal scenario, proposed in the latter part of this chapter (Sec. 7.4), provides a DM candidate having the coupling to the SM-like Higgs, which is dynamically generated by the bosonic seesaw and essentially related to the origin of the EW symmetry breaking. In this scenario the DM, having the mass of TeV scale, dynamically arises as the HC-baryon with the conserved HC-baryon charge, and the thermal relic abundance can be produced enough due to the significantly small coupling to the SM-like Higgs as the consequence of the bosonic seesaw mechanism, namely, the EW symmetry breaking. Since having the extremely small portal coupling, the bosonic-seesaw portal dark matter is fairly insensitive to the direct detection experiments, which would imply other detection proposals.

Chapter 8

Summary and discussion

The SM has been established by the discovery of the Higgs boson, and can explain almost all experimental results obtained until now. In addition, the SM has an approximate scale invariance, so that the hierarchy problem does not arise within the SM. On the other hand, there are unsolvable problems: active neutrino masses, baryon asymmetry of the Universe, dark matter relic abundance, dark energy, and so on. It is, however, well known that the hierarchy problem arises, if one introduces new particles in a high energy scale compared to the EW scale in order to solve these issues. As an attractive idea avoiding the hierarchy problem, we have investigated classically scale invariant extensions, which are classified into almost two types of scale breaking mechanisms: one is the Coleman-Weinberg mechanism; another is the strong-coupling dynamics like the QCD. In this thesis, we have investigated these two types of models, and shown the phenomenological consequences. In addition, we have proposed a new dynamics of the EW symmetry breaking in a classically scale invariant model, i.e., bosonic seesaw mechanism, and found that a dark matter candidate naturally exits in the model.

In our study, we have assumed the classical scale invariance, and regarded it as a boundary condition of the UV complete theory, which can deal with quantum gravity. A conformal field theory (CFT) possesses the scale invariance, and its system has been theoretically studied in several types of spacetime, which are often motivated by the string theory. Although it is difficult to construct a phenomenologically successful model, the CFT may be useful to understand quantum gravity by using the AdS/CFT correspondence [188]. In addition, renormalizable quantum gravity may be described by the CFT as in Ref. [189]. Actually, we need more detailed study about quantum gravity, but it is very difficult and beyond the scope of this thesis. We may, however, expect that there is the conformal symmetry, or equivalently scale invariance, in the UV complete theory.

Appendix A

β functions of the model couplings

In this appendix, we show the β functions of the model couplings, where we omit the SM Yukawa couplings except for the top Yukawa coupling, since they do not contribute significantly to the Higgs quartic coupling and gauge couplings. For our models, we have obtained two-loop β functions by using SARAH [120], while we show them up to the one-loop level, for simplicity.

A.1 Standard model

In the SM, β functions of the coupling constants are given by [109, 190]

$$\beta_{g_1} = \frac{g_1^3}{16\pi^2}\left[\frac{41}{10}\right] + \frac{g_1^3}{(16\pi^2)^2}\left[-\frac{17}{10}y_t^2 + \frac{199}{50}g_1^2 + \frac{27}{10}g_2^2 + \frac{44}{5}g_3^2\right], \tag{A.1}$$

$$\beta_{g_2} = \frac{g_2^3}{16\pi^2}\left[-\frac{19}{6}\right] + \frac{g_2^3}{(16\pi^2)^2}\left[-\frac{3}{2}y_t^2 + \frac{9}{10}g_1^2 + \frac{35}{6}g_2^2 + 12g_3^2\right], \tag{A.2}$$

$$\beta_{g_3} = \frac{g_3^3}{16\pi^2}[-7] + \frac{g_3^3}{(16\pi^2)^2}\left[-2y_t^2 + \frac{11}{10}g_1^2 + \frac{9}{2}g_2^2 - 26g_3^2\right], \tag{A.3}$$

$$\begin{aligned}\beta_{y_t} = {} & \frac{y_t}{16\pi^2}\left[\frac{9}{2}y_t^2 - \frac{17}{20}g_1^2 - \frac{9}{4}g_2^2 - 8g_3^2\right] \\ & + \frac{y_t}{(16\pi^2)^2}\left[y_t^2\left(-12y_t^2 + \frac{393}{80}g_1^2 + \frac{225}{16}g_2^2 + 36g_3^2 - 12\lambda_H\right)\right. \\ & \left. + \frac{1187}{600}g_1^4 - \frac{23}{4}g_2^4 - 108g_3^4 - \frac{9}{20}g_1^2g_2^2 + \frac{19}{15}g_1^2g_3^2 + 9g_2^2g_3^2 + 6\lambda_H^2\right],\end{aligned} \tag{A.4}$$

$$\begin{aligned}\beta_{\lambda_H} = {} & \frac{1}{16\pi^2}\left[\lambda_H\left(24\lambda_H + 12y_t^2 - \frac{9}{5}g_1^2 - 9g_2^2\right) - 6y_t^4 + \frac{27}{200}g_1^4 + \frac{9}{8}g_2^4 + \frac{9}{20}g_1^2g_2^2\right] \\ & + \frac{1}{(16\pi^2)^2}\left[\lambda_H^2\left(-312\lambda_H - 144y_t^2 + \frac{108}{5}g_1^2 + 108g_2^2\right) + \lambda_H y_t^2\left(-3y_t^2 + \frac{17}{2}g_1^2\right.\right. \\ & \left. + \frac{45}{2}g_2^2 + 80g_3^2\right) + \lambda_H\left(\frac{1887}{200}g_1^4 - \frac{73}{8}g_2^4 + \frac{117}{20}g_1^2g_2^2\right) + y_t^4\left(30y_t^2 - \frac{8}{5}g_1^2 - 32g_3^2\right) \\ & \left. + y_t^2\left(-\frac{171}{100}g_1^4 - \frac{9}{4}g_2^4 + \frac{63}{10}g_1^2g_2^2\right) - \frac{3411}{2000}g_1^6 + \frac{305}{16}g_2^6 - \frac{1677}{400}g_1^4g_2^2 - \frac{289}{80}g_1^2g_2^4\right],\end{aligned} \tag{A.5}$$

up to two-loop level.

To solve the RGEs, we take the following boundary conditions [109]:

$$\begin{aligned} g_Y(M_t) &= 0.35761 + 0.00011\left(\frac{M_t}{\text{GeV}} - 173.10\right), \qquad g_1 = \sqrt{\frac{5}{3}}g_Y, \\ g_2(M_t) &= 0.64822 + 0.00004\left(\frac{M_t}{\text{GeV}} - 173.10\right), \\ g_3(M_t) &= 1.1666 - 0.00046\left(\frac{M_t}{\text{GeV}} - 173.10\right) + 0.00314\left(\frac{\alpha_3(M_Z) - 0.1184}{0.0007}\right), \\ y_t(M_t) &= 0.93558 + 0.00550\left(\frac{M_t}{\text{GeV}} - 173.10\right) - 0.00042\left(\frac{\alpha_3(M_Z) - 0.1184}{0.0007}\right), \\ \lambda(M_t) &= 0.12711 - 0.00004\left(\frac{M_t}{\text{GeV}} - 173.10\right) + 0.00206\left(\frac{M_h}{\text{GeV}} - 125.66\right), \\ \alpha_3(M_Z) &= 0.1184 \pm 0.0007, \end{aligned} \tag{A.6}$$

where M_t is the top quark Monte-Carlo mass.

A.2 $U(1)$ gauge extended model I

$$\beta_{g_Y} = \frac{g_Y^3}{(4\pi)^2}\left[\frac{41}{6}\right], \qquad \beta_{g_2} = \frac{g_2^3}{(4\pi)^2}\left[-\frac{19}{6}\right], \qquad \beta_{g_3} = \frac{g_3^3}{(4\pi)^2}\left[-7\right], \tag{A.7}$$

$$\beta_{g_\chi} = \frac{g_\chi}{(4\pi)^2}\left[\frac{196}{25}g_\chi^2 + \frac{41}{6}g_{\rm mix}^2 - \frac{4}{15}g_{\rm mix}g_\chi\right], \tag{A.8}$$

$$\beta_{g_{\rm mix}} = \frac{1}{(4\pi)^2}\left[g_{\rm mix}\left(\frac{41}{6}\left(2g_Y^2 + g_{\rm mix}^2\right) + \frac{196}{25}g_\chi^2\right) - \frac{4}{15}g_\chi\left(g_Y^2 + g_{\rm mix}^2\right)\right], \tag{A.9}$$

$$\beta_{y_t} = \frac{y_t}{(4\pi)^2}\left[\frac{9}{2}y_t^2 - 8g_3^2 - \frac{9}{4}g_2^2 - \frac{17}{12}\left(g_Y^2 + g_{\rm mix}^2\right) - \frac{6}{25}g_\chi^2 + \frac{3}{5}g_{\rm mix}g_\chi\right], \tag{A.10}$$

$$\beta_{y_{M_i}} = \frac{y_{M_i}}{(4\pi)^2}\left[4y_{M_i}^2 + 2{\rm tr}Y_M^2 - 6g_\chi^2\right], \tag{A.11}$$

$$\begin{aligned}\beta_{\lambda_H} = \frac{1}{(4\pi)^2}\Bigg[&\lambda_H\left(24\lambda_H + 12y_t^2 - 3\left(g_Y^2 + g_{\rm mix}^2\right) - 9g_2^2 - \frac{48}{25}g_\chi^2 + \frac{24}{5}g_{\rm mix}g_\chi\right)\\ &+ \lambda_{\rm mix}^2 - 6y_t^4 + \frac{3}{8}\left(2g_2^4 + \left\{g_2^2 + g_Y^2 + \left(g_{\rm mix} - \frac{4}{5}g_\chi\right)^2\right\}^2\right)\Bigg],\end{aligned} \tag{A.12}$$

$$\beta_{\lambda_\Phi} = \frac{1}{(4\pi)^2}\left[\lambda_\Phi\left(20\lambda_\Phi + 8{\rm tr}Y_M^2 - 48g_\chi^2\right) + 2\lambda_{\rm mix}^2 - 16{\rm tr}Y_M^4 + 96g_\chi^4\right], \tag{A.13}$$

$$\begin{aligned}\beta_{\lambda_{\rm mix}} = \frac{1}{(4\pi)^2}\Bigg[&\lambda_{\rm mix}\Bigg(12\lambda_H + 8\lambda_\Phi + 4\lambda_{\rm mix} + 6y_t^2 + 4{\rm tr}Y_M^2 - 24g_\chi^2\\ &- \frac{3}{2}\left\{3g_2^2 + g_Y^2 + \left(g_{\rm mix} - \frac{4}{5}g_\chi\right)^2\right\}\Bigg) + 12\left(g_{\rm mix} - \frac{4}{5}g_\chi\right)^2 g_\chi^2\Bigg].\end{aligned} \tag{A.14}$$

A.3 $U(1)$ gauge extended model II

$$\beta_{g_Y} = \frac{g_Y^3}{16\pi^2}\frac{15}{2}\,, \qquad \beta_{g_2} = \frac{g_2^3}{16\pi^2}\frac{-7}{6}\,, \qquad \beta_{g_3} = \frac{g_3^3}{16\pi^2}(-5)\,, \tag{A.15}$$

$$\beta_{g_X} = \frac{g_X}{16\pi^2}\left[\left(\frac{44}{3}+\frac{64}{3}x_H+30x_H^2\right)g_X^2+\frac{15}{2}g_{\rm mix}^2+\left(\frac{32}{3}+30x_H\right)g_{\rm mix}g_X\right]\,, \tag{A.16}$$

$$\begin{aligned}\beta_{g_{\rm mix}} = \frac{1}{16\pi^2}\Bigg[&g_{\rm mix}\left(\frac{15}{2}(g_{\rm mix}^2+2g_Y^2)+\left(\frac{44}{3}+\frac{64}{3}x_H+30x_H^2\right)g_X^2\right)\\ &+\left(\frac{32}{3}+30x_H\right)g_X(g_Y^2+g_{\rm mix}^2)\Bigg]\,,\end{aligned} \tag{A.17}$$

$$\begin{aligned}\beta_{y_t} = \frac{y_t}{16\pi^2}\Bigg[&\frac{9}{2}y_t^2-\Bigg(8g_3^2+\frac{9}{4}g_2^2+\frac{17}{12}(g_Y^2+g_{\rm mix}^2)+\left(\frac{2}{3}+\frac{10}{3}x_H+\frac{17}{3}x_H^2\right)g_X^2\\ &+\left(\frac{5}{3}+\frac{17}{3}x_H\right)g_{\rm mix}g_X\Bigg)+3(\kappa_1^2+\kappa_2^2)\Bigg]\,,\end{aligned} \tag{A.18}$$

$$\beta_{Y_M} = \frac{Y_M}{16\pi^2}\left[4Y_M^2+2{\rm tr}Y_M^2+2(Y_{N_L}^2+Y_{N_R}^2)-6g_X^2\right]\,, \tag{A.19}$$

$$\beta_{Y_{N_L}} = \frac{1}{16\pi^2}\left[Y_{N_L}\left(6Y_{N_L}^2+f_N^2+2({\rm tr}Y_M^2+Y_{N_R}^2)-6g_X^2\right)+2f_N^2Y_{N_R}\right]\,, \tag{A.20}$$

$$\beta_{Y_{N_R}} = \frac{1}{16\pi^2}\left[Y_{N_R}\left(6Y_{N_R}^2+f_N^2+2({\rm tr}Y_M^2+Y_{N_L}^2)-6g_X^2\right)+2f_N^2Y_{N_L}\right]\,, \tag{A.21}$$

$$\begin{aligned}\beta_{\kappa_1} = \frac{1}{16\pi^2}\Bigg[&\kappa_1\Bigg(-8g_3^2-\frac{9}{4}g_2^2-\frac{5}{12}(g_Y^2+g_{\rm mix}^2)+\frac{1}{3}(1-5x_H)g_{\rm mix}g_X\\ &+\frac{1}{3}(-2+2x_H-5x_H^2)g_X^2+\frac{1}{2}(f_Q^2+f_D^2)+3y_t^2+\frac{9}{2}\kappa_1^2+3\kappa_2^2\Bigg)+2f_Qf_D\kappa_2\Bigg]\,,\end{aligned} \tag{A.22}$$

$$\begin{aligned}\beta_{\kappa_2} = \frac{1}{16\pi^2}\Bigg[&\kappa_2\Bigg(-8g_3^2-\frac{9}{4}g_2^2-\frac{5}{12}(g_Y^2+g_{\rm mix}^2)+\frac{1}{3}(1-5x_H)g_{\rm mix}g_X\\ &+\frac{1}{3}(-2+2x_H-5x_H^2)g_X^2+\frac{1}{2}(f_Q^2+f_D^2)+3y_t^2+\frac{9}{2}\kappa_2^2+3\kappa_1^2\Bigg)+2f_Qf_D\kappa_1\Bigg]\,,\end{aligned} \tag{A.23}$$

$$\begin{aligned}\beta_{f_Q} = \frac{1}{16\pi^2}\Bigg[&f_Q\Bigg(-8g_3^2-\frac{9}{2}g_2^2-\frac{1}{6}(g_Y^2+g_{\rm mix}^2)-\frac{2}{3}(1+x_H)g_{\rm mix}g_X\\ &-\frac{2}{3}(1+x_H)^2g_X^2+\frac{1}{2}(\kappa_1^2+\kappa_2^2)+15f_Q^2+6f_D^2+2f_N^2\Bigg)+2f_D\kappa_1\kappa_2\Bigg]\,,\end{aligned} \tag{A.24}$$

$$\begin{aligned}\beta_{f_D} = \frac{1}{16\pi^2}\Bigg[&f_D\Bigg(-8g_3^2-\frac{2}{3}(g_Y^2+g_{\rm mix}^2)+\frac{4}{3}(1-2x_H)g_{\rm mix}g_X-\frac{2}{3}(1-2x_H)^2g_X^2\\ &+(\kappa_1^2+\kappa_2^2)+12f_Q^2+9f_D^2+2f_N^2\Bigg)+4f_Q\kappa_1\kappa_2\Bigg]\,,\end{aligned} \tag{A.25}$$

$$\beta_{f_N} = \frac{f_N}{16\pi^2}\left[-6g_X^2+2Y_{N_L}^2+8Y_{N_L}Y_{N_R}+2Y_{N_R}^2+12f_Q^2+6f_D^2+5f_N^2\right]\,, \tag{A.26}$$

$$\beta_{\lambda_H} = \frac{1}{16\pi^2}\Big[24\lambda_H^2 + \lambda_{H\Phi}^2 + 2\lambda_{HS}^2 + \lambda_H\Big(12y_t^2 - 9g_2^2 - 3(g_Y^2 + g_{\rm mix}^2) - 12x_H^2 g_X^2 - 12x_H g_{\rm mix} g_X + 12(\kappa_1^2 + \kappa_2^2)\Big) - 6y_t^4 - 6(\kappa_1^4 + \kappa_2^4) + \frac{3}{8}\left\{2g_2^4 + (g_2^2 + g_Y^2 + g_{\rm mix}^2)^2\right\} + 3x_H g_{\rm mix} g_X(g_2^2 + g_Y^2 + g_{\rm mix}^2 + 4x_H^2 g_X^2) + 3x_H^2 g_X^2(g_2^2 + g_Y^2 + 3g_{\rm mix}^2 + 2x_H^2 g_X^2)\Big], \tag{A.27}$$

$$\beta_{\lambda_\Phi} = \frac{1}{16\pi^2}\Big[20\lambda_\Phi^2 + 2\lambda_{H\Phi}^2 + 2\lambda_{\Phi S}^2 + \lambda_\Phi(8({\rm tr}Y_M^2 + Y_{N_L}^2 + Y_{N_R}^2) - 48g_X^2) + 96g_X^4 - 16\left({\rm tr}Y_M^4 + Y_{N_L}^4 + Y_{N_R}^4\right)\Big], \tag{A.28}$$

$$\beta_{\lambda_S} = \frac{1}{16\pi^2}\Big[72\lambda_S^2 + 2\lambda_{HS}^2 + \lambda_{\Phi S}^2 + \lambda_S(48f_Q^2 + 24f_D^2 + 8f_N^2) - 12f_Q^4 - 6f_D^4 - 2f_N^4\Big], \tag{A.29}$$

$$\beta_{\lambda_{H\Phi}} = \frac{1}{16\pi^2}\Big[4\lambda_{HS}\lambda_{\Phi S} + \lambda_{H\Phi}\Big(12\lambda_H + 8\lambda_\Phi + 4\lambda_{H\Phi} - \frac{9}{2}g_2^2 - \frac{3}{2}(g_Y^2 + g_{\rm mix}^2) - 6(4 + x_H^2)g_X^2 - 6x_H g_{\rm mix} g_X + 6y_t^2 + 6(\kappa_1^2 + \kappa_2^2) + 4\left({\rm tr}Y_M^2 + Y_{N_L}^2 + Y_{N_R}^2\right)\Big) + 12g_X^2(g_{\rm mix} + 2x_H g_X)^2\Big], \tag{A.30}$$

$$\beta_{\lambda_{HS}} = \frac{1}{16\pi^2}\Big[2\lambda_{H\Phi}\lambda_{\Phi S} + \lambda_{HS}\Big(12\lambda_H + 24\lambda_S + 8\lambda_{HS} - \frac{9}{2}g_2^2 - \frac{3}{2}(g_Y^2 + g_{\rm mix}^2) - 6x_H^2 g_X^2 - 6x_H g_{\rm mix} g_X + 6y_t^2 + 6(\kappa_1^2 + \kappa_2^2) + 24f_Q^2 + 12f_D^2 + 4f_N^2\Big) - 12(f_Q^2 + f_D^2)(\kappa_1^2 + \kappa_2^2) - 24f_Q f_D \kappa_1\kappa_2\Big], \tag{A.31}$$

$$\beta_{\lambda_{\Phi S}} = \frac{1}{16\pi^2}\Big[4\lambda_{HS}\lambda_{H\Phi} + \lambda_{\Phi S}\Big(24\lambda_S + 8\lambda_\Phi + 8\lambda_{\Phi S} - 24g_X^2 + 24f_Q^2 + 12f_D^2 + 4f_N^2 + 4\left({\rm tr}Y_M^2 + Y_{N_L}^2 + Y_{N_R}^2\right)\Big) - 16f_N^2(Y_{N_L}^2 + Y_{N_R}^2 + Y_{N_L}Y_{N_R})\Big]. \tag{A.32}$$

A.4 Bosonic seesaw model I

$$\beta_{g_Y} = \frac{g_Y^3}{16\pi^2}7\,, \qquad \beta_{g_2} = \frac{g_2^3}{16\pi^2}(-3)\,, \qquad \beta_{g_3} = \frac{g_3^3}{16\pi^2}(-7)\,, \tag{A.33}$$

$$\beta_{g_{B-L}} = \frac{g_{B-L}}{16\pi^2}\left(7g_{\rm mix}^2 + 8g_{\rm mix}g_{B-L} + \frac{68}{3}g_{B-L}^2\right)\,, \tag{A.34}$$

$$\beta_{g_{\rm mix}} = \frac{1}{16\pi^2}\left[g_{\rm mix}\left(14g_Y^2 + 7g_{\rm mix}^2 + 8g_{\rm mix}g_{B-L} + \frac{68}{3}g_{B-L}^2\right) + 8g_{B-L}g_Y^2\right]\,, \tag{A.35}$$

$$\beta_{y_t} = \frac{y_t}{16\pi^2}\left[-8g_3^2 - \frac{9}{4}g_2^2 - \frac{17}{12}(g_Y^2 + g_{\rm mix}^2) - \frac{5}{3}g_{\rm mix}g_{B-L} - \frac{2}{3}g_{B-L}^2 + \frac{9}{2}y_t^2\right]\,, \tag{A.36}$$

$$\beta_{Y_M} = \frac{Y_M}{16\pi^2}\left(-6g_{B-L}^2 + 4Y_M^2 + 2{\rm tr}Y_M^2\right)\,, \tag{A.37}$$

$$\begin{aligned}\beta_{\lambda_1} = \frac{1}{16\pi^2}\Bigg[&\lambda_1\Big(24\lambda_1 - 9g_2^2 - 3(g_Y^2 + g_{\rm mix}^2) + 12y_t^2\Big) + 2\lambda_3^2 + 2\lambda_3\lambda_4 + \lambda_4^2 + \lambda_{H_1\Phi}^2 \\ &+ \frac{3}{8}\Big(2g_2^4 + (g_2^2 + g_Y^2 + g_{\rm mix}^2)^2\Big) - 6y_t^4\Bigg]\,,\end{aligned} \tag{A.38}$$

$$\begin{aligned}\beta_{\lambda_2} = \frac{1}{16\pi^2}\Bigg[&\lambda_2\Big(24\lambda_2 - 9g_2^2 - 3(g_Y^2 + g_{\rm mix}^2) + 48g_{\rm mix}g_{B-L} - 192g_{B-L}^2 + 12y_t^2\Big) \\ &+ 2\lambda_3^2 + 2\lambda_3\lambda_4 + \lambda_4^2 + \lambda_{H_2\Phi}^2 + \frac{3}{8}\Big(2g_2^4 + (g_2^2 + g_Y^2 + g_{\rm mix}^2)^2\Big) \\ &+ 48g_{B-L}^2\left(g_2^2 + g_Y^2 + \frac{1}{3}g_{\rm mix}^2 - 16g_{\rm mix}g_{B-L} + 32g_{B-L}^2\right) \\ &- 12g_{\rm mix}g_{B-L}(g_2^2 + g_Y^2 + g_{\rm mix}^2) - 6y_t^4\Bigg]\,,\end{aligned} \tag{A.39}$$

$$\begin{aligned}\beta_{\lambda_3} = \frac{1}{16\pi^2}\Bigg[&\lambda_3\Big(4\lambda_3 - 9g_2^2 - 3(g_Y^2 + g_{\rm mix}^2) + 24g_{\rm mix}g_{B-L} - 96g_{B-L}^2 + 6y_t^2 \\ &+ 12\lambda_1 + 12\lambda_2\Big) + 4\lambda_1\lambda_4 + 4\lambda_2\lambda_4 + 2\lambda_4^2 + 2\lambda_{H_1\Phi}\lambda_{H_2\Phi} \\ &+ \frac{3}{4}\Big(2g_2^4 + (-g_2^2 + g_Y^2 + g_{\rm mix}^2)^2\Big) + 48g_{\rm mix}^2g_{B-L}^2 - 12g_{\rm mix}g_{B-L}(-g_2^2 + g_{\rm mix}^2 + g_Y^2)\Bigg]\,,\end{aligned} \tag{A.40}$$

$$\begin{aligned}\beta_{\lambda_4} = \frac{1}{16\pi^2}\Bigg[&\lambda_4\Big(4\lambda_4 - 9g_2^2 - 3(g_Y^2 + g_{\rm mix}^2) + 24g_{\rm mix}g_{B-L} - 96g_{B-L}^2 + 6y_t^2 \\ &+ 4\lambda_1 + 4\lambda_2 + 8\lambda_3\Big) + 4\lambda_{\rm mix}^2 + 3g_2^2(g_Y^2 + g_{\rm mix}^2) - 24g_2^2g_{\rm mix}g_{B-L}\Bigg]\,,\end{aligned} \tag{A.41}$$

$$\begin{aligned}\beta_{\lambda_\Phi} = \frac{1}{16\pi^2}\Big[&\lambda_\Phi(20\lambda_\Phi - 48g_{B-L}^2 + 8{\rm tr}Y_M^2) + 2\lambda_{H_1\Phi}^2 + 2\lambda_{H_2\Phi}^2 + 4\lambda_{\rm mix}^2 \\ &+ 96g_{B-L}^4 - 16{\rm tr}Y_M^4\Big]\,,\end{aligned} \tag{A.42}$$

$$\beta_{\lambda_{H_1\Phi}} = \frac{1}{16\pi^2}\Bigg[\lambda_{H_1\Phi}\Bigg(4\lambda_{H_1\Phi} + 12\lambda_1 + 8\lambda_\Phi - \frac{9}{2}g_2^2 - \frac{3}{2}(g_Y^2 + g_{\rm mix}^2) - 24g_{B-L}^2 + 4{\rm tr}Y_M^2 + 6y_t^2\Bigg) + 4\lambda_3\lambda_{H_2\Phi} + 2\lambda_4\lambda_{H_2\Phi} + 8\lambda_{\rm mix}^2 + 12g_{\rm mix}^2 g_{B-L}^2\Bigg], \tag{A.43}$$

$$\beta_{\lambda_{H_2\Phi}} = \frac{1}{16\pi^2}\Bigg[\lambda_{H_2\Phi}\Bigg(4\lambda_{H_2\Phi} + 12\lambda_2 + 8\lambda_\Phi - \frac{9}{2}g_2^2 - \frac{3}{2}(g_Y^2 + g_{\rm mix}^2) - 120g_{B-L}^2 + 24g_{\rm mix}g_{B-L} + 4{\rm tr}Y_M^2\Bigg) + 4\lambda_3\lambda_{H_1\Phi} + 2\lambda_4\lambda_{H_1\Phi} + 8\lambda_{\rm mix}^2 + 12g_{B-L}^2\Bigg(g_{\rm mix}^2 - 16g_{\rm mix}g_{B-L} + 64g_{B-L}^2\Bigg)\Bigg], \tag{A.44}$$

$$\beta_{\lambda_{\rm mix}} = \frac{\lambda_{\rm mix}}{16\pi^2}\Bigg[2\lambda_3 + 4\lambda_4 + 4\lambda_{H_1\Phi} + 4\lambda_{H_2\Phi} + 4\lambda_\Phi - \frac{9}{2}g_2^2 - \frac{3}{2}(g_Y^2 + g_{\rm mix}^2) + 12g_{\rm mix}g_{B-L} - 72g_{B-L}^2 + 4{\rm tr}Y_M^2 + 3y_t^2\Bigg]. \tag{A.45}$$

Here, $g_{\rm mix}$ is a kinetic mixing coupling of the $U(1)$ gauge bosons, and in Chap. 4 we take $g_{\rm mix}(v_\Phi) = 0$ for its boundary condition, so that there is no mixing between Z and Z' bosons.

Bibliography

[1] G. Aad *et al.* [ATLAS Collaboration], Phys. Lett. B **716**, 1 (2012) doi:10.1016/j.physletb.2012.08.020 [arXiv:1207.7214 [hep-ex]].

[2] S. Chatrchyan *et al.* [CMS Collaboration], Phys. Lett. B **716**, 30 (2012) doi:10.1016/j.physletb.2012.08.021 [arXiv:1207.7235 [hep-ex]].

[3] G. Aad *et al.* [ATLAS and CMS Collaborations], Phys. Rev. Lett. **114**, 191803 (2015) doi:10.1103/PhysRevLett.114.191803 [arXiv:1503.07589 [hep-ex]].

[4] N. Cabibbo, Phys. Rev. Lett. **10**, 531 (1963). doi:10.1103/PhysRevLett.10.531

[5] M. Kobayashi and T. Maskawa, Prog. Theor. Phys. **49**, 652 (1973). doi:10.1143/PTP.49.652

[6] B. Pontecorvo, Sov. Phys. JETP **7**, 172 (1958) [Zh. Eksp. Teor. Fiz. **34**, 247 (1957)].

[7] Z. Maki, M. Nakagawa and S. Sakata, Prog. Theor. Phys. **28**, 870 (1962). doi:10.1143/PTP.28.870

[8] [ATLAS and CDF and CMS and D0 Collaborations], arXiv:1403.4427 [hep-ex].

[9] C. Patrignani, Chin. Phys. C **40**, no. 10, 100001 (2016). doi:10.1088/1674-1137/40/10/100001

[10] A. Kobakhidze and K. L. McDonald, JHEP **1407**, 155 (2014) doi:10.1007/JHEP07(2014)155 [arXiv:1404.5823 [hep-ph]].

[11] H. Aoki and S. Iso, Phys. Rev. D **86**, 013001 (2012) doi:10.1103/PhysRevD.86.013001 [arXiv:1201.0857 [hep-ph]].

[12] K. A. Meissner and H. Nicolai, Phys. Lett. B **660**, 260 (2008) doi:10.1016/j.physletb.2007.12.035 [arXiv:0710.2840 [hep-th]].

[13] W. A. Bardeen, FERMILAB-CONF-95-391-T, C95-08-27.3.

[14] S. R. Coleman and E. J. Weinberg, Phys. Rev. D **7**, 1888 (1973). doi:10.1103/PhysRevD.7.1888

[15] A. Salvio and A. Strumia, JHEP **1406**, 080 (2014) doi:10.1007/JHEP06(2014)080 [arXiv:1403.4226 [hep-ph]].

[16] K. Takenaga, Prog. Theor. Phys. **92**, 987 (1994) doi:10.1143/PTP.92.987 [hep-ph/9312321, hep-ph/9312321].

[17] K. A. Meissner and H. Nicolai, Phys. Lett. B **648**, 312 (2007) doi:10.1016/j.physletb.2007.03.023 [hep-th/0612165].

[18] R. Foot, A. Kobakhidze, K. L. McDonald and R. R. Volkas, Phys. Rev. D **76**, 075014 (2007) doi:10.1103/PhysRevD.76.075014 [arXiv:0706.1829 [hep-ph]].

[19] T. Hambye and M. H. G. Tytgat, Phys. Lett. B **659**, 651 (2008) doi:10.1016/j.physletb.2007.11.069 [arXiv:0707.0633 [hep-ph]].

[20] K. A. Meissner and H. Nicolai, Eur. Phys. J. C **57**, 493 (2008) doi:10.1140/epjc/s10052-008-0760-x [arXiv:0803.2814 [hep-th]].

[21] K. Ishiwata, Phys. Lett. B **710**, 134 (2012) doi:10.1016/j.physletb.2012.02.048 [arXiv:1112.2696 [hep-ph]].

[22] J. S. Lee and A. Pilaftsis, Phys. Rev. D **86**, 035004 (2012) doi:10.1103/PhysRevD.86.035004 [arXiv:1201.4891 [hep-ph]].

[23] E. Gabrielli, M. Heikinheimo, K. Kannike, A. Racioppi, M. Raidal and C. Spethmann, Phys. Rev. D **89**, no. 1, 015017 (2014) doi:10.1103/PhysRevD.89.015017 [arXiv:1309.6632 [hep-ph]].

[24] J. Guo and Z. Kang, Nucl. Phys. B **898**, 415 (2015) doi:10.1016/j.nuclphysb.2015.07.014 [arXiv:1401.5609 [hep-ph]].

[25] K. Allison, C. T. Hill and G. G. Ross, Phys. Lett. B **738**, 191 (2014) doi:10.1016/j.physletb.2014.09.041 [arXiv:1404.6268 [hep-ph]].

[26] A. Farzinnia and J. Ren, Phys. Rev. D **90**, no. 1, 015019 (2014) doi:10.1103/PhysRevD.90.015019 [arXiv:1405.0498 [hep-ph]].

[27] M. Lindner, S. Schmidt and J. Smirnov, JHEP **1410**, 177 (2014) doi:10.1007/JHEP10(2014)177 [arXiv:1405.6204 [hep-ph]].

[28] A. Farzinnia and J. Ren, Phys. Rev. D **90**, no. 7, 075012 (2014) doi:10.1103/PhysRevD.90.075012 [arXiv:1408.3533 [hep-ph]].

[29] K. Allison, C. T. Hill and G. G. Ross, Nucl. Phys. B **891**, 613 (2015) doi:10.1016/j.nuclphysb.2014.12.022 [arXiv:1409.4029 [hep-ph]].

[30] Z. Kang, Eur. Phys. J. C **75**, no. 10, 471 (2015) doi:10.1140/epjc/s10052-015-3702-4 [arXiv:1411.2773 [hep-ph]].

[31] K. Endo and Y. Sumino, JHEP **1505**, 030 (2015) doi:10.1007/JHEP05(2015)030 [arXiv:1503.02819 [hep-ph]].

[32] K. Fuyuto and E. Senaha, Phys. Lett. B **747**, 152 (2015). doi:10.1016/j.physletb.2015.05.061

[33] K. Endo and K. Ishiwata, Phys. Lett. B **749**, 583 (2015) doi:10.1016/j.physletb.2015.08.059 [arXiv:1507.01739 [hep-ph]].

[34] A. Ahriche, K. L. McDonald and S. Nasri, JHEP **1602**, 038 (2016) doi:10.1007/JHEP02(2016)038 [arXiv:1508.02607 [hep-ph]].

[35] K. Hashino, S. Kanemura and Y. Orikasa, Phys. Lett. B **752**, 217 (2016) doi:10.1016/j.physletb.2015.11.044 [arXiv:1508.03245 [hep-ph]].

[36] K. Ghorbani and H. Ghorbani, JHEP **1604**, 024 (2016) doi:10.1007/JHEP04(2016)024 [arXiv:1511.08432 [hep-ph]].

[37] A. Ahriche, K. L. McDonald and S. Nasri, JHEP **1606**, 182 (2016) doi:10.1007/JHEP06(2016)182 [arXiv:1604.05569 [hep-ph]].

[38] R. Hempfling, Phys. Lett. B **379**, 153 (1996) doi:10.1016/0370-2693(96)00446-7 [hep-ph/9604278].

[39] A. G. Dias, Phys. Rev. D **73**, 096002 (2006) doi:10.1103/PhysRevD.73.096002 [hep-ph/0604219].

[40] J. R. Espinosa and M. Quiros, Phys. Rev. D **76**, 076004 (2007) doi:10.1103/PhysRevD.76.076004 [hep-ph/0701145].

[41] W. F. Chang, J. N. Ng and J. M. S. Wu, Phys. Rev. D **75**, 115016 (2007) doi:10.1103/PhysRevD.75.115016 [hep-ph/0701254 [HEP-PH]].

[42] S. Iso, N. Okada and Y. Orikasa, Phys. Lett. B **676**, 81 (2009) doi:10.1016/j.physletb.2009.04.046 [arXiv:0902.4050 [hep-ph]].

[43] S. Iso, N. Okada and Y. Orikasa, Phys. Rev. D **80**, 115007 (2009) doi:10.1103/PhysRevD.80.115007 [arXiv:0909.0128 [hep-ph]].

[44] N. Okada and Y. Orikasa, Phys. Rev. D **85**, 115006 (2012) doi:10.1103/PhysRevD.85.115006 [arXiv:1202.1405 [hep-ph]].

[45] S. Iso and Y. Orikasa, PTEP **2013**, 023B08 (2013) doi:10.1093/ptep/pts099 [arXiv:1210.2848 [hep-ph]].

[46] C. Englert, J. Jaeckel, V. V. Khoze and M. Spannowsky, JHEP **1304**, 060 (2013) doi:10.1007/JHEP04(2013)060 [arXiv:1301.4224 [hep-ph]].

[47] E. J. Chun, S. Jung and H. M. Lee, Phys. Lett. B **725**, 158 (2013) Erratum: [Phys. Lett. B **730**, 357 (2014)] doi:10.1016/j.physletb.2013.11.016, 10.1016/j.physletb.2013.06.055 [arXiv:1304.5815 [hep-ph]].

[48] I. Oda, Phys. Lett. B **724**, 160 (2013) doi:10.1016/j.physletb.2013.06.014 [arXiv:1305.0884 [hep-ph]].

[49] V. V. Khoze and G. Ro, JHEP **1310**, 075 (2013) doi:10.1007/JHEP10(2013)075 [arXiv:1307.3764 [hep-ph]].

[50] A. Farzinnia, H. J. He and J. Ren, Phys. Lett. B **727**, 141 (2013) doi:10.1016/j.physletb.2013.09.060 [arXiv:1308.0295 [hep-ph]].

[51] V. V. Khoze, JHEP **1311**, 215 (2013) doi:10.1007/JHEP11(2013)215 [arXiv:1308.6338 [hep-ph]].

[52] R. Foot, A. Kobakhidze, K. L. McDonald and R. R. Volkas, Phys. Rev. D **89**, no. 11, 115018 (2014) doi:10.1103/PhysRevD.89.115018 [arXiv:1310.0223 [hep-ph]].

[53] M. Hashimoto, S. Iso and Y. Orikasa, Phys. Rev. D **89**, no. 1, 016019 (2014) doi:10.1103/PhysRevD.89.016019 [arXiv:1310.4304 [hep-ph]].

[54] M. Lindner, D. Schmidt and A. Watanabe, Phys. Rev. D **89**, no. 1, 013007 (2014) doi:10.1103/PhysRevD.89.013007 [arXiv:1310.6582 [hep-ph]].

[55] M. Hashimoto, S. Iso and Y. Orikasa, Phys. Rev. D **89**, no. 5, 056010 (2014) doi:10.1103/PhysRevD.89.056010 [arXiv:1401.5944 [hep-ph]].

[56] S. Benic and B. Radovcic, Phys. Lett. B **732**, 91 (2014) doi:10.1016/j.physletb.2014.03.018 [arXiv:1401.8183 [hep-ph]].

[57] V. V. Khoze, C. McCabe and G. Ro, JHEP **1408**, 026 (2014) doi:10.1007/JHEP08(2014)026 [arXiv:1403.4953 [hep-ph]].

[58] W. Altmannshofer, W. A. Bardeen, M. Bauer, M. Carena and J. D. Lykken, JHEP **1501**, 032 (2015) doi:10.1007/JHEP01(2015)032 [arXiv:1408.3429 [hep-ph]].

[59] S. Benic and B. Radovcic, JHEP **1501**, 143 (2015) doi:10.1007/JHEP01(2015)143 [arXiv:1409.5776 [hep-ph]].

[60] H. Okada and Y. Orikasa, Phys. Lett. B **760**, 558 (2016) doi:10.1016/j.physletb.2016.07.039 [arXiv:1412.3616 [hep-ph]].

[61] K. Kawana, PTEP **2015**, 073B04 (2015) doi:10.1093/ptep/ptv093 [arXiv:1501.04482 [hep-ph]].

[62] J. Guo, Z. Kang, P. Ko and Y. Orikasa, Phys. Rev. D **91**, no. 11, 115017 (2015) doi:10.1103/PhysRevD.91.115017 [arXiv:1502.00508 [hep-ph]].

[63] P. Humbert, M. Lindner and J. Smirnov, JHEP **1506**, 035 (2015) doi:10.1007/JHEP06(2015)035 [arXiv:1503.03066 [hep-ph]].

[64] N. Haba and Y. Yamaguchi, PTEP **2015**, no. 9, 093B05 (2015) doi:10.1093/ptep/ptv121 [arXiv:1504.05669 [hep-ph]].

[65] S. Oda, N. Okada and D. s. Takahashi, Phys. Rev. D **92**, no. 1, 015026 (2015) doi:10.1103/PhysRevD.92.015026 [arXiv:1504.06291 [hep-ph]].

[66] P. Humbert, M. Lindner, S. Patra and J. Smirnov, JHEP **1509**, 064 (2015) doi:10.1007/JHEP09(2015)064 [arXiv:1505.07453 [hep-ph]].

[67] A. D. Plascencia, JHEP **1509**, 026 (2015) doi:10.1007/JHEP09(2015)026 [arXiv:1507.04996 [hep-ph]].

[68] N. Haba, H. Ishida, N. Okada and Y. Yamaguchi, Phys. Lett. B **754**, 349 (2016) doi:10.1016/j.physletb.2016.01.050 [arXiv:1508.06828 [hep-ph]]; arXiv:1509.01923 [hep-ph].

[69] A. Das, N. Okada and N. Papapietro, arXiv:1509.01466 [hep-ph].

[70] H. Okada, Y. Orikasa and K. Yagyu, arXiv:1510.00799 [hep-ph].

[71] N. Haba, H. Ishida, R. Takahashi and Y. Yamaguchi, JHEP **1602**, 058 (2016) doi:10.1007/JHEP02(2016)058 [arXiv:1511.02107 [hep-ph]].

[72] R. Jinno and M. Takimoto, arXiv:1604.05035 [hep-ph].

[73] A. Das, S. Oda, N. Okada and D. s. Takahashi, Phys. Rev. D **93**, no. 11, 115038 (2016) doi:10.1103/PhysRevD.93.115038 [arXiv:1605.01157 [hep-ph]].

[74] R. Foot, A. Kobakhidze and R. R. Volkas, Phys. Lett. B **655**, 156 (2007) doi:10.1016/j.physletb.2007.06.084 [arXiv:0704.1165 [hep-ph]].

[75] M. Holthausen, M. Lindner and M. A. Schmidt, Phys. Rev. D **82**, 055002 (2010) doi:10.1103/PhysRevD.82.055002 [arXiv:0911.0710 [hep-ph]].

[76] M. Heikinheimo, A. Racioppi, M. Raidal, C. Spethmann and K. Tuominen, Nucl. Phys. B **876**, 201 (2013) doi:10.1016/j.nuclphysb.2013.08.006 [arXiv:1305.4182 [hep-ph]].

[77] T. Hambye and A. Strumia, Phys. Rev. D **88**, 055022 (2013) doi:10.1103/PhysRevD.88.055022 [arXiv:1306.2329 [hep-ph]].

[78] C. D. Carone and R. Ramos, Phys. Rev. D **88**, 055020 (2013) doi:10.1103/PhysRevD.88.055020 [arXiv:1307.8428 [hep-ph]].

[79] S. Abel and A. Mariotti, Phys. Rev. D **89**, no. 12, 125018 (2014) doi:10.1103/PhysRevD.89.125018 [arXiv:1312.5335 [hep-ph]].

[80] C. T. Hill, Phys. Rev. D **89**, no. 7, 073003 (2014) doi:10.1103/PhysRevD.89.073003 [arXiv:1401.4185 [hep-ph]].

[81] A. Karam and K. Tamvakis, Phys. Rev. D **92**, no. 7, 075010 (2015) doi:10.1103/PhysRevD.92.075010 [arXiv:1508.03031 [hep-ph]].

[82] V. V. Khoze and A. D. Plascencia, arXiv:1605.06834 [hep-ph].

[83] A. Karam and K. Tamvakis, Phys. Rev. D **94**, no. 5, 055004 (2016) doi:10.1103/PhysRevD.94.055004 [arXiv:1607.01001 [hep-ph]].

[84] T. Hur and P. Ko, Phys. Rev. Lett. **106**, 141802 (2011) doi:10.1103/PhysRevLett.106.141802 [arXiv:1103.2571 [hep-ph]].

[85] M. Heikinheimo, A. Racioppi, M. Raidal, C. Spethmann and K. Tuominen, Mod. Phys. Lett. A **29**, 1450077 (2014) doi:10.1142/S0217732314500771 [arXiv:1304.7006 [hep-ph]].

[86] M. Holthausen, J. Kubo, K. S. Lim and M. Lindner, JHEP **1312**, 076 (2013) doi:10.1007/JHEP12(2013)076 [arXiv:1310.4423 [hep-ph]].

[87] J. Kubo, K. S. Lim and M. Lindner, Phys. Rev. Lett. **113**, 091604 (2014) doi:10.1103/PhysRevLett.113.091604 [arXiv:1403.4262 [hep-ph]].

[88] J. Kubo, K. S. Lim and M. Lindner, JHEP **1409**, 016 (2014) doi:10.1007/JHEP09(2014)016 [arXiv:1405.1052 [hep-ph]].

[89] O. Antipin, M. Redi and A. Strumia, JHEP **1501**, 157 (2015) doi:10.1007/JHEP01(2015)157 [arXiv:1410.1817 [hep-ph]].

[90] M. Heikinheimo and C. Spethmann, JHEP **1412**, 084 (2014) doi:10.1007/JHEP12(2014)084 [arXiv:1410.4842 [hep-ph]].

[91] Y. Ametani, M. Aoki, H. Goto and J. Kubo, Phys. Rev. D **91**, no. 11, 115007 (2015) doi:10.1103/PhysRevD.91.115007 [arXiv:1505.00128 [hep-ph]].

[92] C. D. Carone and R. Ramos, Phys. Lett. B **746**, 424 (2015) doi:10.1016/j.physletb.2015.05.044 [arXiv:1505.04448 [hep-ph]].

[93] J. Kubo and M. Yamada, Phys. Rev. D **93**, no. 7, 075016 (2016) doi:10.1103/PhysRevD.93.075016 [arXiv:1505.05971 [hep-ph]].

[94] J. Kubo and M. Yamada, PTEP **2015**, no. 9, 093B01 (2015) doi:10.1093/ptep/ptv114 [arXiv:1506.06460 [hep-ph]].

[95] N. Haba, H. Ishida, N. Kitazawa and Y. Yamaguchi, Phys. Lett. B **755**, 439 (2016) doi:10.1016/j.physletb.2016.02.052 [arXiv:1512.05061 [hep-ph]].

[96] H. Ishida, S. Matsuzaki and Y. Yamaguchi, arXiv:1604.07712 [hep-ph].

[97] K. Kannike, G. M. Pelaggi, A. Salvio and A. Strumia, JHEP **1607**, 101 (2016) doi:10.1007/JHEP07(2016)101 [arXiv:1605.08681 [hep-ph]].

[98] H. Hatanaka, D. W. Jung and P. Ko, JHEP **1608**, 094 (2016) doi:10.1007/JHEP08(2016)094 [arXiv:1606.02969 [hep-ph]].

[99] J. Kubo and M. Yamada, arXiv:1610.02241 [hep-ph].

[100] H. Ishida, S. Matsuzaki and Y. Yamaguchi, arXiv:1610.07137 [hep-ph].

[101] H. Ishida, S. Matsuzaki, S. Okawa and Y. Omura, arXiv:1701.00598 [hep-ph].

[102] N. Haba and T. Yamada, arXiv:1701.02146 [hep-ph].

[103] K. Tsumura, M. Yamada and Y. Yamaguchi, in preparation.

[104] Y. Yamaguchi and Y. Yoshimochi, in preparation.

[105] P. Minkowski, Phys. Lett. B **67**, 421 (1977) doi:10.1016/0370-2693(77)90435-X;
T. Yanagida, Conf. Proc. C **7902131**, 95 (1979);
M. Gell-Mann, P. Ramond and R. Slansky, Conf. Proc. C **790927**, 315 (1979) [arXiv:1306.4669 [hep-th]];
R. N. Mohapatra and G. Senjanovic, Phys. Rev. Lett. **44**, 912 (1980) doi:10.1103/PhysRevLett.44.912;
J. Schechter and J. W. F. Valle, Phys. Rev. D **22**, 2227 (1980); Phys. Rev. D **25** 774 (1982).

[106] P. Langacker, Rev. Mod. Phys. **81**, 1199 (2009) doi:10.1103/RevModPhys.81.1199 [arXiv:0801.1345 [hep-ph]].

[107] G. Degrassi, S. Di Vita, J. Elias-Miro, J. R. Espinosa, G. F. Giudice, G. Isidori and A. Strumia, JHEP **1208**, 098 (2012) doi:10.1007/JHEP08(2012)098 [arXiv:1205.6497 [hep-ph]].

[108] J. Chakrabortty, P. Konar and T. Mondal, Phys. Rev. D **89**, no. 5, 056014 (2014) doi:10.1103/PhysRevD.89.056014 [arXiv:1308.1291 [hep-ph]].

[109] D. Buttazzo, G. Degrassi, P. P. Giardino, G. F. Giudice, F. Sala, A. Salvio and A. Strumia, JHEP **1312**, 089 (2013) doi:10.1007/JHEP12(2013)089 [arXiv:1307.3536 [hep-ph]].

[110] N. Haba, H. Ishida, R. Takahashi and Y. Yamaguchi, Nucl. Phys. B **900**, 244 (2015) doi:10.1016/j.nuclphysb.2015.09.004 [arXiv:1412.8230 [hep-ph]].

[111] [ATLAS Collaboration], ATLAS-CONF-2012-129.

[112] CMS Collaboration [CMS Collaboration], CMS-PAS-EXO-12-015.

[113] M. Carena, A. Daleo, B. A. Dobrescu and T. M. P. Tait, Phys. Rev. D **70**, 093009 (2004) doi:10.1103/PhysRevD.70.093009 [hep-ph/0408098].

[114] G. Cacciapaglia, C. Csaki, G. Marandella and A. Strumia, Phys. Rev. D **74**, 033011 (2006) doi:10.1103/PhysRevD.74.033011 [hep-ph/0604111].

[115] The ATLAS collaboration [ATLAS Collaboration], ATLAS-CONF-2016-045.

[116] CMS Collaboration [CMS Collaboration], CMS-PAS-EXO-16-031.

[117] A. Pilaftsis and T. E. J. Underwood, Nucl. Phys. B **692**, 303 (2004) doi:10.1016/j.nuclphysb.2004.05.029 [hep-ph/0309342].

[118] S. Iso, N. Okada and Y. Orikasa, Phys. Rev. D **83**, 093011 (2011) doi:10.1103/PhysRevD.83.093011 [arXiv:1011.4769 [hep-ph]].

[119] N. Okada, Y. Orikasa and T. Yamada, Phys. Rev. D **86**, 076003 (2012) doi:10.1103/PhysRevD.86.076003 [arXiv:1207.1510 [hep-ph]].

[120] F. Staub, arXiv:0806.0538 [hep-ph].

[121] I. Gogoladze, B. He and Q. Shafi, Phys. Lett. B **690**, 495 (2010) doi:10.1016/j.physletb.2010.05.076 [arXiv:1004.4217 [hep-ph]].

[122] F. Bazzocchi and M. Fabbrichesi, Phys. Rev. D **87**, no. 3, 036001 (2013) doi:10.1103/PhysRevD.87.036001 [arXiv:1212.5065 [hep-ph]].

[123] G. Barenboim, F. J. Botella and O. Vives, Nucl. Phys. B **613**, 285 (2001) doi:10.1016/S0550-3213(01)00390-X [hep-ph/0105306].

[124] J. Heeck, Phys. Lett. B **739**, 256 (2014) doi:10.1016/j.physletb.2014.10.067 [arXiv:1408.6845 [hep-ph]].

[125] G. Aad *et al.* [ATLAS Collaboration], JHEP **1508**, 105 (2015) doi:10.1007/JHEP08(2015)105 [arXiv:1505.04306 [hep-ex]].

[126] V. Khachatryan *et al.* [CMS Collaboration], Phys. Rev. D **93** (2016) no.11, 112009 doi:10.1103/PhysRevD.93.112009 [arXiv:1507.07129 [hep-ex]].

[127] V. Khachatryan *et al.* [CMS Collaboration], Phys. Rev. D **93**, no. 1, 012003 (2016) doi:10.1103/PhysRevD.93.012003 [arXiv:1509.04177 [hep-ex]].

[128] L. Lavoura and J. P. Silva, Phys. Rev. D **47**, 2046 (1993). doi:10.1103/PhysRevD.47.2046

[129] N. Maekawa, Phys. Rev. D **52**, 1684 (1995). doi:10.1103/PhysRevD.52.1684

[130] G. Aad *et al.* [ATLAS Collaboration], Phys. Rev. D **90**, no. 5, 052005 (2014) doi:10.1103/PhysRevD.90.052005 [arXiv:1405.4123 [hep-ex]].

[131] V. Khachatryan *et al.* [CMS Collaboration], JHEP **1504**, 025 (2015) doi:10.1007/JHEP04(2015)025 [arXiv:1412.6302 [hep-ex]].

[132] M. Fukugita and T. Yanagida, Phys. Lett. B **174**, 45 (1986). doi:10.1016/0370-2693(86)91126-3

[133] S. Davidson and A. Ibarra, Phys. Lett. B **535**, 25 (2002) doi:10.1016/S0370-2693(02)01735-5 [hep-ph/0202239].

[134] M. Duerr, P. Fileviez Perez and J. Smirnov, Phys. Rev. D **92**, no. 8, 083521 (2015) doi:10.1103/PhysRevD.92.083521 [arXiv:1506.05107 [hep-ph]].

[135] D. S. Akerib *et al.* [LUX Collaboration], Phys. Rev. Lett. **112**, 091303 (2014) doi:10.1103/PhysRevLett.112.091303 [arXiv:1310.8214 [astro-ph.CO]].

[136] D. S. Akerib *et al.*, arXiv:1608.07648 [astro-ph.CO].

[137] A. Tan *et al.* [PandaX-II Collaboration], Phys. Rev. Lett. **117**, no. 12, 121303 (2016) doi:10.1103/PhysRevLett.117.121303 [arXiv:1607.07400 [hep-ex]].

[138] R. Adam *et al.* [Planck Collaboration], Astron. Astrophys. **594**, A10 (2016) doi:10.1051/0004-6361/201525967 [arXiv:1502.01588 [astro-ph.CO]].

[139] N. Okada and S. Okada, arXiv:1611.02672 [hep-ph].

[140] X. Calmet, Eur. Phys. J. C **28**, 451 (2003) doi:10.1140/epjc/s2003-01213-6 [hep-ph/0206091].

[141] H. D. Kim, Phys. Rev. D **72**, 055015 (2005) doi:10.1103/PhysRevD.72.055015 [hep-ph/0501059].

[142] N. Haba, N. Kitazawa and N. Okada, Acta Phys. Polon. B **40**, 67 (2009) [hep-ph/0504279].

[143] C. Vafa and E. Witten, Phys. Rev. Lett. **53**, 535 (1984). doi:10.1103/PhysRevLett.53.535

[144] G. 't Hooft, Phys. Rev. Lett. **37**, 8 (1976). doi:10.1103/PhysRevLett.37.8

[145] E. Witten, Nucl. Phys. B **156**, 269 (1979). doi:10.1016/0550-3213(79)90031-2

[146] G. Veneziano, Nucl. Phys. B **159**, 213 (1979). doi:10.1016/0550-3213(79)90332-8; Phys. Lett. **95B**, 90 (1980). doi:10.1016/0370-2693(80)90406-2

[147] The ATLAS collaboration, ATLAS-CONF-2015-081.

[148] CMS Collaboration [CMS Collaboration], collisions at 13TeV," CMS-PAS-EXO-15-004.

[149] The ATLAS collaboration [ATLAS Collaboration], ATLAS-CONF-2016-059.

[150] CMS Collaboration [CMS Collaboration], CMS-PAS-EXO-16-027.

[151] J. Gasser and H. Leutwyler, Nucl. Phys. B **250**, 465 (1985). doi:10.1016/0550-3213(85)90492-4

[152] J. Wess and B. Zumino, Phys. Lett. **37B**, 95 (1971). doi:10.1016/0370-2693(71)90582-X

[153] S. Fichet, G. von Gersdorff and C. Royon, Phys. Rev. D **93**, no. 7, 075031 (2016) doi:10.1103/PhysRevD.93.075031 [arXiv:1512.05751 [hep-ph]].

[154] C. Csaki, J. Hubisz and J. Terning, Phys. Rev. D **93**, no. 3, 035002 (2016) doi:10.1103/PhysRevD.93.035002 [arXiv:1512.05776 [hep-ph]].

[155] C. Csaki, J. Hubisz, S. Lombardo and J. Terning, Phys. Rev. D **93**, no. 9, 095020 (2016) doi:10.1103/PhysRevD.93.095020 [arXiv:1601.00638 [hep-ph]].

[156] S. Fichet, G. von Gersdorff and C. Royon, Phys. Rev. Lett. **116**, no. 23, 231801 (2016) doi:10.1103/PhysRevLett.116.231801 [arXiv:1601.01712 [hep-ph]].

[157] L. A. Harland-Lang, V. A. Khoze and M. G. Ryskin, JHEP **1603**, 182 (2016) doi:10.1007/JHEP03(2016)182 [arXiv:1601.07187 [hep-ph]].

[158] N. D. Barrie, A. Kobakhidze, M. Talia and L. Wu, Phys. Lett. B **755**, 343 (2016) doi:10.1016/j.physletb.2016.02.010 [arXiv:1602.00475 [hep-ph]].

[159] A. Ahriche, G. Faisel, S. Nasri and J. Tandean, arXiv:1603.01606 [hep-ph].

[160] E. Molinaro, F. Sannino and N. Vignaroli, Nucl. Phys. B **911**, 106 (2016) doi:10.1016/j.nuclphysb.2016.07.032 [arXiv:1602.07574 [hep-ph]].

[161] G. Aad *et al.* [ATLAS Collaboration], Phys. Rev. D **92**, no. 3, 032004 (2015) doi:10.1103/PhysRevD.92.032004 [arXiv:1504.05511 [hep-ex]].

[162] CMS Collaboration [CMS Collaboration], CMS-PAS-EXO-12-045.

[163] G. Aad *et al.* [ATLAS Collaboration], Phys. Lett. B **738**, 428 (2014) doi:10.1016/j.physletb.2014.10.002 [arXiv:1407.8150 [hep-ex]].

[164] G. Aad *et al.* [ATLAS Collaboration], Eur. Phys. J. C **76**, no. 1, 45 (2016) doi:10.1140/epjc/s10052-015-3820-z [arXiv:1507.05930 [hep-ex]].

[165] V. Khachatryan *et al.* [CMS Collaboration], JHEP **1510**, 144 (2015) doi:10.1007/JHEP10(2015)144 [arXiv:1504.00936 [hep-ex]].

[166] G. Aad *et al.* [ATLAS Collaboration], JHEP **1601**, 032 (2016) doi:10.1007/JHEP01(2016)032 [arXiv:1509.00389 [hep-ex]].

[167] P. Lebiedowicz, M. Luszczak, R. Pasechnik and A. Szczurek, Phys. Rev. D **94**, no. 1, 015023 (2016) doi:10.1103/PhysRevD.94.015023 [arXiv:1604.02037 [hep-ph]].

[168] H. Baer, K. Y. Choi, J. E. Kim and L. Roszkowski, Phys. Rept. **555**, 1 (2015) doi:10.1016/j.physrep.2014.10.002 [arXiv:1407.0017 [hep-ph]].

[169] Y. Mambrini, S. Profumo and F. S. Queiroz, Phys. Lett. B **760**, 807 (2016) doi:10.1016/j.physletb.2016.07.076 [arXiv:1508.06635 [hep-ph]].

[170] G. G. Raffelt, Lect. Notes Phys. **741**, 51 (2008) doi:10.1007/978-3-540-73518-2_3 [hep-ph/0611350].

[171] E. Di Valentino, S. Gariazzo, M. Gerbino, E. Giusarma and O. Mena, Phys. Rev. D **93**, no. 8, 083523 (2016) doi:10.1103/PhysRevD.93.083523 [arXiv:1601.07557 [astro-ph.CO]].

[172] F. Bezrukov, D. Gorbunov and M. Shaposhnikov, JCAP **0906**, 029 (2009) doi:10.1088/1475-7516/2009/06/029 [arXiv:0812.3622 [hep-ph]].

[173] J. Garcia-Bellido, D. G. Figueroa and J. Rubio, Phys. Rev. D **79**, 063531 (2009) doi:10.1103/PhysRevD.79.063531 [arXiv:0812.4624 [hep-ph]].

[174] D. G. Figueroa and C. T. Byrnes, arXiv:1604.03905 [hep-ph].

[175] K. Choi, K. Hwang, H. B. Kim and T. Lee, Phys. Lett. B **467**, 211 (1999) doi:10.1016/S0370-2693(99)01156-9 [hep-ph/9902291].

[176] P. Sikivie, Phys. Rev. Lett. **51**, 1415 (1983) Erratum: [Phys. Rev. Lett. **52**, 695 (1984)]. doi:10.1103/PhysRevLett.51.1415, 10.1103/PhysRevLett.52.695.2

[177] P. Sikivie, Phys. Rev. D **32**, 2988 (1985) Erratum: [Phys. Rev. D **36**, 974 (1987)]. doi:10.1103/PhysRevD.36.974, 10.1103/PhysRevD.32.2988

[178] P. Sikivie, D. B. Tanner and Y. Wang, Phys. Rev. D **50**, 4744 (1994) doi:10.1103/PhysRevD.50.4744 [hep-ph/9305264].

[179] R. Bradley, J. Clarke, D. Kinion, L. J. Rosenberg, K. van Bibber, S. Matsuki, M. Muck and P. Sikivie, Rev. Mod. Phys. **75**, 777 (2003). doi:10.1103/RevModPhys.75.777

[180] T. Appelquist *et al.* [Lattice Strong Dynamics (LSD) Collaboration], Phys. Rev. D **89**, no. 9, 094508 (2014) doi:10.1103/PhysRevD.89.094508 [arXiv:1402.6656 [hep-lat]].

[181] T. Appelquist *et al.*, Phys. Rev. D **92**, no. 7, 075030 (2015) doi:10.1103/PhysRevD.92.075030 [arXiv:1503.04203 [hep-ph]].

[182] T. Appelquist *et al.*, Phys. Rev. Lett. **115**, no. 17, 171803 (2015) doi:10.1103/PhysRevLett.115.171803 [arXiv:1503.04205 [hep-ph]].

[183] J. L. Feng *et al.*, arXiv:1401.6085 [hep-ex].

[184] H. Ohki *et al.*, Phys. Rev. D **78**, 054502 (2008) doi:10.1103/PhysRevD.78.054502 [arXiv:0806.4744 [hep-lat]].

[185] H. Ohki *et al.* [JLQCD Collaboration], Phys. Rev. D **87**, 034509 (2013) doi:10.1103/PhysRevD.87.034509 [arXiv:1208.4185 [hep-lat]].

[186] J. Hisano, K. Ishiwata and N. Nagata, JHEP **1506**, 097 (2015) doi:10.1007/JHEP06(2015)097 [arXiv:1504.00915 [hep-ph]].

[187] J. Billard, L. Strigari and E. Figueroa-Feliciano, Phys. Rev. D **89**, no. 2, 023524 (2014) doi:10.1103/PhysRevD.89.023524 [arXiv:1307.5458 [hep-ph]].

[188] J. M. Maldacena, Int. J. Theor. Phys. **38**, 1113 (1999) [Adv. Theor. Math. Phys. **2**, 231 (1998)] doi:10.1023/A:1026654312961 [hep-th/9711200].

[189] K. Hamada, S. Horata and T. Yukawa, "Background Free Quantum Gravity and Cosmology," *Focus on Quantum Gravity Research*, Nova Science Publisher, (2006), Chap. 1 (pp. 1-47).

[190] C. Ford, I. Jack and D. R. T. Jones, Nucl. Phys. B **387**, 373 (1992) Erratum: [Nucl. Phys. B **504**, 551 (1997)] doi:10.1016/0550-3213(92)90165-8, 10.1016/S0550-3213(97)00532-4 [hep-ph/0111190].